OCS Study MMS 2009-017

Final Report

MAPPING SEA ICE OVERFLOOD USING REMOTE SENSING: SMITH BAY TO CAMDEN BAY

DF Dickins Associates, LLC

Coastal Frontiers Corporation

Aero-Metric Inc.

University of Alaska Fairbanks, Geophysical Institute

June 2009

MMS Contract No. M06 PC 00034

US Department of the Interior
Minerals Management Service
Alaska OCS Region
Anchorage, Alaska

Disclaimer:

This report was prepared under contract between the Mineral Management Service (MMS) and DF Dickins Associates, LLC. It has been technically reviewed by the MMS and approved for publication. Approval does not signify that the contents necessarily reflect the views and policies of the Service, nor does mention of trade names or commercial products constitute endorsement or recommendation for use. The report is, however, exempt from review and compliance with the MMS editorial standards.

Citation for Referencing

The correct citation for this study reads:

Hearon, G., D. Dickins, K. Ambrosius, and K. Morris. 2009. Mapping Sea Ice Overflood Using Remote Sensing: Smith Bay to Camden Bay. Report prepared by DF Dickins Associates, Coastal Frontiers Corporation, Aerometric, and The Geophysical Institute, University of Alaska for US Department of Interior, Minerals Management Service, Alaska OCS Region under Contract M06PC00034.

MAPPING SEA ICE OVERFLOOD USING REMOTE SENSING SMITH BAY TO CAMDEN BAY

DF Dickins Associates, LLC.
9463 Poole Street
La Jolla, CA 92037

Coastal Frontiers Corporation
9420 Topanga Canyon Blvd., Suite #101
Chatsworth, CA 91311

Aero-Metric Inc.
2014 Merrill Field Drive
Anchorage, Alaska 99501

Geophysical Institute, University of Alaska Fairbanks
903 Koyuktuk Drive
Fairbanks, AK 99775

June 2009

This study was funded by the U.S. Department of Interior, Minerals Management Service (MMS), Alaska Outer Continental Shelf Region, Anchorage Alaska, under Contract Number M06 PC 00034, as part of the MMS Alaska Environmental Studies Program.

The opinions, findings, conclusions, or recommendations expressed in this report or product are those of the authors and do not necessarily reflect the view of the U.S. Department of the Interior, nor does mention of trade names or commercial products constitute endorsement or recommendation for use by the federal Government.

Corresponding authors
Email: dfdickinsickins@scbglobal.net, ghearon@coastalfrontiers.com

Acknowledgements

The study team would like to recognize the support of BP Exploration (Alaska) Inc., Pioneer Natural Resources Alaska, and Shell Exploration and Production Inc. for providing open access to historical strudel drain and scour mapping data.

PROJECT ORGANIZATION

David Dickins
DF Dickins Associates, LLC
Principal Investigator and Program Manager

- Project oversight and team coordination
- Visual satellite image archive screening
- Visual satellite image acquisition
- Overflood limit interpretation from satellite images
- Primary report author

Greg Hearon
Coastal Frontiers Corporation
Co-Program Manager

- 2007 field operations
- Historical overflood limit and strudel scour data integration
- Overflood limit interpretation from satellite images
- Environmental variables assessment
- Facilities access
- Strudel scour potential assessment
- Primary report author

Ken Ambrosius
Aero-Metric, Anchorage
GIS Manager

- Image catalog and metadata development
- Image processing and ArcGIS shapefile generation
- ArcGIS database compilation and management
- Cartographic support

Kim Morris
Geophysical Institute, University of Alaska Fairbanks
Radar Satellite Imagery Lead

- Radar satellite image archive screening and image acquisition
- Radar Satellite image interpretation

Additional Support
Craig Leidersdorf, Coastal Frontiers Corporation – strudel scour potential assessment
Peter Gadd, Coastal Frontiers Corporation – ice road database development
Chris Scott, Coastal Frontiers Corporation – field operations support
Marcy Compton Aero-Metric – GIS manager (former)
Ray Norman, Aero-Metric – GIS support (2007)
Richard Reich, BTS Professional Services – permitting support for 2007 field operations

TABLE OF CONTENTS

APPENDICES

LIST OF FIGURES

LIST OF TABLES

GLOSSARY OF ABBREVIATIONS

ALOS	Advanced Land Observing Satellite (Japan)
ASF	Alaska Satellite Facility (Fairbanks)
AVNIR-2	Advanced Visible and Near Infrared Radiometer type 2 (Japan)
BPXA	British Petroleum Exploration Alaska
ERS 1&2	European Remote Sensing Satellites – 1 and 2
FDD	Freezing Degree Days
GIS	Geographic Information System
Landsat	Series of earth observing satellites 1972 to present (LS-7)
MMS	Minerals Management Service
MODIS	MODerate resolution Imaging Spectroradiometer (NASA)
NASA	National Aeronautics and Space Administration
NOAA	National Oceanic and Atmospheric Administration
NRCS	National Resource Conservation Service
Radarsat	Radar Satellite (Canada)
SPOT	Satellite Pour l'Observation de la Terre (France)
PALSAR	Phased Array type L-band Synthetic Aperture Radar (Japan)
PRISM	Panchromatic Remote-sensing Instrument for Stereo Mapping (Japan)
TDD	Thawing Degree Days
UAF	University of Alaska Fairbanks
USGS	United States Geological Survey
WRCC	Western Regional Climate Center

ABSTRACT

This study was commissioned by the U.S. Department of Interior, Minerals Management Service (MMS), Alaska Outer Continental Shelf Region to map the extent of peak river overflooding onto the landfast ice in the nearshore region of the Alaskan Beaufort Sea during the 13-year period between 1995 and 2007. River overflood on the sea ice occurs annually in the nearshore region of the study area during a brief period in the spring when river break-up precedes the break-up of the landfast sea ice. River overflood constitutes a potential hazard to offshore oil and gas development, as it relates to facilities access, oil spill spreading, and the associated phenomenon of strudel drainage and potential seabed scouring. While the overall goal of this study is to improve the knowledge of the spatial and temporal variability in overflooding and related pipeline and facility siting concerns, the specific study objectives are to 1) document maximum river overflood boundaries from Smith Bay to Camden Bay between 1995 and 2007 using remote sensing and historical helicopter-based surveys, 2) assess and compare different remote sensing platforms for mapping river overflood, 3) investigate environmental factors that contribute to river overflood, 4) assess hazards associated with river overflood, and 5) incorporate the overflood and strudel mapping information into a GIS database.

EXECUTIVE SUMMARY

River overflood on the sea ice occurs annually in the nearshore region of the Beaufort Sea during a brief period in the spring when river break-up precedes the break-up of the landfast ice. Upon arrival at the coast, the river water flows on top of the grounded and floating sea ice, spreading up to 10 km offshore. This brief but energetic phenomenon constitutes a potential hazard to offshore oil and gas development in that it can impede access to facilities, disperse spilled oil, and expose buried subsea pipelines through scouring of the seabed below the landfast ice (strudel scouring).

This study was designed to map the annual extent of peak river overflooding onto the landfast ice of the Alaskan Beaufort Sea during the 13-year period between 1995 and 2007. The study area covers a 430-km stretch of shoreline between Smith Bay on the west and Camden Bay on the east. The Minerals Management Service (MMS) will use the findings for environmental assessment and hazard mitigation for present and future oil and gas facilities that may be located within or adjacent to the areas influenced by the overflood. The specific objectives of the study were as follows:

- Document the maximum river overflood boundaries (peak seaward extent) in the study area using remote sensing and historical helicopter-based survey data;
- Assess and compare the effectiveness of different remote sensing platforms for mapping river overflood;
- Investigate environmental factors that contribute to river overflood; and
- Assess the hazards associated with overflood (primarily strudel scour).

Overflood boundaries have been mapped previously to support oil and gas development on a site specific basis using both helicopter-based surveys and visible satellite imagery. Synthetic Aperture Radar (SAR) satellite imagery has not been used in the past for overflood mapping. The ability to accurately map river overflood boundaries from various remote sensing platforms (both visible and SAR) was evaluated by comparing the results of a 2007 helicopter-based overflood survey off the Colville River Delta with the overflood boundaries mapped from a variety of satellite image platforms.

River overflood on the sea ice is a complex phenomenon that likely is affected by the interaction of multiple variables. An analysis was undertaken to search for correlations between each suspected environmental driving force and overflood area to provide a means of predicting the severity of future overflood events. The correlation between the suspected environmental driving forces also was investigated to determine if one can be used as a proxy for others.

Strudel scouring occurs when the overflood water drains through holes or discontinuities in the sea ice (strudel drains) and impinges on the seabed. The resulting depressions can constitute significant design considerations for subsea pipelines. Strudel drain and strudel scour data obtained from various industry studies were used to provide an indication of the scour potential associated with river overflood.

The study products were incorporated into an ArcGIS database that includes satellite images, interpreted overflood boundaries, strudel drain and scour data, and an inventory of offshore ice roads. The database constitutes one of the study deliverables.

The generosity of BP Exploration (Alaska) Inc. (BPXA), Pioneer Natural Resources Alaska (Pioneer), and Shell Exploration and Production Inc.(Shell) is gratefully acknowledged for providing access to industry overflood mapping and strudel scour data.

Salient findings from the study are summarized below:

1. *Field Survey Program and Satellite Image Validation*: Helicopter-based mapping techniques provide the most accurate depiction of river overflood limits. The helicopter-derived 2007 Colville River overflood boundary was compared to the boundaries mapped using images from three visible spectrum satellite platforms (Landsat 7, SPOT, and MODIS) and two SAR satellite platforms (ERS-2 and Radarsat) to gain an understanding of the accuracy and limitations of various image platforms. Landsat 7, MODIS, and ERS-2 performed equally well among the satellite platforms and provided the most accurate depiction of the overflood limit relative to the helicopter survey. The SPOT and Radarsat imagery provided the least accurate results. The findings suggest that satellite imagery can be used to derive overflood limits that approach the accuracy of helicopter-based results under favorable conditions. However, late in the overflood period and under unfavorable conditions, overflood boundaries derived from satellite-based imagery can differ materially from those derived from helicopter-based mapping. Because the availability of images from multiple satellite platforms in a given year is rare, however, none of the satellite platforms investigated should be excluded from consideration when mapping historical overflood limits.

2. *Historical Overflood Boundary Mapping*: River overflood boundaries were mapped for all major rivers and streams in the study area for the 13-year period between 1995 and 2007 using a combination of historical helicopter surveys and satellite images. Satellite imagery, and particularly radar satellite imagery, formed the key data source needed to develop the final mapped boundaries. To increase the probability of capturing the peak overflood, a maximum composite overflood limit was developed for each watercourse by integrating all of the mapped overflood limits for a given year. When the 11 major river systems in the study are considered, overflood limits were mapped for 129 out of 143 possible river and year combinations, resulting in a mapping success of 90%. This result exceeded expectations, and would not have been possible without having access to both the radar imagery and helicopter surveys.

3. *Correlation of River Overflood with Environmental Variables*: No meaningful correlations were identified between annual overflood areas and the corresponding values of streamflow, precipitation, and temperature. Attempts to correlate streamflow with either precipitation or temperature also proved to be fruitless. The most important implication of these findings is that the extent of river overflood onto the sea ice cannot be predicted by any single environmental variable for which historical data currently

exist. The overflood phenomenon appears to be governed by complex interactions between a number of environmental forces, some of which, such as ice jams in distributary channels, roughness and snow cover on the sea ice, and the density of drainage features on the sea ice, have not been quantified to date.

4. *Hazards Related to Strudel Scours*: Strudel scouring can constitute a significant design consideration for subsea pipelines in nearshore areas adjacent to river and stream mouths. Strudel scour concerns have resulted in the burial of the two existing subsea pipelines in the Alaskan Beaufort Sea (BPXA's Northstar and Pioneer's Oooguruk). In the event that a strudel drain is located directly above a buried subsea pipeline, a sufficiently deep strudel scour may expose the pipeline and lead to an unsupported span. A strudel scour that forms directly over a buried pipeline also can remove the backfill material that is needed to prevent damage from ice keels and forestall upheaval buckling. An additional concern is that strudel drainage provides a potential mechanism to transport spilled oil below the ice sheet.

5. *Strudel Scour Zonation*: Strudel scour frequency and severity can be segregated into zones according to water depth. Strudel scouring typically is most common and severe in the Primary Strudel Zone, which extends offshore from the bottomfast ice edge at approximately 1.5 m to approximately 6 m water depth. In the zone of bottomfast ice (the "Secondary Strudel Zone") and offshore of the Primary Zone (the "Tertiary Strudel Zone"), scouring tends to be more modest and occur less frequently. When the major rivers in this region were considered, the Secondary Strudel Zone accounted for the greatest portion of the overflood area in any given year. On average, this zone encompassed 66% of the total average overflood area. The Primary Strudel Zone accounted for 32% of the total average overflood area, while the Tertiary Zone accounted for a mere 2%. Strudel zone information should be used to assess the risk to prospective pipeline routes posed by strudel scouring in different coastal areas.

6. *Strudel Scour Pipeline Encounter Frequency*: A case study of strudel scours in the vicinity of the BPXA Northstar Development suggests that the presence of the operational pipeline materially altered the scour regime, and has led to a substantially higher than expected scour encounter frequency with the pipelines. This phenomena is most prominent in the Secondary Zone, and is believed to be attributable to radiant heat from the pipelines propagating through the backfill and degrading the overlying ice cover. While less pronounced, a statistical analysis of strudel occurrence also indicates an increased encounter frequency in the Primary Zone. Radiant heat from the pipelines also may explain the high encounter frequency in this zone. However, it is not known whether the impact is direct (degradation of the ice sheet), indirect (increased biological activity in the warmer water), or a combination of the two. Because scouring is more severe in the Primary Zone, the potential consequences of scour depressions forming over the pipelines are greater in this zone than in the Secondary Zone.

7. *Hazards Related to Facilities Access*: Rapid deterioration of the ice sheet can render ice roads impassable within the zone of river overflood, impacting both facilities access and oil spill response.

1 INTRODUCTION

This study was designed to map the extent of peak river overflooding onto the landfast ice in the nearshore region of the Alaskan Beaufort Sea during the 13-year period between 1995 and 2007. The findings will be used by the MMS for environmental assessment and hazard mitigation for present and future oil and gas facilities that may be located within or adjacent to the areas influenced by the overflood.

River overflood on the sea ice occurs annually in the nearshore region of the Beaufort Sea during a brief period in the spring when river break-up precedes the break-up of the landfast sea ice. Upon arrival at the coast, the river water flows on top of the grounded and floating sea ice, spreading up to 10 km offshore. This brief but energetic phenomenon constitutes a potential hazard to offshore oil and gas development in that it can impede access to facilities, disperse spilled oil, and expose buried subsea pipelines through strudel scouring.

The study area covers a 430 km stretch of shoreline between Smith Bay on the west and Camden Bay on the east (Figure 1-1). Located at the northern extremity of the Arctic Coastal Plain province, this area is part of the North Slope physiographic unit. The region is characterized by a gently sloping tundra-covered plain extending from the foothills of the Brooks Range to the Beaufort Sea. The coastal plain consists of alluvial and glacial sediments overlying continuous permafrost (TAPS, 2001). Numerous drainage basins discharge to the Beaufort sea, ranging from large rivers to small creeks and streams. Figures 1-2 and 1-3 show all of the coastal drainages considered in the study, while the major rivers are listed in Table 1-1.

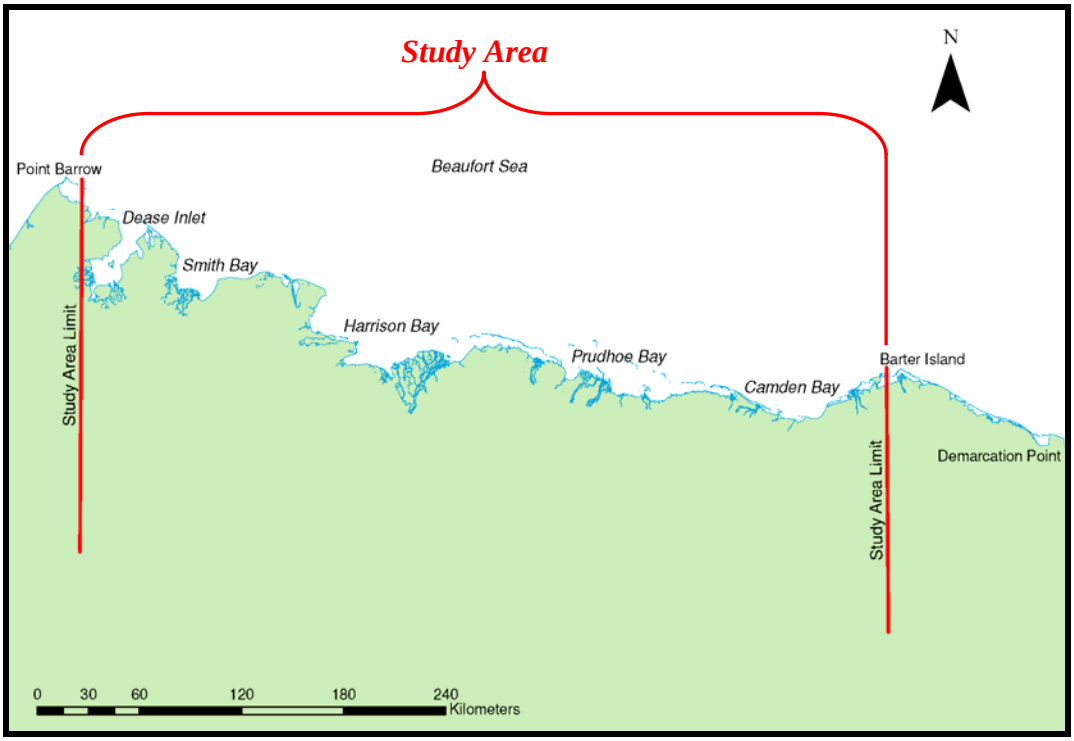

Figure 1-1. Project Location Map

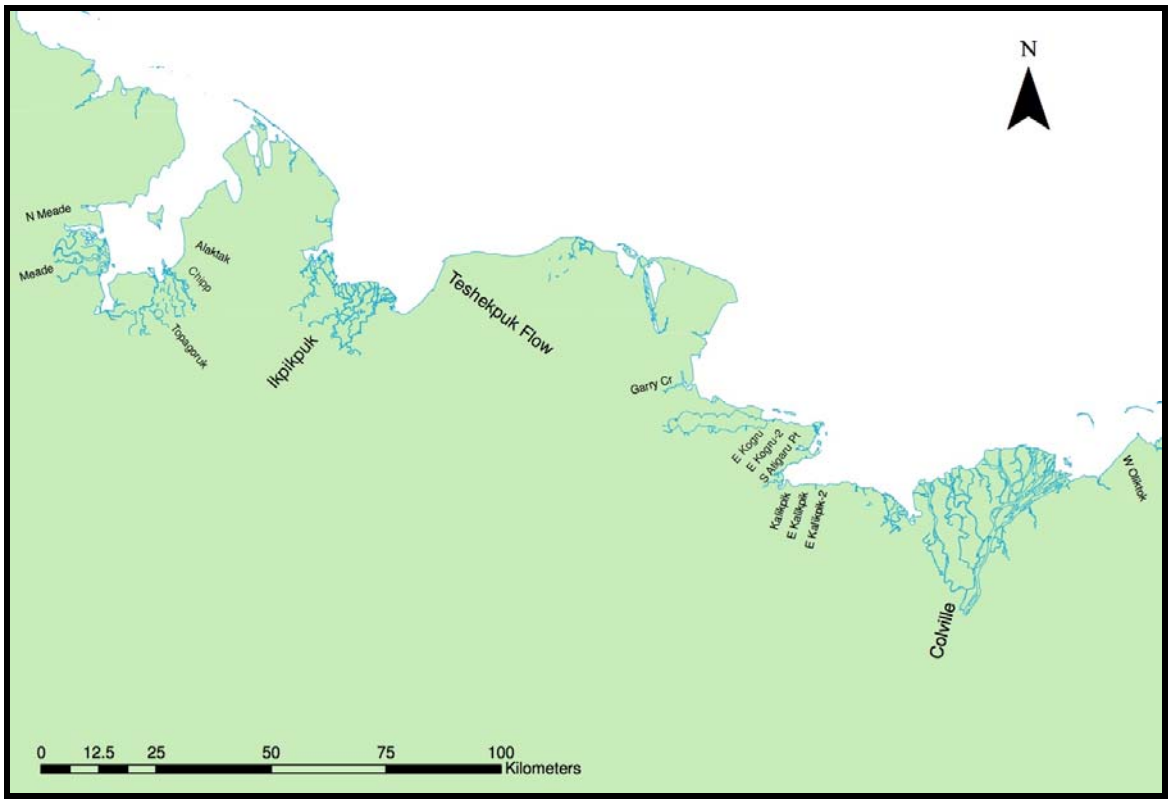

Figure 1-2. Western Study Region

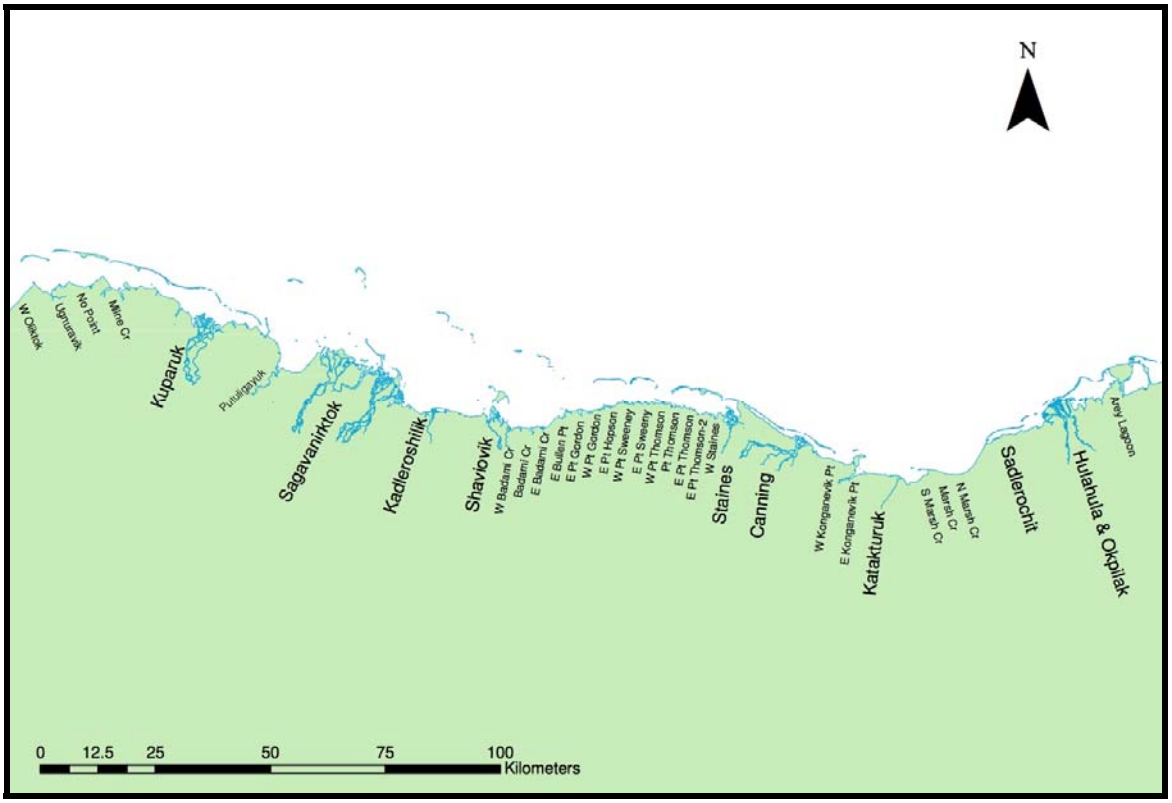

Figure 1-3. Eastern Study Region

Table 1-1. Main Rivers Discharging into Alaskan Beaufort Sea

River	LOCATION (approximate)
Topagoruk River	70°45'24"N, 155°55'35"W
Ikpikpuk River	70°49'25"N, 154°18'09"W
Teshekpuk Lake outflow near Lonely	70°54'38"N, 153°14'31"W
Colville River	70°23'02"N, 150°48'24"W
Kuparuk River	70°24'42"N, 148°52'38"W
Sagavanirktok River	70°16'39"N, 147°59'55"W
Kadleroshilik River	70°12'23"N, 147°37'00"W
Shaviovik River	69°40'19"N, 147°45'41"W
Staines River	70°08'17"N, 145°59'57"W
Canning River	70°04'42"N, 145°33'56"W
Katakturuk River	69°58'33'N, 144°59'51"W
Sadlerochit River	70°01'22"N, 144°26'08"W
Hulahula River	70°03'54"N, 144°04'57"W
Okpilak River	70°04'40"N, 144°03'09"W

As indicated earlier, the general objective of the study is to map river overflooding. The specific objectives are as follows:

1. Document the maximum river overflood boundaries (peak seaward extent) from Smith Bay to Camden Bay between 1995 and 2007 using remote sensing and historical helicopter-based surveys;
2. Assess and compare the effectiveness of different remote sensing platforms for mapping river overflood;
3. Investigate environmental factors that contribute to river overflood;
4. Assess the hazards associated with overflood (primarily strudel scour); and
5. Incorporate the overflood and strudel mapping information into a GIS database.

Overflood boundaries have been mapped using helicopter-based surveys on numerous prior occasions to support oil and gas development. While visible satellite imagery also has been used to document overflood limits, radar satellite imagery has not been used extensively prior to this study. Furthermore, the accuracy of remote sensing methods has not been assessed.

The ability to accurately map river overflood boundaries from various remote sensing platforms was evaluated in this study by comparing the results of a 2007 helicopter-based overflood survey of the Colville River with the overflood limits mapped from a variety of satellite image products.

River overflood is a complex phenomenon that is governed by a number of environmental influences. Correlations between environmental variables and overflood extent were investigated to determine if such variables can be used to predict the magnitude of the overflood in a given year, and to understand how climate change might influence overflood in

the future. The primary factors considered consisted of streamflow, precipitation, and air temperature during breakup.

As indicated at the outset, river overflood can impact nearshore facilities by impeding access via ice roads, dispersing spilled oil and hampering clean-up efforts, and exposing and even undermining buried subsea pipelines. Of particular concern is the phenomenon of strudel scouring, which represents a major design consideration for subsea pipelines. Strudel drain and strudel scour data obtained from various industry studies were used to provide an indication of the scour potential associated with river overflood.

The study products were incorporated into an ArcGIS database that includes satellite images, interpreted overflood boundaries, strudel drain and scour data, and an inventory of offshore ice roads. The database constitutes one of the study deliverables.

This report presents a detailed account of the overflood mapping study. Section 2 provides an overview of the river overflood phenomenon, including a summary of previous research. Overflood mapping methods are described in Section 3. The 2007 field study of the Colville River overflood and satellite image validation is discussed in Section 4, while Section 5 describes the historical overflood mapping results. Section 6 discusses the influence of environmental variables on river overflood. The facilities hazards associated with overflood are assessed in Section 7. Key conclusions are summarized in Section 8, followed by references in Section 7. Figures and tables are interspersed with the text. The bibliographic database and map products are provided in Appendices A through G.

2 BACKGROUND AND STATE OF KNOWLEDGE

Overflooding of fresh water onto sea ice from rivers draining into the Alaskan Beaufort Sea is a dramatic natural phenomenon on a grand scale, clearly visible by satellite or from the Space Shuttle. Figure 2-1 is a Defense Meteorological Satellite Program (DMSP) image (600-m resolution) acquired May 29, 1980 that shows discharge onto the sea ice from all of the major rivers between the Colville Delta on the west and the Mackenzie Delta in the Canadian Northwest Territories.

Figure 2-1. Satellite Image from May 29, 1980 Showing All Major Rivers in Overflood
Source: DF Dickins internal satellite archive – original DMSP photographic image from NSIDC.

Walker (1974) describes key features of the overflood process using the Colville River as an example. This river generates by far the largest fresh water discharge volume into the Alaskan Beaufort Sea and gives rise to the largest peak overflood area. The rapid buildup in stream flow before the river mouth is free of ice leaves the water no other pathway but to flow seawards on top of the ice. Once the river stage rises sufficiently, river ice in the deeper channels fractures and lifts off the seabed on the rising flood. The sea ice overflood builds in area and in seaward extent over a ten to twenty-day period. As defined by Walker, the so-called "pre break-up" flooding continues until the river ice begins to move downstream. This period can be very short, lasting less than 2 days. Most of the initial floodwater moves out rapidly from the delta front over the nearshore bottomfast sea ice.

> *Note: Delta Front - The sloping portion of a delta, developed offshore from the bar at the mouth of the river and passing at its toe into the pro-delta. Delta fronts are the site of active, and often rapid, sedimentation.*

While each river system has its own unique characteristics depending on the geometry of channels feeding the delta and flow characteristics, the general pattern of overflood stages is

repeated at other drainages along the entire Alaskan Beaufort Sea Coast within a relatively short time window of a few weeks or less.

The overflood layer can reach a depth of 1.5 m in places on top of the ice however, depths of 0.6 to 0.9 m are considered more typical (Vaudrey 1984, 1985, 1986). In deeper water (typically over 2 m) seaward of the bottomfast ice boundary, for a week to ten days following peak water depths on the ice, the overflood waters drain through holes and discontinuities in the ice sheet such as tidal, thermal and stress cracks, and seal breathing holes. Once the floating offshore ice drains, the remaining bottomfast ice may remain in a flooded state for a brief period of time before the grounded ice separates from the seabed and floats free in large broken floes.

As the overflood drains through the ice, powerful strudel jets in areas with high drainage rates can create strudel scours in the sea floor. These sea floor craters were documented in US Geological Survey investigations off the North Slope in the 1970's (*e.g.*, Reimnitz, *et al*., 1974; Reimnitz and Kempema, 1982). The processes of strudel drainage and sea floor scouring tend to be more severe in the floating fast ice zone than the bottomfast zone (Leidersdorf, *et al*., 2007).

Strudel scours can constitute significant design considerations for subsea pipelines in cold regions (Lanan, *et al*., 2008). In the event that a strudel drain is located directly above a buried subsea pipeline, a sufficiently deep strudel scour may expose the pipeline and lead to an unsupported span. A strudel scour that forms directly over a buried pipeline also removes backfill material that is needed to help prevent upheaval buckling and protect against ice keels. Chapter 6 discusses the strudel drain and scour processes and related databases in greater detail.

An additional concern is that strudel drainage may provide a pathway to transport an oil spill below the ice sheet. This topic is introduced in Section 7.2. Refer to Dickins and Owens (2002) for a more in-depth discussion of this topic.

In order to provide historical context for the current study, the following sections summarize the findings of previous investigations concerned with the river overflood phenomenon.

2.1 Early Studies (1970-1980)

The early 1970's saw the first use of relatively high-resolution (100 m) Landsat imagery to document the overflood boundaries for some rivers in the study area, but this record was limited by cloud cover and the long orbit repeat cycle of the satellites (16 to 18 days). Much of the original documentation of river overflood in the Prudhoe Bay area was generated through field studies carried out by the US Geological Survey, the University of Alaska and NOAA (See example in Figure 2-2).

In one of the earliest published papers dealing specifically with overflood in Alaska, Barnes and Reimnitz (1974) describe the phenomenon and provide a sequence of consecutive Landsat images acquired on May 24, 26 & 27, 1973. The authors state that flooding of the Sagavanirktok Delta started May 23 and reached a maximum on May 28. From the image sequence shown in the paper, it appears that the over-ice flooding peaked on May 26. Twenty-four hours later, the next image shows signs of drainage and a reduction in the flooded ice area.

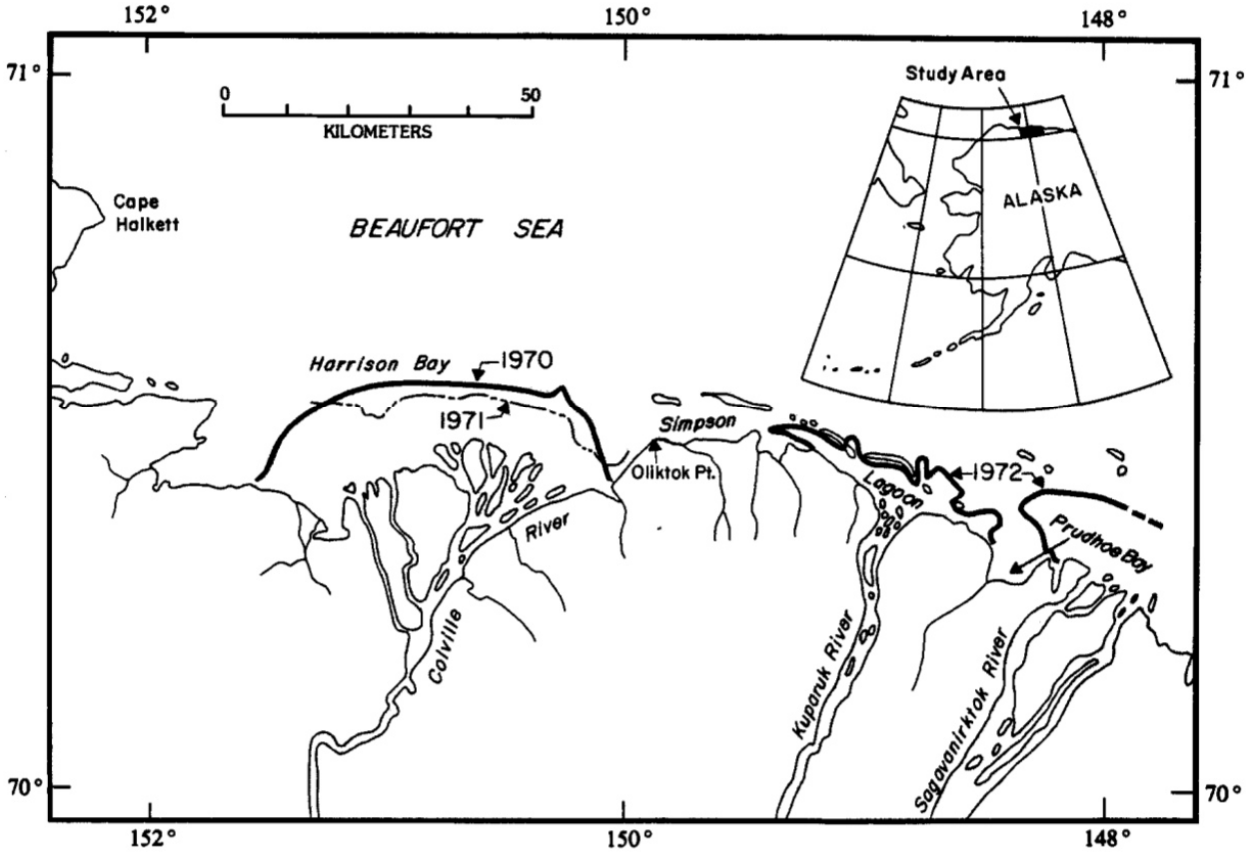

Figure 2-2. Areas of River Flooding onto Sea Ice 1970-72
(published in Labelle and Wise, 1983, based on Reimnitz, *et al*., 1974)

A map in Reimnitz, *et al*. (1974) shows overflood limits in 1970 and 1971 for the Colville River, and in 1972 for the Kuparuk and western delta of the Sagavanirktok River. Reimnitz and Kempema (1982) also reported on the results of surveys of specific strudel scour depressions at the mouths of the Kuparuk and Sagavanirktok Rivers.

Barry, *et al*. (1979), report the average river overflooding date for the central Alaskan Beaufort Coast as May 25 (based on Landsat imagery from 1973 through 1977). Barry cites Carlson (1977) as reporting that the area of flooded ice off the mouth of the Sagavanirktok River in 1975 was 208 km^2. A similar area was reported in 1974, although the extent of the overflood at other rivers was greatly reduced that year. The areas of overflood mapped in the unusually clear June 6, 1976 image were calculated by Reimnitz as only about 101 km^2 for both the Sagavanirktok and the Colville Rivers. On this basis, the 1974 and 1975 overflood areas appear to represent close to the maximum historical values from published sources at the time.

The potential for flooding off the Colville River is dramatic. For example, in 1971, 404 km^2 of the delta, and 630 km^2 of the sea ice were estimated to be flooded (Walker, 1974). In a typical year, the overflood waters reach an average distance of 10 to 12 km off the delta front, but there is evidence of the overflood front extending out to as much as 18 km (Carlson, 1977). Figure 2-3 shows the extent of the overflood from the Colville River mapped by a helicopter survey on June 2, 1985.

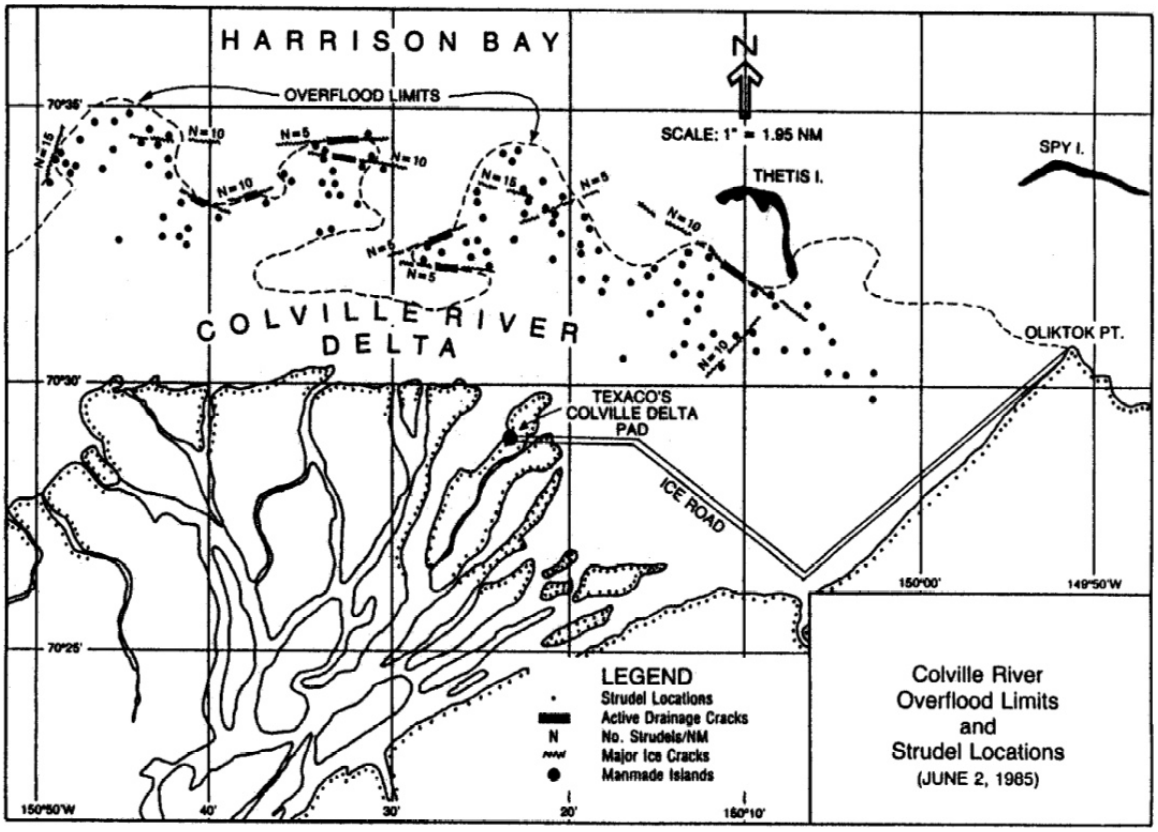

Figure 2-3. Colville Overflood Limits for 1985 Mapped by Vaudrey (1986)

Table 2-1, developed by Carlson from the relatively low-resolution NOAA imagery, shows areas of flooded ice in 1974 and 1975 for the Kuparuk, Sagavanirktok and Colville Rivers. Although the trends in overflood area with time are probably correct, absolute values must be considered approximate, given the limitations of the imagery.

Table 2-1. Historical Estimates of Flooded Ice Areas

	Estimated Overflood Area (km ^{2})		
Date	**Kuparuk River**	**Sagavanirktok R.**	**Colville River**
21 May 1974	No Data	61	15
26 May 1974	10	151	50
4 Jun 1974	30	185	61
6 June 1974	30	40	120
4 June 1975	101	208	219
9 June 1975	69	179	276

Source: Carlson, 1977

2.2 Historical Industry Studies

This section summarizes a number of industry-sponsored projects beginning in the early 1980's that mapped the peak overflood extent and strudel drain locations for specific rivers based on a combination of helicopter surveys and visible satellite interpretations. Additional details regarding the available airborne survey data sponsored by different companies are provided in Sections 5 and 7.

The early overflood studies undertaken by the petroleum industry tended to focus on two main areas:

1. Off the Sagavanirktok River Delta and Stefansson Sound to the east, associated with the Endicott Development and proposals to develop the Liberty Prospect in Foggy Island Bay.
2. Within Simpson Lagoon from Oliktok Point to West Dock, associated with the impact of Kuparuk River overflood on the Northstar pipeline corridor.

In some of the original helicopter overflood surveys carried out without the benefit of GPS navigation, Vaudrey & Associates (1984, 1985, and 1986) mapped the overflood limits of the Sagavanirktok River and adjacent rivers to the east in 1983, 1984 and 1985. Figure 2-4 reproduces a map developed by Vaudrey (in Dickins, *et al*., 2001) to show the typical maximum overflood boundaries from the Kuparuk and Sagavanirktok Rivers based on a limited number of annual observations in the 1980's.

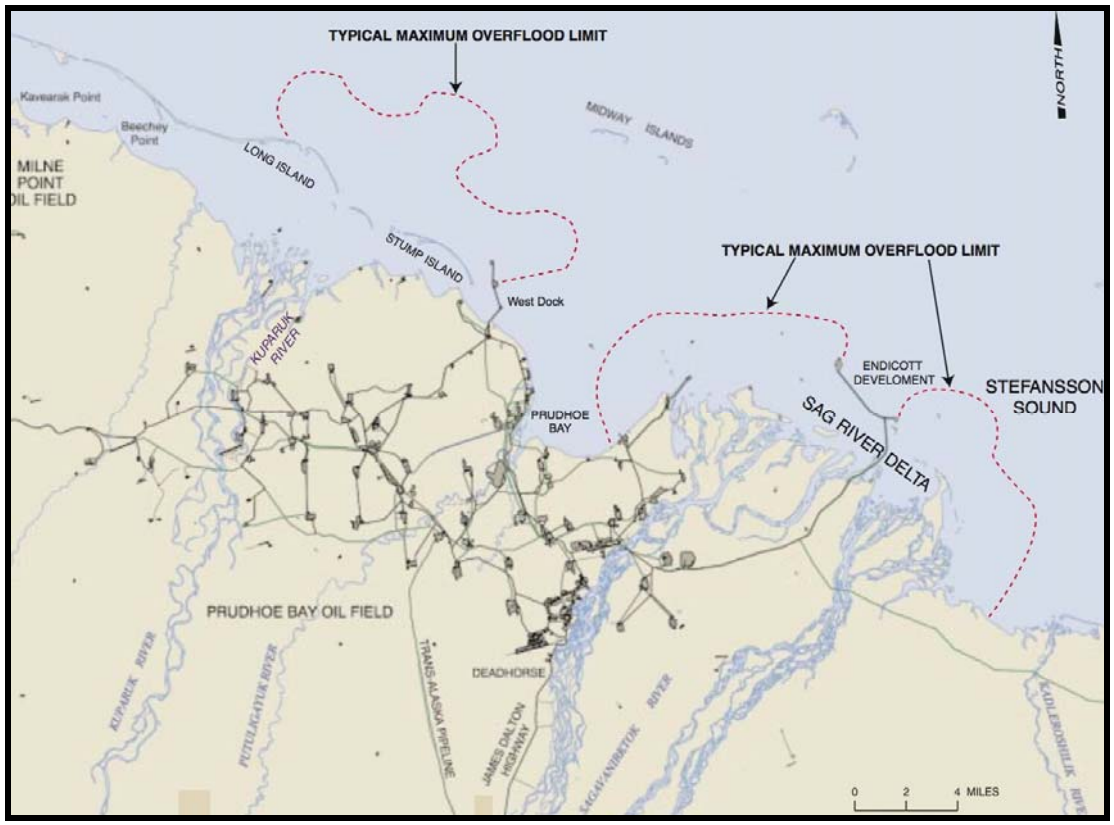

Figure 2-4. Typical Maximum Overflood Limits from the Kuparuk and Sag Rivers (from Vaudrey in Dickins, *et al*., 2001)

Dickins, *et al*. (2001) summarized findings from an original study conducted by DF Dickins, *et al*. (1999) as part of BP Exploration's Liberty Development pipeline project. The purpose of that study was to delineate the seaward limits of sea ice overflood originating mainly from the Sagavanirktok River but also from the Shaviovik and Kadleroshilik Rivers. The primary data source was historical Landsat imagery, supplemented by available helicopter survey observations. Figure 2-5 shows an example of overflood boundaries interpreted from a Landsat image of June 3, 1980 at 100-m resolution. All of the rivers shown were close to full flood at the time the image was acquired, and the seaward boundaries approach the maximum historical limits of overflood extent observed over the 11 years when data were available for the Sagavanirktok River (up to 1999).

During the past five years, area-specific studies have examined the overflood off the Colville River on behalf of Pioneer's Oooguruk Project (Coastal Frontiers, 2006b; 2007b) and off the Staines and Canning Rivers in planning for possible future pipeline routes to service Shell's Sivulliq Prospect (Coastal Frontiers, 2007c; 2008b). In Canada, federal government studies recently have focused on the break-up patterns within the Mackenzie Delta, including documentation of overflood and extent of bottomfast ice using radar imagery (Solomon 2006, 2007, 2008).

A recent study funded by the Alaska Department of Environmental Conservation (ADEC) used all available visible imagery (Landsat and MODIS) in documenting patterns of ice clearing along the entire Alaskan Beaufort Sea Coast. Particular attention was paid to evaluating the influence of overflood on the timing of nearshore break-up, but a number of cases used selected Landsat images to demonstrate the peak overflood extent in different areas (Dickins and Oasis, 2006). For example, Figure 2-6 shows an exceptionally clear Landsat 4 scene depicting conditions an estimated 48 hours after significant overflood drainage based on the timing of overflood milestone events for that year tabulated in Atwater (1991). The dark areas on the image include a mix of still-flooded ice and drained ice with sediment deposited by the overflood.

Although too small to show on most historical satellite images, localized areas of overflooding have been observed at the mouths of numerous creeks that drain small sections of the Arctic Coastal Plain. Not all of these streams or creeks will have sufficient discharge to flood the coastal sea ice, but some could produce periodic (not necessarily annual) local overflooding.

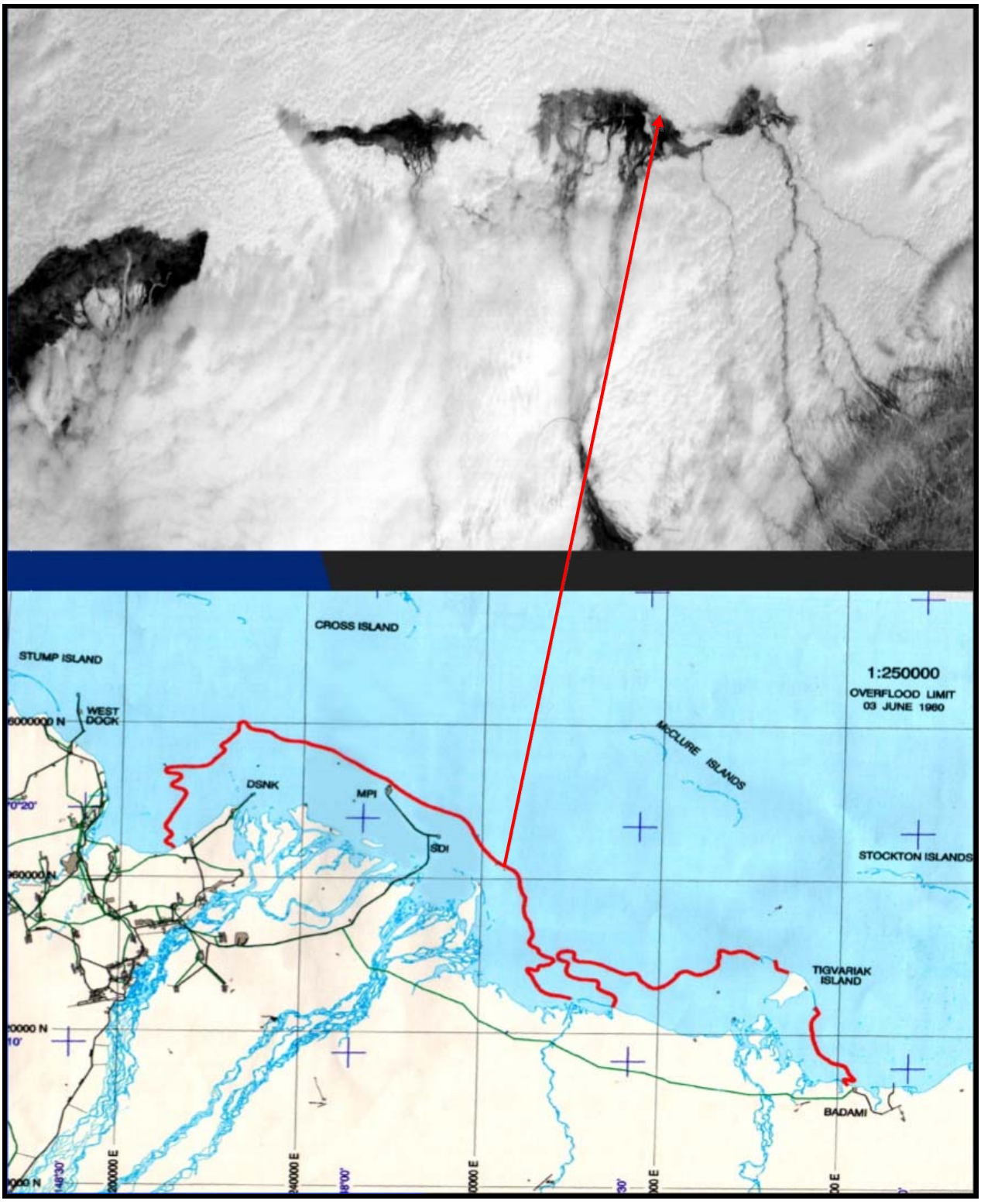

Figure 2-5. Overflood Limits for the Stefansson Sound Area on June 3, 1980

Note: The flooding river channels are clearly visible through a thin overcast sky condition. Heavier cloud cover often obliterates surface details in Landsat and prevents the development of a consistent long-term database relying on visible imagery alone. Source: Dickins, *et al.*, 2001

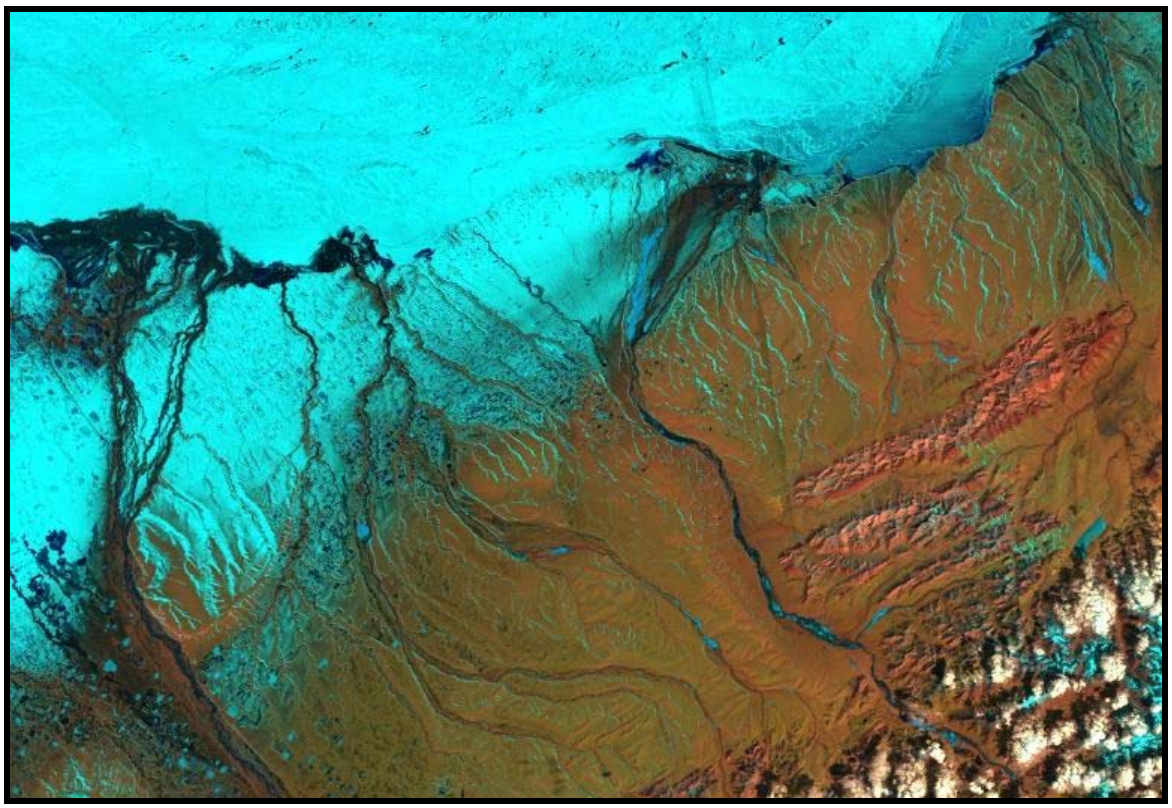

Figure 2-6. Landsat 4 scene from June 13, 1986 showing Close-to-Peak Overflood
Note: This image spans the coastal section from Prudhoe Bay (far left) to the Hulahula River (far right).

3 OVERFLOOD MAPPING METHODS

The overflood boundary database developed for this study was derived from a combination of historical helicopter-based surveys and satellite image mapping. Overflood boundaries have been mapped using helicopter-based surveys on numerous prior occasions to support oil and gas development. Visible satellite imagery also has been used to document river overflood, however, radar satellite imagery has not been used extensively prior to this study. This section describes the methods used to map overflood boundaries with helicopter surveys and from satellite images.

3.1 Helicopter-Based Overflood Surveys

Overflood boundaries derived from helicopter surveys performed during the 1995 to 2007 study period were obtained from industry studies conducted on behalf of BPXA's Northstar and Liberty Developments, Pioneer's Oooguruk Development, and Shell's Sivulliq Prospect (Coastal Frontiers, 1997, 1998a, 1998b, 1999a, 1999b, 2000a, 2000b, 2001a, 2002, 2003a, 2003b, 2004, 2005, 2006a, 2006b, 2007a, 2007b, 2007c, 2008a, 2008b). In each case, the study objectives included mapping river overflood boundaries in the vicinity of proposed or existing subsea pipelines. While the mapping methods have been refined during the past decade, the general approach was similar for each of the surveys.

The helicopter missions were conducted at the end of the overflood period rather than at its peak to insure that the maximum extent of the flood was documented. Prior to mobilizing for the surveys, several sources are consulted to assess the stage of overflood development. The United States Geological Survey (USGS) streamflow gauges located on the Colville, Kuparuk, and Sagavanirktok Rivers provide a quantitative indication of break-up. Based on past experience, overflood onto the sea ice typically occurs several days after the peak discharge is recorded at these streamflow stations. Several North Slope resources also are queried as break-up approaches. Observations of flood waters at the Sagavanirktok River Bridge and closure of the Kuparuk River Bridge (both located near Deadhorse, AK) are obtained from FR Bell and Associates. Past experience suggests that the overflood from these rivers typically reaches its maximum extent within one to two weeks of the flood waters reaching the respective bridges. Observations from personnel associated with the BPXA Northstar Development (located offshore of the Kuparuk River Delta), the ConocoPhilips Alpine Development (located within the Colville River Delta), and Pioneer's Oooguruk Development (located offshore of the Colville River Delta) also provide insight into the appropriate time to map the river overflood boundaries.

Mapping was performed using a survey-grade GPS unit operated from a helicopter. The GPS antennae typically was installed in an overhead window of the aircraft. In recent years, the GPS unit was interfaced to a laptop computer using navigation software which displays a map of the region to allow the survey crew to view the aircraft's position relative to coastal landmarks in real-time. Prior to 2004, the surveys were conducted with the GPS unit operated in autonomous mode, resulting in a position accuracy of approximately 100 m. In 2000, the U.S. Government discontinued Selective Availability, thereby increasing the accuracy of autonomous positions to approximately 7 m (Milbert, 2001). Commencing in 2004, differential corrections broadcast in real time via the Wide Area Augmentation System (WAAS) were used. Equipment

manufacturers Trimble and Magellan report an accuracy of 1 to 3 m for WAAS corrected positions in the Continental U.S. (Lewis, 2001; Magellan, 2001). The higher accuracy attainable with site-specific differential corrections (DGPS) was judged to be unwarranted, due to the imprecision inherent in mapping features on the ice from a helicopter hovering overhead.

The offshore boundary of the river overflood on the sea ice was delineated by recording successive positions with the GPS unit while flying over the observed boundary at typical altitudes of 30 to 200 m, and at a speed of approximately 60 knots. Although mapping often was conducted after the overflood waters have started to drain or retreat, evidence of the seaward extent of the overflood limit typically was readily identifiable. The overflooded area typically was characterized by sediment-laden water or discolored ice on the inshore side of the boundary. Evidence of strudel drainage also was frequently apparent inside the overflood boundary. In contrast, the ice offshore of the boundary generally was a pristine white or blue color with areas of snow cover. Figure 3-1 shows a well defined overflood boundary off of the Kuparuk River.

In cases where the overflood limit was difficult to discern during the initial flight path, additional mapping was conducted from the opposite direction or at different altitudes. Approaching from an alternate direction often provides a different perspective, particularly reflection off of the ice during sunny conditions. Higher altitudes provide a broader view of the overflood area, while lower altitudes allow detailed investigation of features such as strudel drains and sediment-laden ice. On occasions when the boundary was mapped multiple times, a single merged boundary was created based on field notes and observations (including mapping confidence and flight precision).

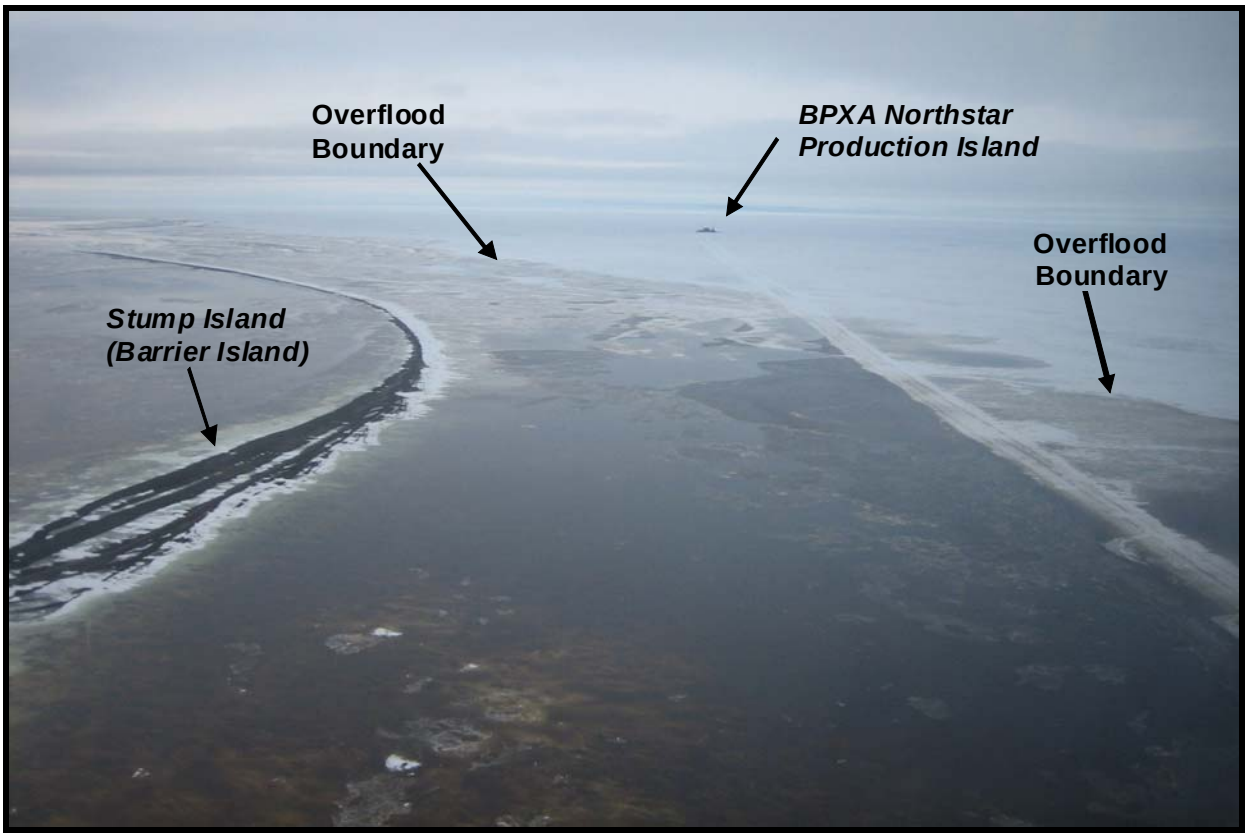

Figure 3-1. Overflood Boundary on Eastern Portion of Kuparuk River Delta, 2006

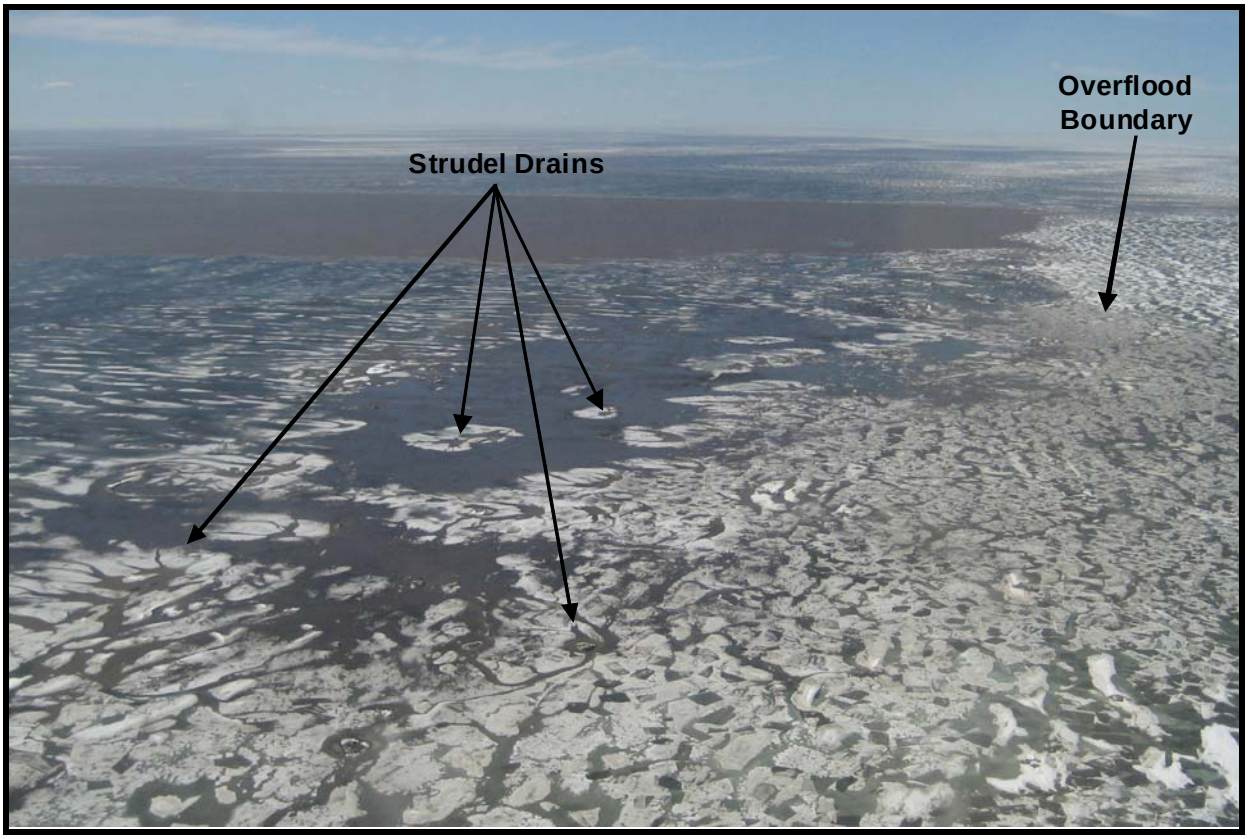

Figure 3-2. Evidence of Strudel Drainage within Colville River Overflood Boundary, 2007

3.2 Satellite Image-Based Overflood Mapping

This section discusses the steps taken to search the available archives for all imagery between 1995 and 2007 with the potential to capture the peak overflood extent, screen-browse the selected imagery to eliminate scenes that clearly miss the timing of peak overflood, acquire images that have a moderate to high probability of showing the peak overflood, and map images that actually capture the peak overflood seaward boundary. Through this process, the number of useable images was steadily reduced from hundreds at the initial search stage to the final number of 64 images actually mapped (Appendix F). As discussed below, radar satellite imagery was adopted as the primary satellite mapping tool due to the limitations inherent with satellites relying upon the visible spectrum. Accordingly, this section provides additional details and a case study specific to the family of SAR satellites.

3.2.1 Available Satellite Platforms

A limited number of historical satellite platforms provide an archive of useful images that can be used to document peak overflood. The satellite platforms and their onboard sensors are highlighted below. Further specifications and descriptions are provided in Appendix G.

NOAA/DMSP: The NOAA satellites provide visual and infrared coverage, with multiple daily passes dating back to the early 1970's. Most of these images are available with a

resolution of approximately 2 km, considered inadequate (by current standards) for accurate mapping of the overflood boundary. In addition, the Defense Meteorological Satellite Program (DMSP) provides slightly better quality images (down to 600 m resolution) dating back to 1973. A representative older DMSP image is provided in Figure 2-1. This study made no attempt to use NOAA Advanced Very High Resolution Radiometer (AVHRR) or DMSP imagery, focusing instead on higher-resolution products offered by other visible-spectrum and radar satellites (see below). *Note: NOAA's definition of "High Resolution" is relative to other satellite capabilities common in the 1970's and is misleading now when compared with present generation of sensors.*

SAR imagery from Radar Satellites: The original group of commercially-available radar satellites included Japan's JERS-1, Europe's ERS-1 and 2, and Canada's Radarsat 1 launched in the late 1990's. Of these, only the Canadian satellite was designed as a true commercial system with frequent repeat cycles and incidence angles optimized for ice mapping. Depending on the swath width, ground resolutions down to 8-12 m were possible with these first-generation systems. The latest generation of radar satellites, launched in late 2007 by Canada, Italy, Germany and Japan (Radarsat-2, CosmoSkymed, TeraSAR-X and ALOS), can deliver much finer resolution (down to 1 meter) at the expense of coverage area and cost. Desired scenes must be programmed and ordered in advance, and there is no database of routinely-archived products.

Landsat: This satellite series (1 through 7) provides the only cost-effective source of high-resolution imagery with a comprehensive historical archive for Alaska (dating back to 1972). Ground resolution has improved from 80 to 100 m for the earlier satellites (LS 1-5) to 12 m for the latest Landsat 7 in panchromatic band. The primary drawback of Landsat (and other visible-spectrum satellites) is the need for minimal cloud cover at the time when the satellite orbits over the target area. With coverage over a given ground target repeated only every 16 to 18 days, a search over 20 years or more can result in a very small number of useable overflood scenes.

SPOT: The Satellite Earth Observation System was designed in France, and developed with the participation of Sweden and Belgium. The SPOT satellites capture panchromatic and multispectral imagery in resolutions ranging from 2.5 to 20 m. SPOT satellites can be programmed to target client-specific areas of interest Two satellites are currently operational with imagery available by advance order only (no archives). SPOT 5 was launched on May 4, 2002 with 2.5-, 5-, and 10-m capability, as well as along-track stereoscopic sensors. *Note: There is no historical archive of SPOT images for the study area. SPOT was only used in this study to document the 2007 Colville overflood.*

NASA MODIS (Aqua and Terra): The MODIS system consists of two visible band satellites acquiring daily imagery at 250-m resolution. Although theoretically available since 1999, only scenes from 2004 on are readily accessible in a convenient browsable archive. Scenes are available for earlier years through the ASF Gina search routine, but the identification of useable images is very time-consuming. The most user-friendly link to browse daily MODIS images of the study area is:
http://rapidfire.sci.gsfc.nasa.gov/subsets/?AERONET_Barrow/

Other commercial satellites can provide custom-order visual imagery at much higher resolution than that of historical Landsat scenes, but at much higher cost, for example: Russian SPIN-2 (2 to 10 m), Indian IRS (5 m) and the IKONOS system (1 m). All of these satellites require pre-booking for specific dates, and there are no historical archives. ALOS is a new multi-sensor satellite from Japan that combines radar and visible sensors. Availability is limited at present to the scientific research community.

3.2.2 Image Search, Screening and Acquisition

For this study, only three satellite systems had historical archives of images with sufficient temporal coverage to serve as a potential primary data source:

- Radarsat-1 in Standard Beam and ScanSAR mode (available only through ASF)
- ERS-1 and 2 (available only through ASF to approved researchers)
- NASA MODIS (available to the general public)

In addition, three publicly available USGS Landsat products provided an additional potential source of high-resolution images:

- Landsat 4 and 5 TM (Thematic Mapper) Jul 82 to present, 30-m spatial resolution
- Landsat 7 ETM (Enhanced Thematic Mapper) available from June 1999 to May 2003 at 15-m resolution (Panchromatic band)
- Landsat 7 ETM (SLC Off Mode) from July 2003 to present*

**Note:* Due to a satellite malfunction in 2003, LS7 scenes suffer from data gaps and although sold "as is", are still useable for mapping purposes.*

In searching the NASA MODIS and USGS Landsat archives, it quickly became apparent that visible images alone could never provide the basis for a consistent overflood database either temporally or spatially. The Landsat images have a 16-day repeat cycle and cover an area approximately 170 x 183 km. At the latitude of the study area there is sufficient east/west overlap between scenes that a location is theoretically observable on three consecutive days. In practice, however, only a very small percentage (generally 10 to 20%) of all scenes acquired have sufficiently low cloud cover to be useable (based on a cloud threshold of 30% from past experience). As a result, the availability of predominantly cloud-free scenes that happen to match the timing of the overflood becomes close to coincidental. The MODIS image gallery, in spite of providing daily coverage, still misses too many of the peak overflood windows to provide a consistent record, again due to the problem of persistent cloud cover often lasting for ten days or more in May and June.

As a result of the limitations inherent with any satellite that uses the visible spectrum, the SAR imagery was adopted as the primary satellite mapping data source, supplemented by Landsat 7 imagery where available. Given its relatively low resolution of 250 m, MODIS was used sparingly only to fill in a few data gaps where higher-resolution imagery was unavailable.

A series of steps was required to move from searching available archives to screening browse scenes and finally to ordering the full data files. First, historical industry observations of the Kuparuk and Sagavanirktok break-up dates (FR Bell and Associates, 2007) were used together with an earlier spatial analysis of overflood trends between different river systems (Atwater, 1991) to develop conservative overflood time windows as an aid in searching satellite archives for useful historical imagery (Table 3-1). Three different archives were then searched to identify images falling within the likely time windows shown in Table 3-1:

- USGS Earth Explorer for Landsat 5TM and/or Landsat 7
- NASA Rapid Response Gallery (Aeronet Barrow) for MODIS (Aqua or Terra)
- Alaska Satellite Facility for ERS 1&*2* and Radarsat

Table 3-1. Estimated Overflood Windows Used to Guide the Satellite Searches

	Colville		Kuparuk		Sag		Canning	
Year	Start	Stop	Start	Stop	Start	Stop	Start	Stop
1995	13-May	26-May	13-May	25-May	10-May	26-May	13-May	26-May
1996	21-May	2-Jun	25-May	2-Jun	26-May	7-Jun	21-May	2-Jun
1997	19-May	31-May	22-May	1-Jun	17-May	30-May	19-May	31-May
1998	16-May	28-May	20-May	1-Jun	20-May	1-Jun	16-May	28-May
1999	22-May	3-Jun	26-May	3-Jun	27-May	8-Jun	22-May	3-Jun
2000	5-Jun	17-Jun	10-Jun	18-Jun	2-Jun	14-Jun	5-Jun	17-Jun
2001	4-Jun	16-Jun	7-Jun	15-Jun	3-Jun	15-Jun	4-Jun	16-Jun
2002	19-May	1-Jun	23-May	1-Jun	21-May	2-Jun	19-May	1-Jun
2003	30-May	11-Jun	2-Jun	10-Jun	1-Jun	13-Jun	30-May	11-Jun
2004	21-May	2-Jun	25-May	2-Jun	18-May	30-May	21-May	2-Jun
2005	20-May	1-Jun	24-May	1-Jun	14-May	28-May	20-May	1-Jun
2006	24-May	5-Jun	28-May	3-Jun	18-May	30-May	24-May	5-Jun

***Note**: Dates presented here were used only as a conservative guide to times when the imagery was most likely to show some stage of overflood. In practice, extensive overflood from any given river usually persists for a much smaller duration than the periods shown in the table.*

The final optimal suite of SAR images (ERS 1&2 and Radarsat) was assembled by restricting the geographic areas and time periods of interest. Using these criteria, a list of candidate images was developed by searching the Alaska Satellite Facility (ASF) SAR data archive. The basic attributes of the SAR data are summarized in Table 3-2.

The search engine for the ASF archive does not have a browse function. The footprint of an image can be displayed on a map of the target area, and its usefulness can be assessed only with respect to its spatial coverage. This limitation led to processing a much greater number of images than were eventually used in mapping. Initially, 155 scenes were ordered from ASF as raw image files for the period 1995-2006 (14 ERS-1, 71 ERS-2, 12 RADARSAT Standard Beam and 58 RADARSAT ScanSAR). These so-called CEOS (Level 1) data were then processed using the ASF Convert tool. For initial evaluation, the images were converted to amplitude data,

geocoded to a UTM projection and exported in jpeg format. This approach represents one of the least computationally-intensive methods to process the data and conduct a visual assessment.

A preliminary subset of 91 potentially useful images was compiled by visual inspection, and the resulting CEOS (Level 1) data were converted to a GeoTiff format. The GeoTiff format allows the image to be imported directly into a GIS application where its projection can be changed as required. Before the images were loaded into the GIS and mapped, a further level of screening was performed by examining lower-resolution jpeg images to determine whether the image quality, timing and coverage area justified further interpretation. This process resulted in a final subset of 38 SAR images, with the selection based on the probability of showing the most developed overflood extent and the field experience of the project team.

3.2.3 Image Mapping

The project image catalogue (attached as Appendix F) provides details for all scenes from all satellites ultimately selected for use in mapping the 1995-2007 overflood boundaries. Image quality was ranked according to the level of confidence that the image displayed the peak overflood extent.

1. Quality 1 – Level of confidence that the image captures the timing of the overflood at close to the peak flood (maximum seaward extent of the flood water).

2. Quality 2 – Level of confidence in being able to visually identify the overflood limit as an unambiguous boundary.

Note: *In some cases, the tonal value on a visible image within the overflood area (Landsat or MODIS) tends to merge with the clearly non-flooded ice offshore. This situation becomes more severe towards the last few days of the overflood cycle as the sea ice beyond the river overflood zone can become nearly completely flooded on the surface through snow melt alone. See examples in the 2000 case study discussed in Section 3.2.5.*

A total of 64 images was used for the 13-year historical mapping task: 21 Landsat, 38 Radarsat/ERS, 4 MODIS and 1 SPOT (2007 only). A comparison of the 2007 overflood limits from these images with those from the Colville 2007 helicopter survey is provided in Chapter 4.

Before mapping the overflood limits from Landsat, the study team evaluated a number of different band combinations and image stretching to highlight or improve the discrimination of the flood boundaries. In some cases, it was possible to see clear overflood boundaries through thin overcast. After trying recommended band combinations used in previous ice studies, it was decided to use the higher resolution (12 vs. 30 m) Panchromatic band with stretching to enhance the overflood contrast. The Landsat and Standard Beam SAR imagery could be easily mapped at scales on the order of 1:50,000 or better. MODIS and ScanSAR imagery, which has 3 to 10 times less resolution, required mapping at scales of 1:150,000 to 1:250,000 depending on the level of pixilation that could be accepted in digitizing a meaningful boundary.

The image files shown in the catalogue were entered into ArcGIS v. 9.1 and the boundaries were digitized as closed polygons (closed where the boundaries intersected the shoreline). The base map was derived from the BPXA cartographic database acquired for this

project. This methodology used the procedures developed for and experience derived from the 2007 Colville River mapping program described in Chapter 3.

Every effort was made to map fine features along the overflood boundary (localized undulations), but interior features within the overflood area such as early openings where the ice had rotted out off the delta front or dry patches (islands of bare ice) were not mapped. As a quality control measure, every mapped overflood limit was reviewed by at least two members of the study team. To a large extent, the overall error in mapping an overflood limit depends on the quality and timing of the image relative to the peak overflood.

3.2.4 SAR Imagery

A synopsis of the fundamentals of microwave remote sensing is provided here to facilitate an understanding of some of the natural influences and technical characteristics that contribute to the often-marked differences between SAR images that may be closely spaced in time and location. For an expanded treatment the reader is referred to (Canada Centre for Remote Sensing, 2008).

Active microwave instruments differ from those that acquire visible band and near infrared (IR) data in two important ways: 1) an active microwave system provides its own source of energy illumination (microwave bursts) and is therefore not dependent on the sun; and 2) it operates in wavelengths at which clouds are nominally transparent. As a consequence of these two characteristics, satellite active microwave data can be acquired at any time of day and under any sky (cloud) conditions. The most common active microwave imaging instrument is the synthetic aperture radar (SAR).

Each pixel value (brightness) in a SAR image is based on that portion of the total amount of energy emitted that is returned to the sensor. The amount of returned energy depends on how the initial energy burst interacts with the surface it encounters (backscatter). This energy/target interaction can be characterized by the: 1) surface roughness of the target, 2) radar system viewing and surface geometry relationship, and 3) moisture content and electrical properties.

A surface is considered "smooth" if the height variations are much smaller than the radar wavelength (C- band – 5.6/5.66 cm: L-band – 23.5 cm). When the surface height variations begin to approach the wavelength, then the surface will appear "rough" as will surface height variations greater than the SAR wavelength (Figure 3-3). Consequently, small-scale height variations on sea ice can yield a similar backscatter coefficient to large very rough ridged ice fields, which contain both large and small-scale roughness (Mahoney, *et al*., 2005). This ambiguity often leads to difficulties in interpreting SAR images.

A smooth surface (A) causes specular reflection away from the sensor resulting in only a small amount of energy returning to the radar and making smooth surfaces appear as darker-toned areas on an image. A calm water surface would be an example of a smooth surface. A rough surface (B) will scatter the energy in all directions (*i.e.* diffusely) and a significant portion of the energy will be backscattered to the radar. Rough surfaces will appear lighter in tone on an image. A wind-roughened water surface could appear lighter (brighter) in a SAR image. Fetterer, *et al*. (1994), found that new ice and open water can exhibit a wide range of backscatter coefficients because the surfaces of both can be very smooth or roughened by small-

scale ice deformation or wind-induced waves. This ambiguity affects the interpretation of SAR imagery during the overflood period.

The presence (or absence) of moisture affects the electrical properties of the target, which, in turn, influence the absorption, transmission, and reflection of the microwave energy. When a target is moist or wet, scattering from the topmost portion (surface scattering) is the dominant process. The type of reflection (ranging from specular to diffuse) and the magnitude will depend on how rough the material appears to the radar. For example, overflood water on the ice reduces the backscatter coefficient relative to that of calm open water (Mahoney, *et al*., 2005). Barber, *et al*. (1995), demonstrated that the production of superimposed ice nodules in the snow early in the spring (increased roughness), followed by flooding (smooth surface) and then draining of the ice surface (renewed roughness) can lead to an increase, a sudden decrease and then another increase in backscatter, respectively. As a result, radar imagery during these different overflood phases can range from dark to bright white, back to dark and then light in texture. The following section describes a case study developed as part of this project that demonstrates some of these effects.

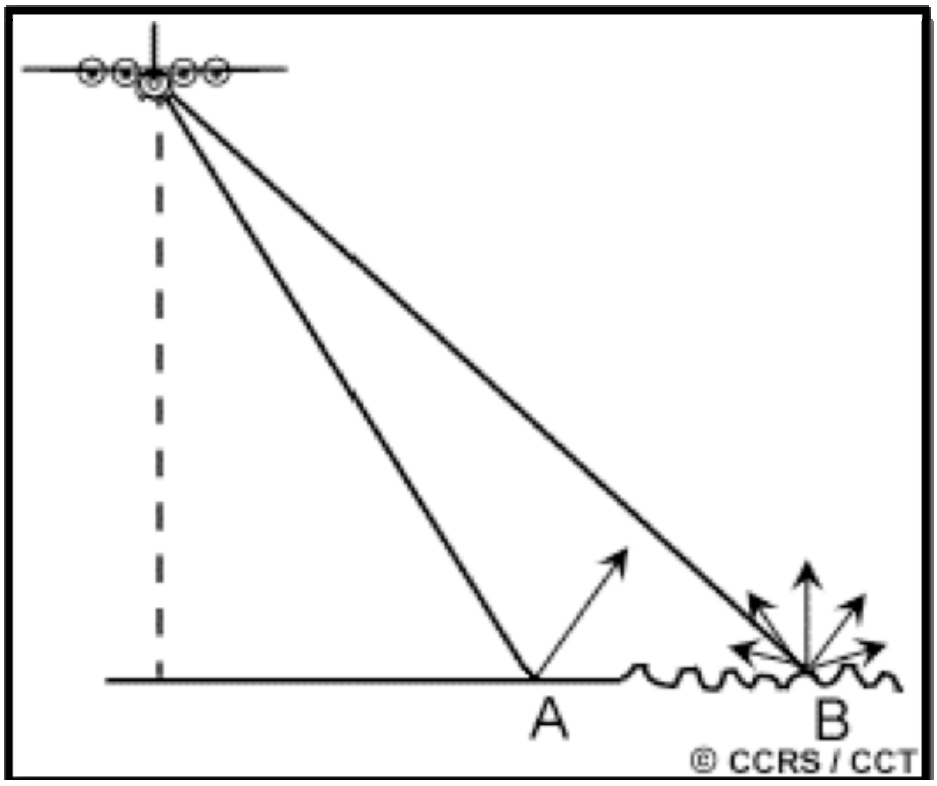

Figure 3-3. Schematic Illustration of Roughness Effects on Radar Returns

3.2.5 2000 SAR Case Study to Examine Overflood Mapping Potential

A time series of SAR images for 2000 was assembled to explore the potential for this type of imagery to map sea ice overflood. The goal was to determine if radar imagery could be relied on to identify and map the peak overflood extent from a time series of close-to-daily images. The work was conducted early in the study prior to relying on the imagery as the primary source for historical mapping.

Full resolution ERS-2, RADARSAT standard beam and RADARSAT ScanSAR (wide beam) images for the 2000 break-up/ice overflood season in the vicinity of Prudhoe Bay were identified and ordered from the Alaska Satellite Facility (ASF). Table 3-2 summarizes the fundamental characteristics of these data. Refer to Appendix G for the different radar satellite product specifications.

Table 3-2. SAR Imagery Used for the 2000 Case Study

Data Type	Frequency	Resolution	Areal coverage
ERS-2 [1]	5.3 GHz (5.6 cm)	30 m	100 x 100 km
RADARSAT (Standard Beam)	5.3 GHz (5.6 cm)	30 m	100 x 100 km
RADARSAT ScanSAR (wide)	5.3 GHz (5.6 cm)	100 m	500 x 500 km

1. Both ERS-1 and 2 imagery were used in the full mapping program. See Section 5.4

The example images shown in Figures 3-4 to 3-14 were processed using the ASF Convert tool. These images were converted from CEOS (Level 1) data to amplitude (digital number) data, geocoded to a UTM projection and exported in jpeg format order to "see" the data (first look). This is one of the least computationally-intensive ways to process the data in order to visually assess them. The subscenes of ScanSAR images are displayed at 20% of their original size while the RADARSAT and ERS-2 standard beam images are displayed at 10% of their original size. Full RADARSAT Standard Beam images are about 20 MB, ERS-2 images are 20-21 MB, and ScanSAR images are 25-30 MB. A single Landsat image available for this time period is included as a visual reference in Figure 3-12.

If necessary, SAR data can be reprocessed in a variety of different ways to facilitate more rigorous scientific evaluation. However, as evidenced by the following examples, the images clearly show the peak overflood boundary at only a basic processing level and further processing proved unnecessary in this study. It should be noted that interpreting any SAR image in the absence of ground data is never straightforward. The commentary on the 2000 images should be treated as "informed speculation" that is based on what is known about surface conditions at the time the image is acquired (wind speeds and temperatures) and the visual texture of the image.

In each example, one or two colored boxes are used to provide some orientation on the images. The red boxes on the images enclose Prudhoe Bay, the Sagavanirktok River Delta and the Endicott Causeway; the blue boxes enclose the Kuparuk River Delta. These were the primary areas of interest for this case-study exercise. Where possible, other areas of the Beaufort Sea coast are also depicted to give some indication of the range in image quality and tonal values with varying local conditions (wind, water on the ice, snow cover, etc.).

Over the time period selected for the case study, the USGS stream gauge data (USGS, 2008) indicates that the flow of the Sagavanirktok River increased from May 30, 2000 to June 9, 2000 (crest) and decreased to "normal" flow beyond that. On the Kuparuk River, the discharge increased from June 8, 2000 to June 13, 2000 (crest) and decreased to "normal" flow beyond that. Wind speed and air temperature data were obtained from the NOAA NOS/CO-OP station located on West Dock (NOAA, 2008). All times are Coordinated Universal Time (UTC).

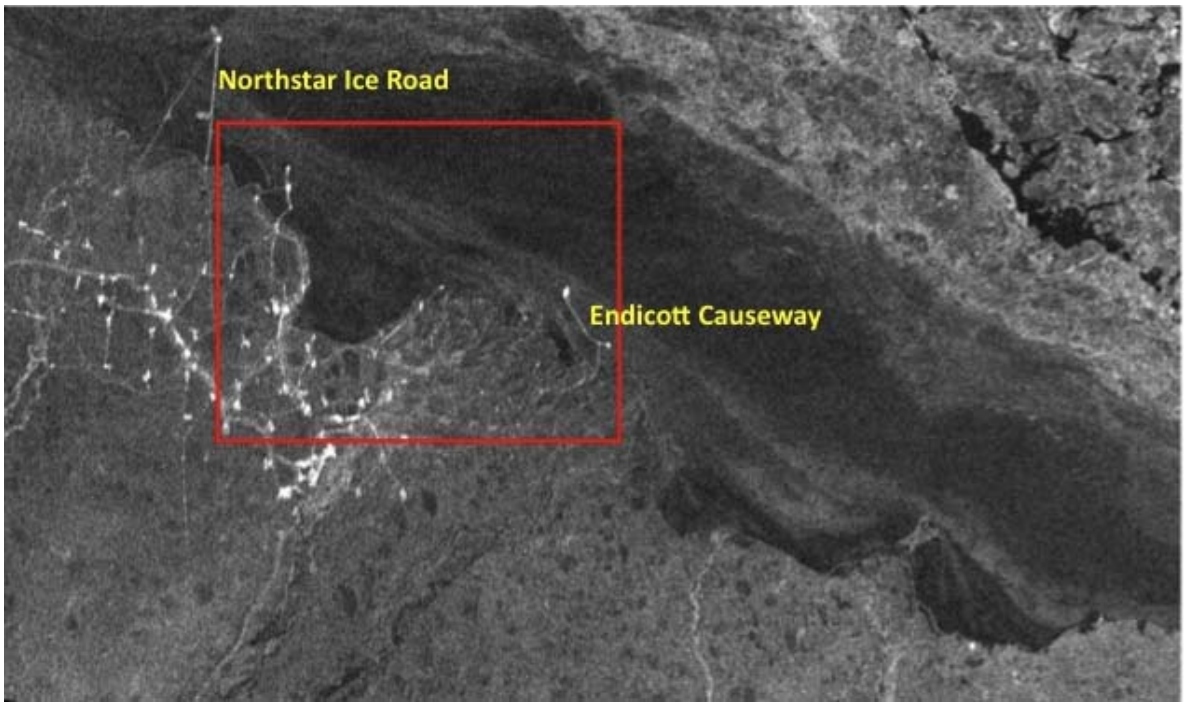

ScanSAR subscene R1_23883_270 June 1, 2000 (1616 UTC)

The roads, buildings, West Dock and the Endicott causeway present very high return (bright) targets. The low return (dark) areas indicate smooth cold ice. Air temperatures were well below freezing on 1 June and the wind speeds were 4.5 m/s (1600) to 6.0 m/s (1700).

Figure 3-4. ScanSAR Subscene June 1, 2000

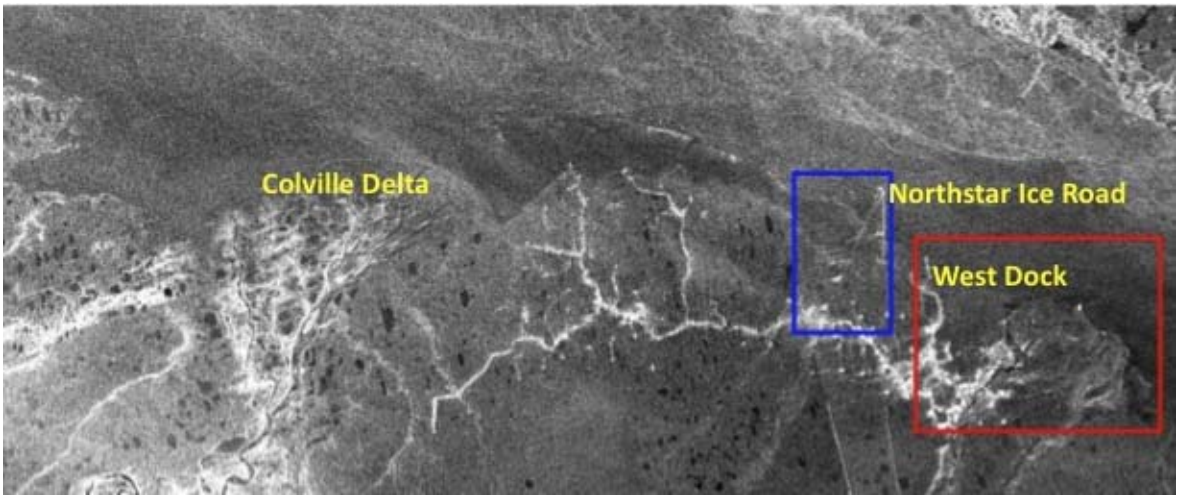

ScanSAR subscene R1_23961_182 June 7, 2000 (0306 UTC)

The roads, buildings and causeway present very high return targets. The Northstar ice road with its snow berms on either side appeared in this image as a distinct linear feature (see blue box upper right). It is not possible to see any well-defined water forms on the sea ice in this image. The generally "higher" radar returns from some of the river channels indicated that the river ice is still intact, especially on the Kuparuk River. However, on the Sagavanirktok River, there were reaches of very low radar return, indicating water flowing in the channel (either the ice was completely melted in that section of channel or water was flowing over the ice). This observation correlates to the increase in water flow observed at the gauging station from 30 May 2000 to 9 June 2000 (crest). The *smeared* appearance of the image may be due to the acquisition time (>1 minute) and rapidly changing conditions on the ground during that time (gusting winds) or may simply be a function of the resolution/pixel size. Air temperatures were near freezing at the time of data acquisition, -0.5°C (0200) to -1.5°C (0400), and wind speeds ranged from 9.6 m/s (0300) to 10.7 m/s (0400).

Figure 3-5. ScanSAR Subscene June 7, 2000

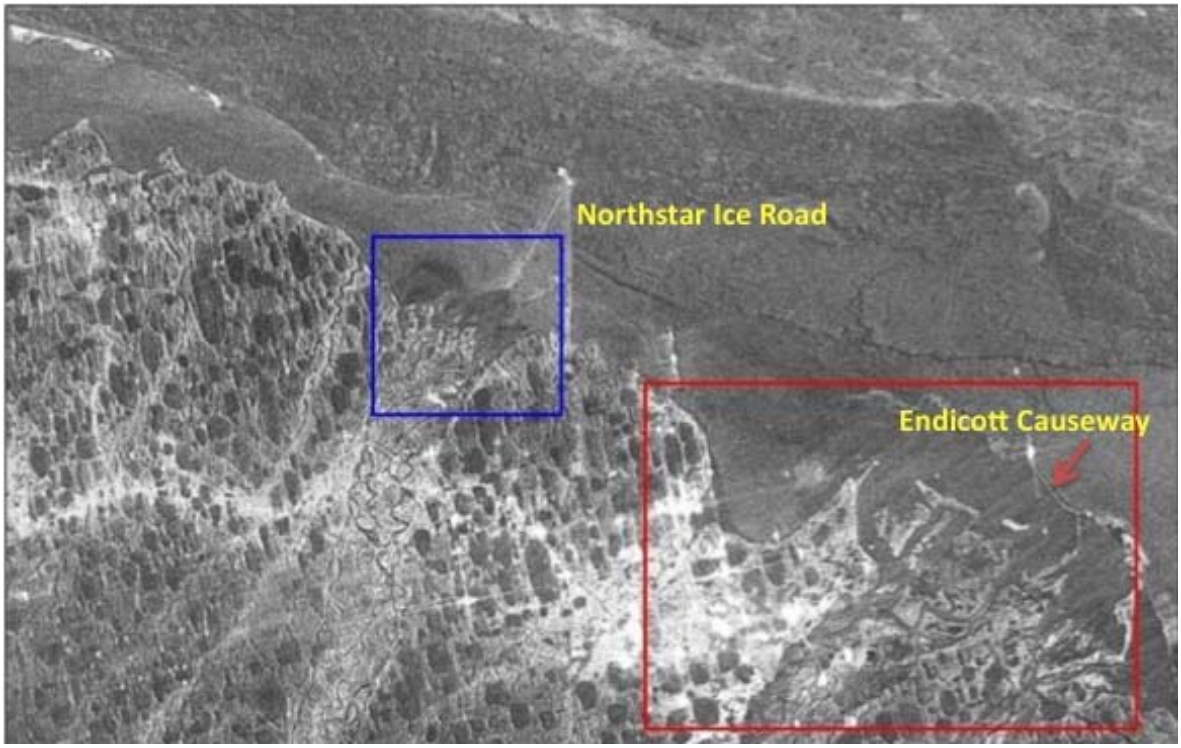

RADARSAT Standard Beam subscene R1_2004177 June 10, 2000 (0317 UTC)

Once again it is difficult to clearly discern water on the ice in this image. However, when viewed in conjunction with the 10-11 June 2000 Subscenes below, it becomes obvious that there was a substantial area of water in front of the Kuparuk River (blue box). Off the Sagavanirktok Delta there is a distinct tonal difference between the area inside the causeway and outside (the area to the north shows ice roughness features and fracturing while the inshore area is uniformly streaked). There appears to be a margin of flooded water (darker return) along the west shore of Prudhoe Bay. Air temperatures were near -10°C (-9.5°C at 0300 and -10.0°C at 0400) and wind speeds were decreasing compared to the previous day (4.7 m/s at 03:00 and 2.7 m/s at 0400). At these temperatures, there is likely to be a thin skim of new ice on the overflood, being broken in places by wind action. This situation creates a complex interface in terms of radar scattering.

Figure 3-6. **RADARSAT Standard Beam Subscene June 10, 2000**

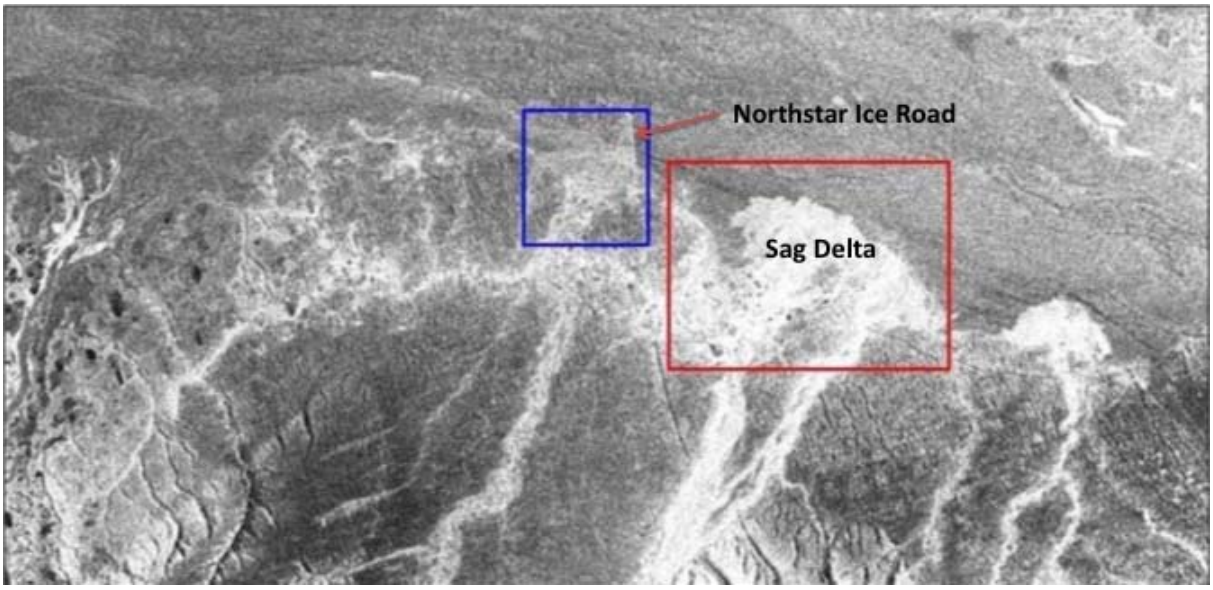

ScanSAR subscene R1_24012_269 June 10, 2000 (1654 UTC)

This scene was acquired later the same day as the previous image (Figure. 3-6) but approximately 13 hours later. From 0600 onward, wind speeds increased to >8.0 m/s and air temperatures increased to -1.7°C (1700). It appears from the radar reflection strength in this image that the wind was sufficiently strong off the Sagavanirktok River Delta to roughen the surface of the overflood water on the ice, creating a very clear outline of the flooded area even at this degraded resolution. The flooded zone adjacent to the Kuparuk River Delta is less well-defined although the water boundaries are very obvious in the standard beam image below. See Fig. 3-8 following.

Figure 3-7. ScanSAR Subscene June 10, 2000

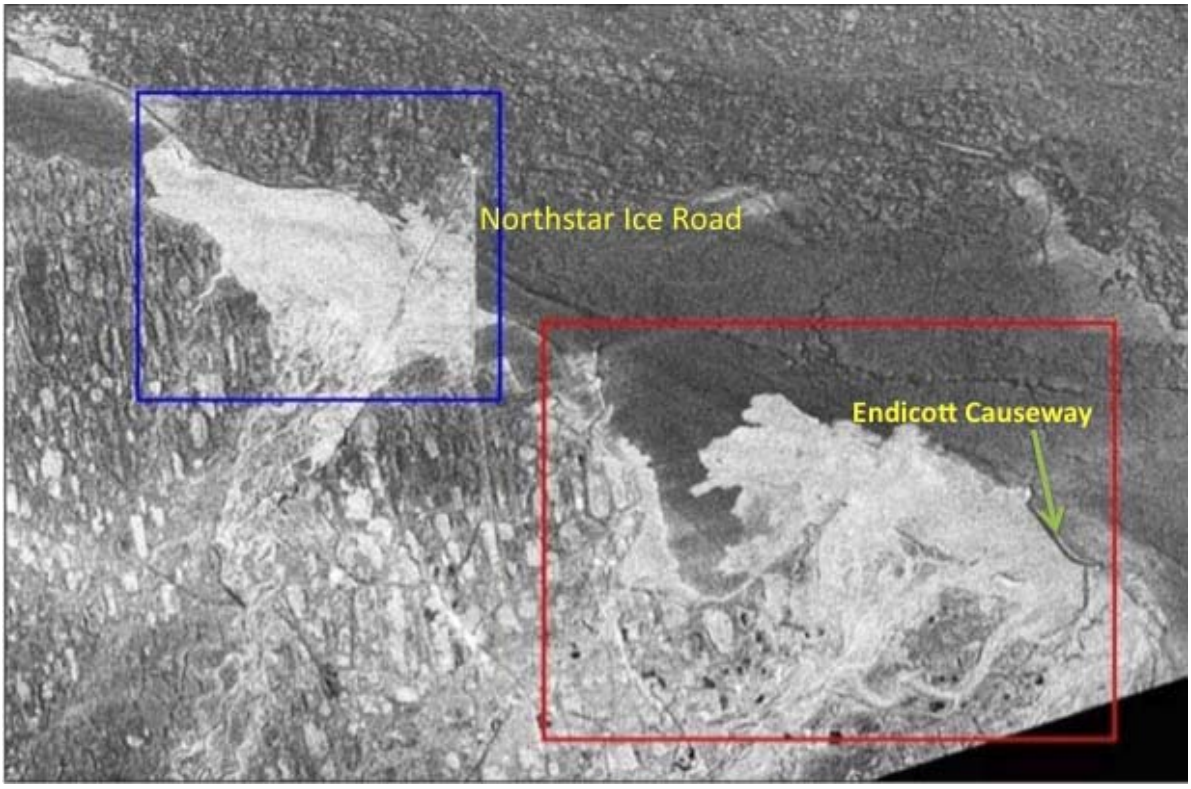

RADARSAT Standard Beam subscene R1_24018178 June 11, 2000 (0248 UTC)

These data were acquired about 7 hours after the previous scene (Figure 3-7). The water on the ice appears very bright because the wind is strong enough to roughen the water surface sufficiently to interact with the radar signal. Wind speeds increased to 17.5 m/s by 10 June, 2300 and remained high (>10.0 m/s) until 11 June, 0500. It is obvious that the Endicott Causeway to the east presented a sharply-defined obstacle to over-ice water flow, as do other man-made features, notably the ice road to Northstar defining the offshore eastern boundary of the Kuparuk River overflood. The barrier islands off the Kuparuk Delta constrained overflood spreading to the north. From 10 June, 2000 to 11 June, 0700, air temperatures were >-1.0°C, indicating continued surface melting and a lack of new ice forming.

Figure 3-8. RADARSAT Standard Beam Subscene June 11, 2000

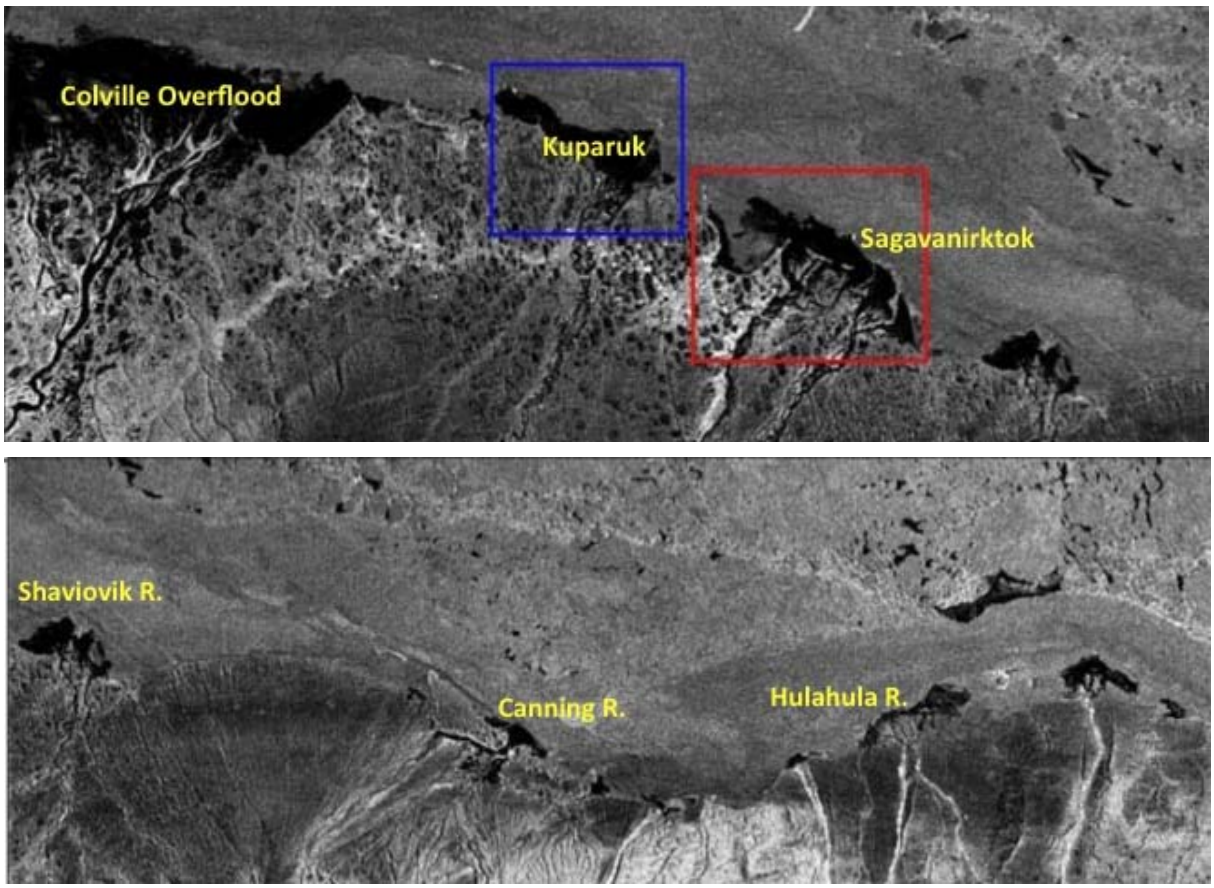

ScanSAR subscene R1_24026_270 June 11, 2000 (1625 UTC)

These data were acquired about 13 hours later than the last image (Figure 3-8). The wind speeds during this period ranged from 9.9 m/s (16:00) to 10.7 m/s (1700), sufficient to sustain a rough water surface normally associated with a strong (bright) radar return. Air temperatures had fallen to ~ -6°C, but the formation of a thin new ice layer is considered unlikely with the strong winds. The distinct low-energy black returns from all the overfloods in this image are not consistent with the environmental factors. With the strong contrast, even floodwater plumes off the smaller river to the east are very obvious. In the case of both the Kuparuk and Sagavanirktok rivers, the channels in the delta all appear wide and very dark, indicating a large volume of water flowing (Kuparuk River crested on 13 June at gauge; Sagavanirktok on 9 June).

Figure 3-9. ScanSAR Subscene June 11, 2000

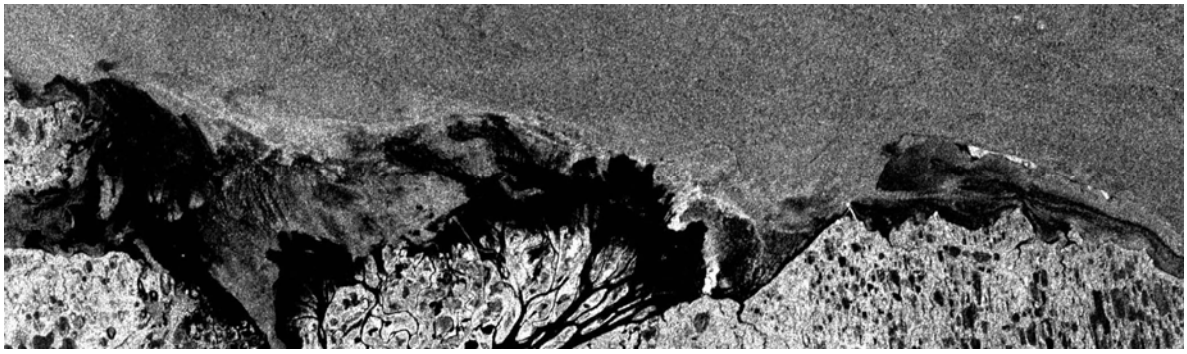

Colville Delta to Simpson Lagoon

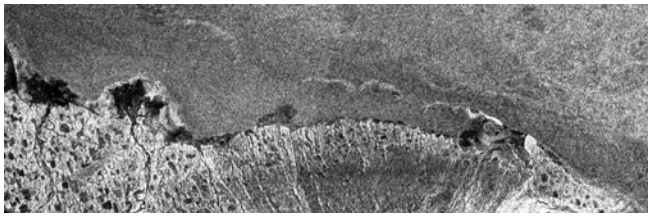

Kadleroshilik to Canning River

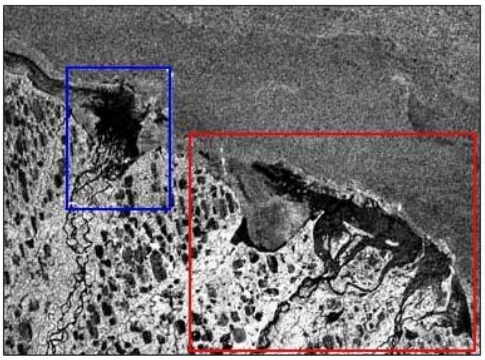

Kuparuk to the Sagavanirktok Delta

ScanSAR subscene R1_24069_269 June 14, 2000 (1638 UTC)

These image panels show different coastal sections from the Colville Delta to the Canning River. The overflood areas in these images are less dark and uniform than in the previous data set (Figure 3-9). ***Note:*** *Differences in pixel saturation are not clearly visible at the degraded resolution necessary for publication*. Wind speeds were close to calm (0.0 m/s at 1600 and 2.8 m/s at 1700). Air temperatures were also low (-17.8°C at 1600 rising to 15.3°C at 1700). The lack of uniformity in return signatures could be a consequence of minor differences in ice roughness. This complex surface roughness pattern may also indicate that water has drained through the sea ice cover in some areas, leaving bare sea ice surrounded by standing water with a thin layer of smooth ice (producing a very low return). Some of the "standing water" areas immediately off the deltas are likely open water; *i.e*., the sea ice has melted out completely.

Figure 3-10. ScanSAR Subscene June 14, 2000

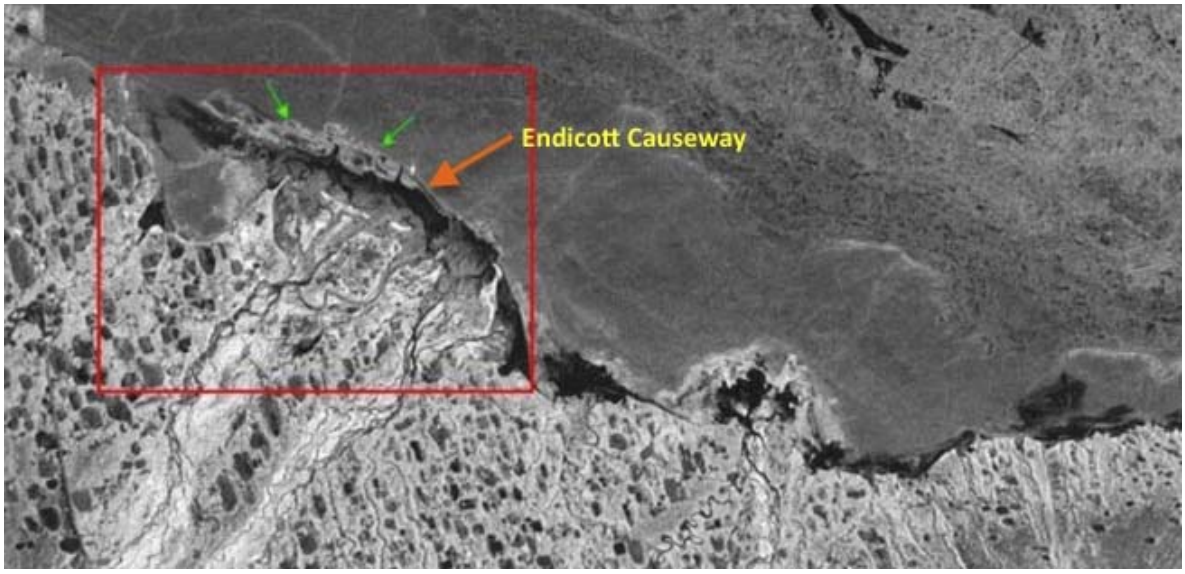

ERS2 subscene E2_26951273 June 15, 2000 (2123 UTC)

Air temperatures corresponding to this image were moderate (-6.8°C at 2100 and -5.7°C at 2200) and wind speeds were 6.3 m/s (2100) to 7.2 m/s (2200). It is much easier to see the variation in the radar return in front of the Sagavanirktok River Delta (due, in part, to the greater resolution of this image compared to the previous). The channels in the delta have a higher radar return than in previous images indicating that the water level has passed flood stage. The very low return south of the Endicott Causeway (orange arrow) may be standing floodwater with a thin layer of smooth ice on it or, more likely open water. It is unclear what is causing the zone of high return off the end of the causeway (indicated by the green arrows). One possibility is that the remains of previously bottomfast ice have floated free and now appear as a drained irregular ice surface. This area represents the extreme seaward limits of the overflood waters shown in the June 11 standard beam image (Figure 3-8) and a zone of sediment and/or debris deposited during drainage could create a rough surface leading to a patchy high return.

Figure 3-11. ERS-2 Subscene June 15, 2000

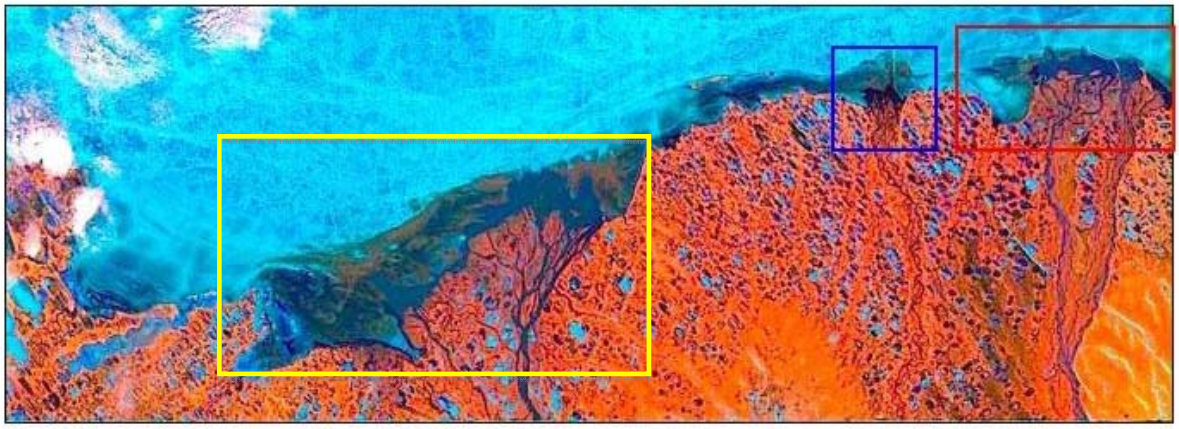

Landsat subscene June 16, 2000)

In this Landsat image, the very dark blue areas off the Colville (yellow box), Kuparuk (blue box) and Sag (red box) Deltas represent partial open water within the area previously covered with overflood water. The brown color represents sediment deposited on the sea ice at the outer edge of the floodwater plume and can be used to gain some indication of what may have been the peak overflood extent. The only way to accurately map the overflood boundary once the floodwaters have drained from the ice is by low-level helicopter surveys that can utilize other visual clues to locate the flood boundary (*e.g.*, the presence of old strudel drains looking into shore and an absence looking seaward).

Figure 3-12. Landsat Subscene June 16, 2000

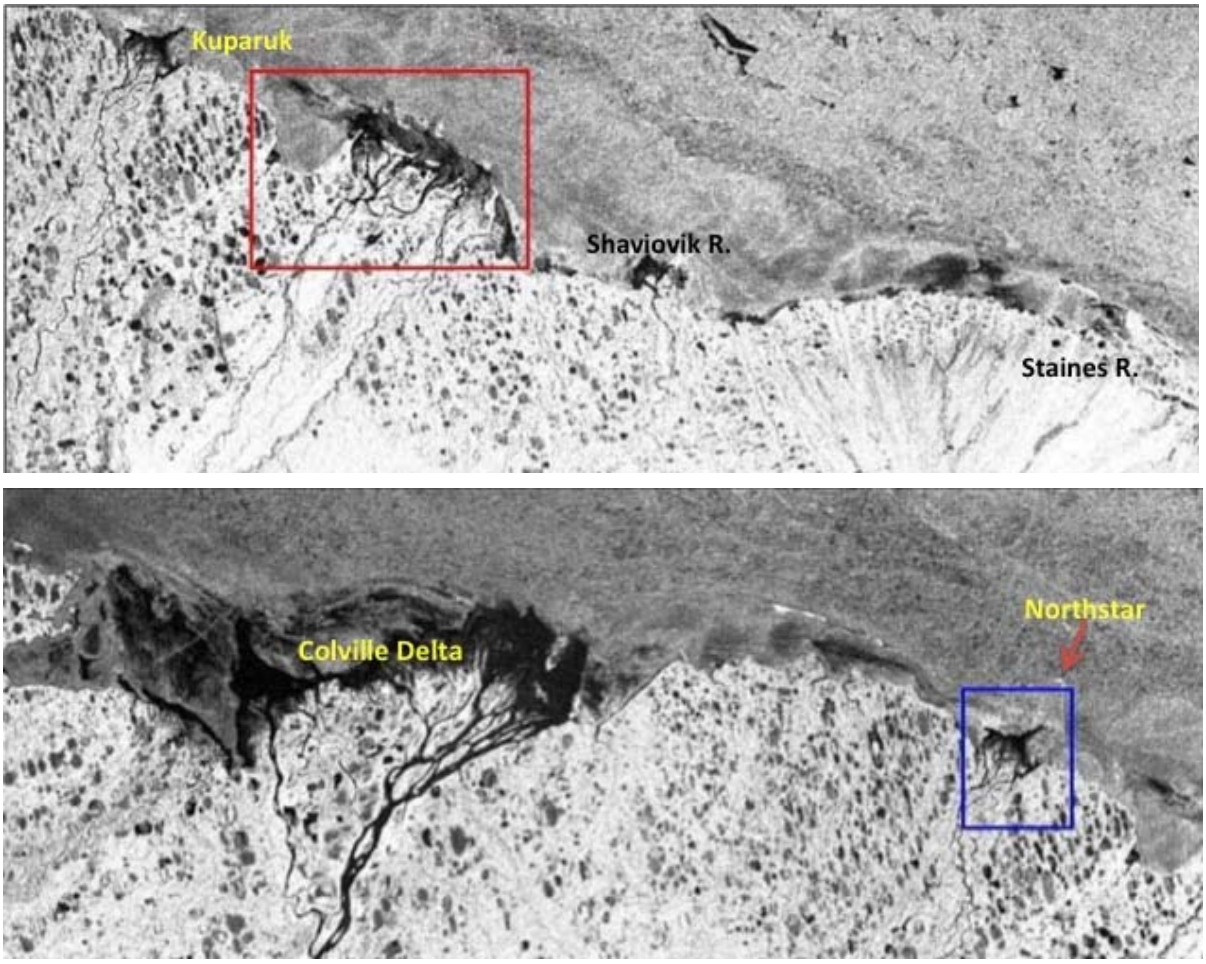

R1_24069_ScanSAR subscene R1_24112_269 June 17, 2000 (1649 UTC)

During the data acquisition period, the air temperature was ~ -10°C (-10.7°C at 1600 and -9.7°C at 1700) with moderate winds (5.2 m/s at 16:00 and 3.3 m/s at 1700). The nearshore zones off the Colville, Kuparuk and Sag deltas show a non-uniform return. This likely represents areas of open water (*i.e.*, the sea ice has completely melted out) in combination with areas of drained sea ice with or without some sediment deposited on the surface. See the Landsat visible image from the previous day in Figure 3-12.

Figure 3-13. ScanSAR Subscene June 17, 2000

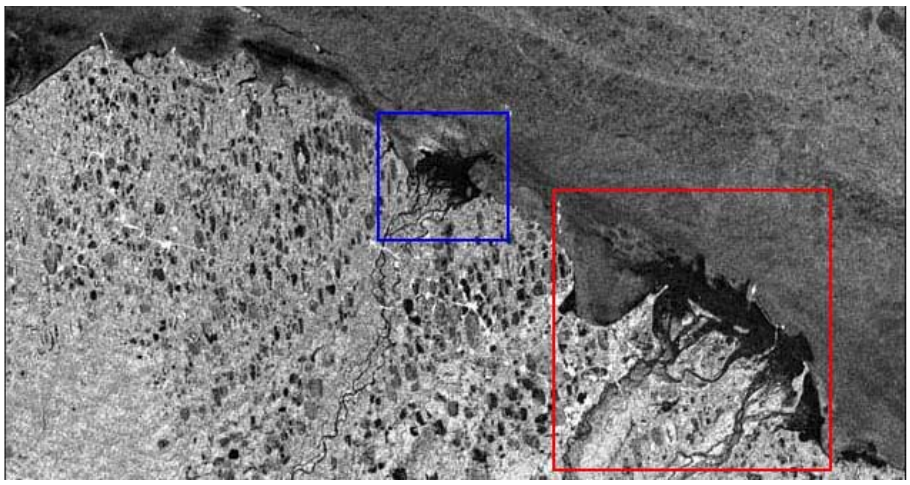

Oliktok Point (left) to Sag Delta (right)

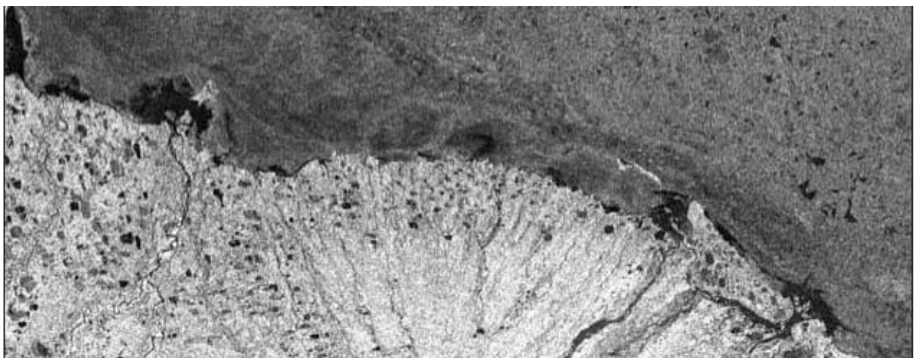

Shaviovik River to Canning River

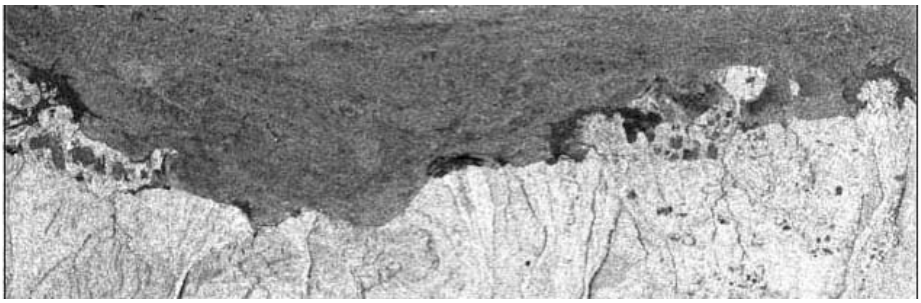

Canning River to Avery Lagoon (see Figure 1-1)

R1_24069_ScanSAR subscene R1_24126_270 June 18, 2000 (1602 UTC)

The fairly uniform, low return (dark) zones adjacent to the deltas in these images likely represents the initial areas of open water following overflood drainage and close to complete melting of former bottomfast ice. The wind speed was low (2.1 m/s at 1600) and air temperature was approximately -9.5°C. At this late stage, more than a week after the overflood has drained, it is very difficult to delineate the peak overflood boundary.

Figure 3-14. ScanSAR Subscene June 18, 2000

The overall conclusion from the 2000 SAR case study was that radar imagery (either Radarsat or ERS) is capable of accurately defining the peak overflood, recognizing that the brightness associated with the overflood as a radar target can change in a very brief period of time depending mainly on fluctuations in wind strength. Other observations from interpreting surface features at different stages in the overflood cycle include:

1) The RADARSAT ScanSAR does not appear to be very useful at the beginning of the melt season, although the returns from the oil and gas field infrastructure are easily discerned. This may be because the sea ice and land cover are both "wet" due to snow melting. See Figures 3-4 and 3-5.

2) The over-ice flooding is visible in the ScanSAR data on June 10 as a high return zone related to the surface roughness of the windswept water. The overflood boundaries are much better-defined in the higher-resolution RADARSAT standard beam image acquired six hours later (Comparing Figures 3-7 and 3-8).

3) Under low-wind conditions and with relatively high volumes of water on the ice, the over-ice flooded areas, although still visible in the low-resolution ScanSAR imagery show better contrast and more distinct boundaries in the Standard Beam imagery.

4) As the floodwater drains through the ice and deposits sediment and debris on the sea ice surface, the texture of the flood zone changes significantly on the radar imagery. Without ground truth data it is impossible to fully interpret the ScanSAR images except in very general terms (*e.g.*, June 14, 17 and 18). Under calm or low wind conditions, at this late stage in the overflood process, it will not always be possible to distinguish between substantial standing floodwater remaining on the ice and the first appearance of open water off the delta fronts.

5) Once drainage has occurred, visible Landsat images (example shown in Figure 3-12) also become difficult to accurately interpret without a detailed understanding of the chronology of the overflood event or access to other imagery immediately before and after.

4 2007 FIELD STUDY AND SATELLITE IMAGE VALIDATION

This section describes the helicopter-based reconnaissance and mapping of the Colville River overflood that were conducted in 2007. The specific objective of the reconnaissance mission was to map the seaward limit of the river overflood on the sea ice. The results were compared to overflood limits mapped from satellite images to gain an understanding of the accuracy and limitations of various mapping techniques and image platforms, and to provide guidance for mapping historical overflood limits (1995 to 2007). The project area is shown in Figure 4-1.

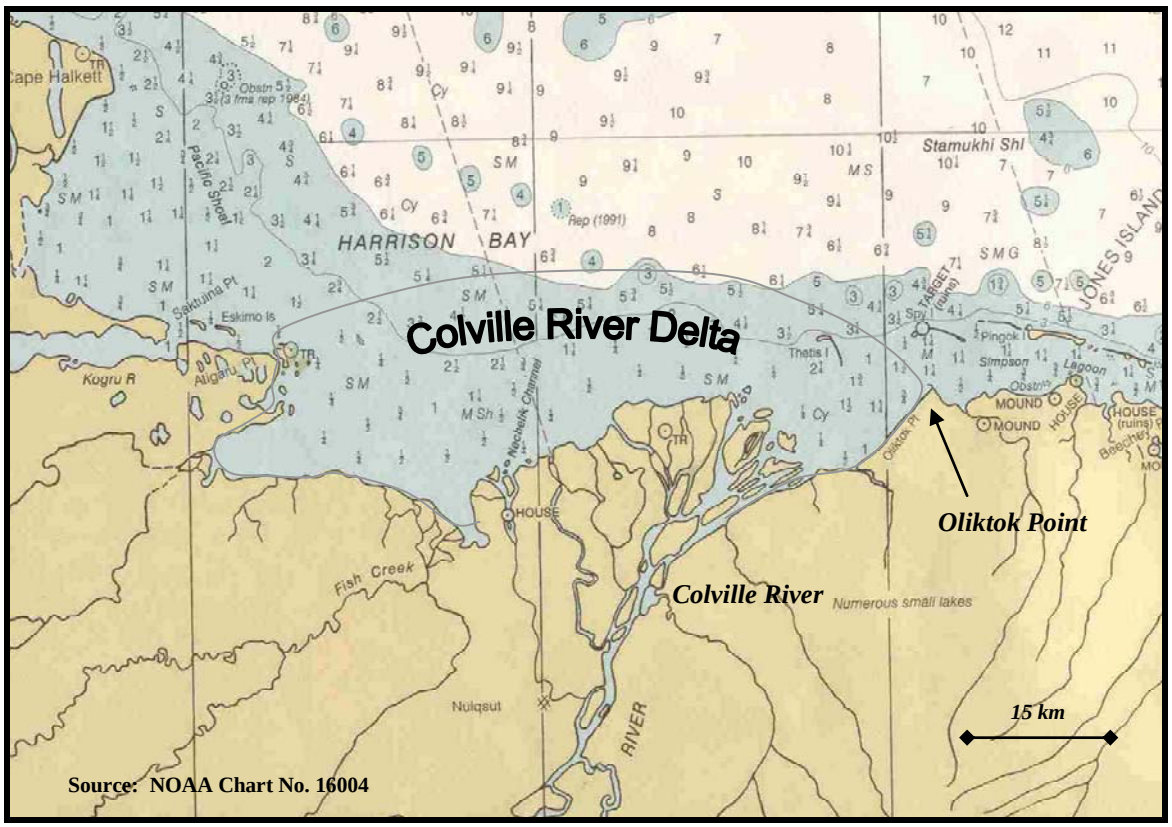

Figure 4-1. 2007 Field Study Location Map

A description of the 2007 Colville River overflood is provided in Section 4.1. The field operations are discussed in Section 4.2, while the overflood limits derived from satellite imagery are presented in Section 4.3. The results of the 2007 helicopter and satellite mapping, and a comparison of the overflood boundaries are discussed in Section 4.4.

4.1 2007 River Overflood

The floodwaters of the Colville River arrived at the delta on May 28, 2007, with water reaching the nearshore region shortly thereafter (Alexander, 2007). It is difficult to place this break-up into historical context due to the lack of available long-term streamflow data and break-

up observations. However, streamflow measurements on the Colville and observations at other North Slope rivers suggest that breakup at the Colville occurred later than usual and was modest compared to flood events in the recent past.

Daily streamflow data from 2003 through 2007 for the U.S. Geological Survey (USGS) gauge on the Colville River at Umiat are shown in Figure 4-2 (USGS, 2008), while the streamflow characteristics are summarized in Table 4-1. The station is located approximately 140 km south of the river mouth. A detailed discussion of streamflow data at this station and other North Slope locations is provided in Section 6.1.

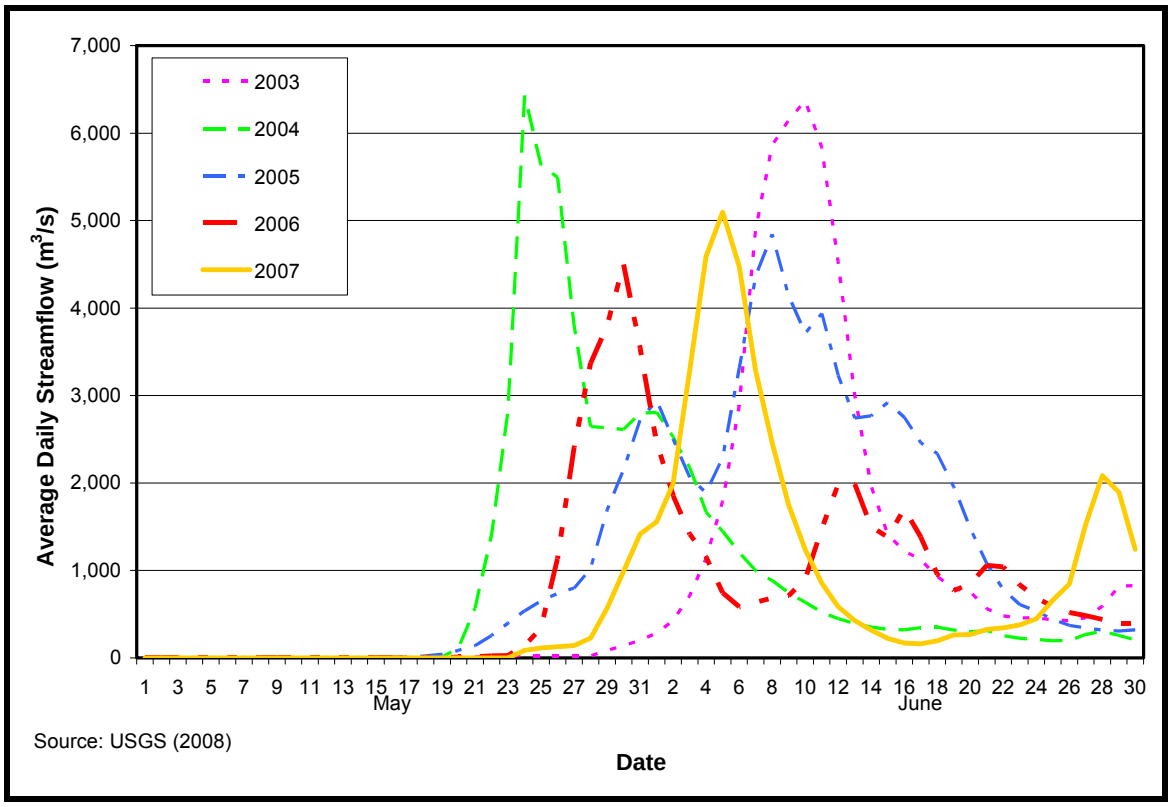

Figure 4-2. Average Daily Streamflow in the Colville River during Spring Break-up

During the four-year period preceding 2007, the date of peak streamflow (Q) at the USGS gauge ranged from May 24 to June 10, with an average date of June 2. The 2007 peak streamflow occurred three days later, on June 5. The peak streamflow, average streamflow, flood volume and flood intensity in 2007 all were below the respective pre-2007 averages.

Although individual drainage basins have different thermal exposures and responses, a general indication of the timing of 2007 Colville River break-up is given by long-term break-up observations at two nearby North Slope rivers. Table 4-2 summarizes the break-up observations at the Sagavanirktok and Kuparuk Rivers for the 28-year period between 1980 and 2007. The observations for the Sagavanirktok and Kuparuk Rivers suggest that break-up at North Slope rivers occurred later than usual in 2007. The 2007 Sagavanirktok River break-up was observed on May 26, one day beyond the average break-up date (May 25). Based on the closure date at the Kuparuk River bridge, break-up occurred at this river 11 days after the average date (May 26) on June 6.

Table 4-1. Colville River Streamflow Characteristics during Break-up Period

Year	Date of Peak Q	Peak Q (m^3/s)	Average Q (m^3/s)	Flood Volume (m^3)	Flood Intensity ($m^3/s/day$)
2003	*June 10*	*6,372*	*2,617*	*4,521,775,104*	*661*
2004	*May 24*	*6,429*	*2,385*	*4,532,541,235*	*1,466*
2005	*June 8*	*4,843*	*2,247*	*6,212,791,757*	*269*
2006	*May 30*	*4,503*	*2,100*	*2,358,272,102*	*694*
2007	***June 5***	***5,098***	***2,276***	***2,949,675,264***	***566***
Pre-2007 Ave.	***June 2***	***5,537***	***2,337***	***4,406,345,050***	***772***
Pre-2007 Max.	*June 10*	*6,429*	*2,617*	*6,212,791,757*	*1466*
Pre-2007 Min.	*May 24*	*4,503*	*2,100*	*2,358,272,102*	*269*

Table 4-2. Break-up Observations at the Sagavanirktok and Kuparuk Rivers

River	Break-up Date				Difference 2007 – Ave.
	Range (1980-2006)	Average (1980-2006)	Std. Dev. (1980-2006)	2007	
Sagavanirktok	5/8 – 6/14	5/25	8 days	5/26	+ 1 day
Kuparuk	5/13 – 6/10	5/26	7 days	6/6	+11 days

Notes: *Source: FR Bell and Associates, 2007*

1. Sagavanirktok River break-up dates based on observations at the Sagavanirktok River bridge (Deadhorse, AK).
2. Kuparuk River break-up dates based on closure dates for the Kuparuk River bridge (Deadhorse, AK).

Figure 4-3 shows the progression of the 2007 Colville River overflood through a series of RadarSat images. The beginning of river overflood on the sea ice is visible at the eastern and western portions of the river delta on May 30. A linear demarcation corresponding to the location of the ice road constructed to support the Oooguruk Development flowline installation (Hall, 2008) is evident at the eastern edge of the flood water. The progressive westward spreading of the overflood boundary is apparent in the consecutive images from June 1 through 4. These images also indicate that the eastern boundary of the overflood (near the Oooguruk project site) remained essentially unchanged during this period. The June 9 image suggests that the overflood waters had started to recede and the nearshore ice was deteriorating.

The westward spreading of the Colville River overflood boundary is attributable, at least in part, to the predominance of easterly winds during the overflood period. Figure 4-4, which displays wind speeds measured at the Seawater Treatment Plant (STP) on West Dock, indicates

that wind speeds exceeded 20 kts on five occasions between May 29 and June 10. Two of these events produced wind speeds exceeding 40 kts.

If freezing air temperatures occur for extended periods after river overflood has begun, the flood waters may re-freeze, thereby limiting their progression offshore. As indicated in Figure 4-5, this phenomenon did not play a major role in 2007. The daytime temperatures exceeded 0˚C from June 1 to 3, while both day and night temperatures remained above this threshold from June 4 to 11.

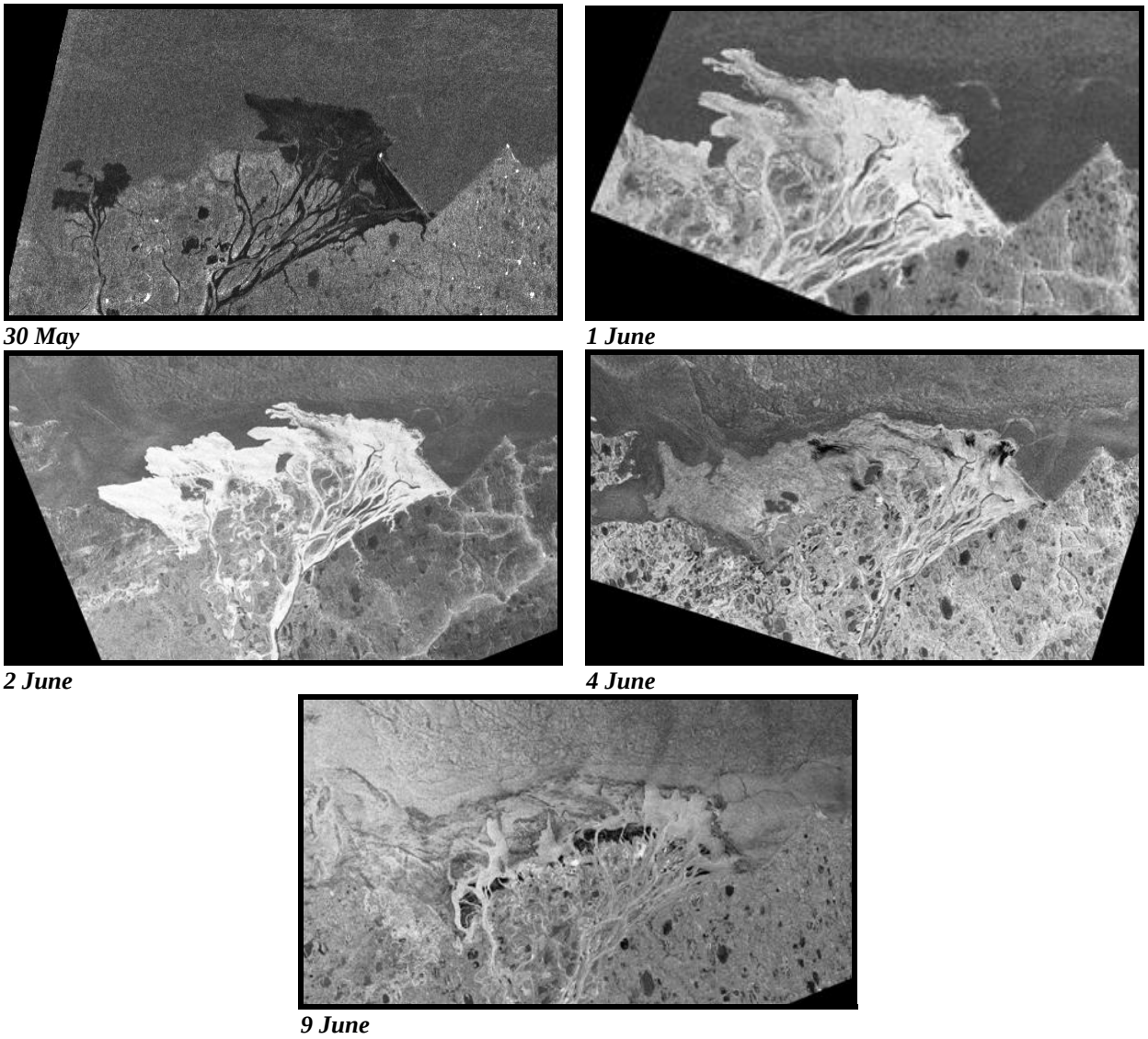

Figure 4-3. RadarSat and ERS Images Showing the Progression of the 2007 Colville River Overflood

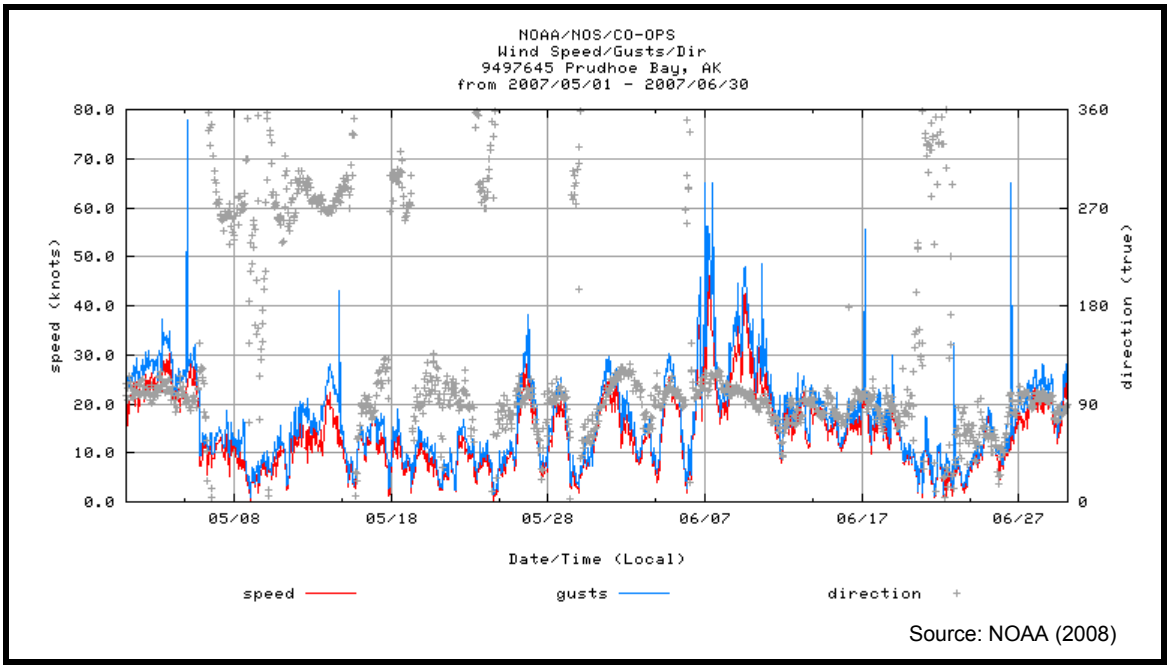

Figure 4-4. Wind Speed Observations at West Dock STP during Overflood

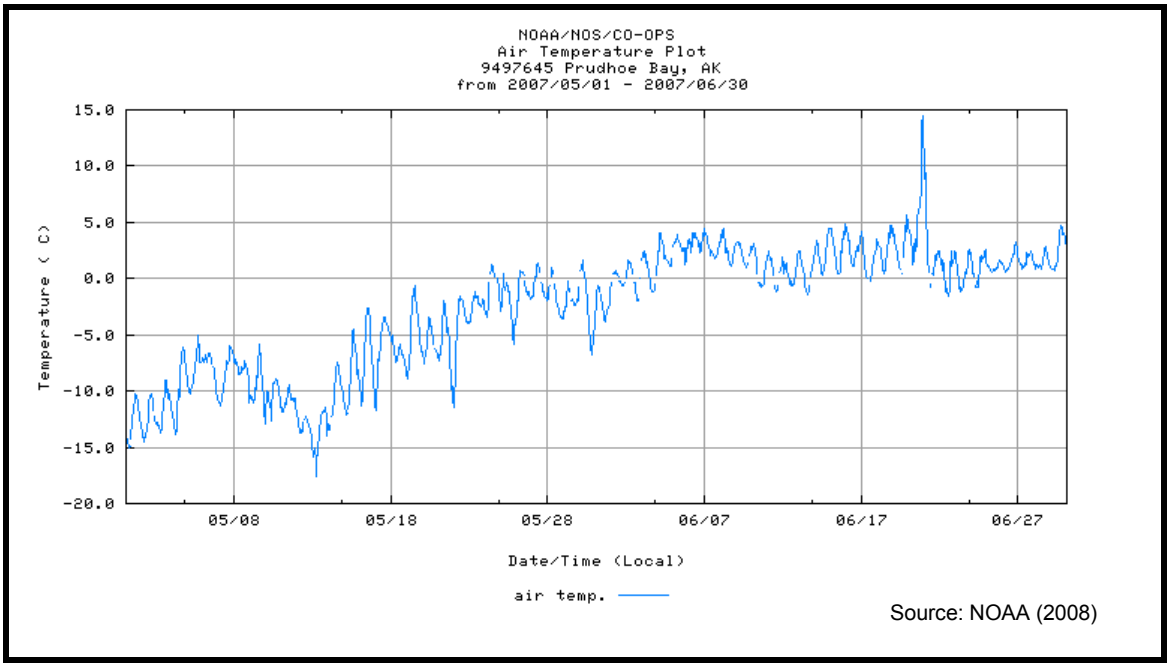

Figure 4-5. Temperature Observations at West Dock STP during Overflood

4.2 Field Survey Activities

The field mapping activities were conducted on June 8, 2007. To insure that the maximum offshore extent of the flood was documented, the mapping was performed near the end of the overflood period rather than at its peak. The following sections summarize the pre-

survey agency coordination, describe the timing, and discuss the methods used for the field operations.

4.2.1 Agency Coordination

The necessary permits for the overflood reconnaissance were obtained prior to the field effort with the assistance of Mr. Richard Reich of BTS Professional Services. The permit application was submitted to the North Slope Borough on January 24, 2007. The permit approval was received on January 29, 2007. Prior to conducting the aerial reconnaissance, the following entities in the community of Nuiqsut were notified: North Slope Borough Village Coordinator, City of Nuiqsut, Kuupik Village Corporation, Native Village of Nuiqsut, and the Kuukpik Subsistence Oversight Panel.

4.2.2 Timing

Several sources were consulted to determine the most appropriate time to mobilize the scientific team to the North Slope. Based on an assessment of the available information, the complete field crew was mobilized to the North Slope on June 7, 2007. The sources used to monitor breakup are summarized below.

A quantitative indication of break-up in the Colville River was provided by the aforementioned USGS streamflow gauge located at Umiat. Based on past experience, overflood onto the sea ice typically occurs several days after the peak discharge is recorded at Umiat.

Several North Slope sources were contacted on a regular basis as break-up approached, including personnel associated with the BPXA Northstar Development, the ConocoPhilips Alpine Development (through contractor Michael Baker, Jr., Inc.), and FR Bell and Associates. In addition, a Coastal Frontiers field crew was stationed on-site to map strudel drainage features in the vicinity of Pioneer's Oooguruk Development (located offshore of the Colville River Delta). This work was initiated soon after the overflood began to best capture strudel drainage in the project area. This field crew provided firsthand insight into the most appropriate time to map the peak overflood of the Colville River.

4.2.3 Survey Methods

Coastal Frontiers Corporation has performed more than twenty helicopter-based river overflood and strudel drain mapping projects in the Alaskan Beaufort Sea during the past decade. The methods developed and refined during these surveys were used for the 2007 Colville River mapping effort.

The work was performed using a Bolkow BO-105, a small twin-engine helicopter, operated by Air Logistics (Figure 4-6). Weather conditions were nearly ideal, with clear skies and visibility of several kilometers. Winds speeds exceeded 30 kts during the initial flight, but subsided to about 20 knots by the end of the reconnaissance period (NOAA, 2008).

Figure 4-6. Bolkow BO-105 Helicopter Operated by Air Logistics

Mapping was performed using a Trimble Pathfinder Pro XR GPS unit operated from the helicopter. To improve the accuracy of the GPS position data, differential corrections broadcast in real time via satellite by the U.S. Government's Wide Area Augmentation System (WAAS) were received by the GPS unit. The higher accuracy attainable with differential corrections broadcast from a local source was judged to be unwarranted, due to the imprecision inherent in mapping features on the ice from a helicopter flying overhead. To assist with navigation, the GPS unit was interfaced to a laptop computer using the Hypack Max survey software package. The software display included a map of the region, allowing the field crew to view the aircraft's position relative to coastal landmarks in real-time.

Three flights were required to map the entire area of overflood due to fuel limitations. For each mission, the helicopter departed from and returned to Deadhorse Airport with a scientific team of three persons and the pilot. On the first flight, the aircraft traveled over land to the vicinity of Oliktok Point guided by GPS navigation.

Upon reaching Oliktok Point, the easternmost edge of the overflood was identified by flying along the coastline. The seaward edge of the river overflood was mapped by recording successive positions with the GPS unit while flying over the observed boundary at altitudes of 30 to 200 m and a speed of approximately 60 knots. Starting at the shoreline, the aircraft proceeded to the west along the overflood limit and continued until it intersected the shoreline on the opposite (west) side of the Colville River. The flight path then was reversed, with mapping conducted from west to east. In addition, the helicopter paused briefly at 15 locations along or near the overflood limit to allow the scientific team to obtain photographs.

After each flight, the GPS files were downloaded to a laptop computer and checked for completeness. When data acquisition was complete, the field crew merged the overflood limits mapped during the westbound and eastbound flights into a single overflood limit based on field notes and observations (including mapping confidence and flight precision). The data files then were backed up, and transmitted to the Coastal Frontiers office electronically for archiving.

4.3 Satellite-Derived 2007 Overflood Limits for the Colville River

As indicated at the outset of this section, the primary objective of the 2007 field program was to enable a quantitative comparison between the overflood limits derived from helicopter-based and satellite-based mapping. Accordingly, the 2007 Colville River overflood limit was derived from satellite imagery without reference to the results of the helicopter-based mapping effort to ensure that the results were unbiased. Suitable images from multiple satellite platforms were available for this purpose, thanks to a fortuitous combination of favorable atmospheric conditions and appropriately-timed satellite passes during the period of interest. Considering the high frequency of cloud cover that typically prevails in the study area during the month of June (including a long-term average of approximately 80% in Barrow; Curtis, 2003), the availability of a full suite of visible satellite imagery was both unexpected and extremely serendipitous.

Satellite images generated within ±6 days of the June 8 helicopter reconnaissance were acquired from various archives. The Landsat archives were searched through USGS EarthExplorer, and selected scenes were purchased from USGS EROS as GeoTiff files. The MODIS archives for the Aqua and Terra visible satellites were searched through the NASA Aeronet Barrow website, and the desired scenes were identified and downloaded with the accompanying GIS data files. The Alaska Satellite Facility (ASF) was used to search for and acquire available Synthetic Aperture Radar (SAR) images. SPOT imagery was pre-ordered prior to conducting the field survey, and without knowledge of when the peak overflood would occur. This approach was necessary because SPOT imagery is not archived, and users must schedule the time and location for image acquisition. Four images spanning a 48-hour period from June 9 to 10 were acquired. A detailed description of the satellite image platforms and the data acquisition process is provided in Section 4.

Only the best images from each platform were selected for interpretation, based on image quality and confidence that the scene depicted the fully-developed overflood. The images utilized from the five satellite platforms are described in Table 4-3. The satellite image dates ranged from June 2 to June 10, and encompassed the helicopter overflight date (June 8). The image quality was judged to be medium to high, while the confidence that each image captured the maximum overflood extent ranged from low to high.

Before mapping the overflood boundaries, the study team evaluated a number of different band combinations (in the case of Landsat) and image stretching to highlight or improve their ability to discern the flood boundaries. Every effort was made to map fine details and local undulations along the overflood boundary. Interior features within the overflood area, such as open water where the ice had melted and dry patches where the ice protruded from the flood water, generally were not mapped. The overflood boundaries were digitized as polygons, and closed where the boundaries intersected the shoreline. A detailed description of the mapping methods was provided in Section 3.

Table 4-3. Satellite Images used to Map 2007 Colville River Overflood

Satellite Platform	Image Date	Resolution	Image Quality	Max Overflood Confidence
Landsat 7	June 4	12-30 m	High	High
MODIS	June 3	250 m	Medium	High
SPOT	June 9 and 10	10 m	Medium	Med-Low
ERS-2	June 2 and 5	30 m	High	High
RadarSat	June 4	30 m	Medium	Med

4.4 Results

The results of the field survey and satellite mapping for the 2007 Colville River overflood are discussed in the sections below. A detailed comparison of the helicopter- and satellite-mapped overflood boundaries also is proved, followed by conclusions.

4.4.1 Helicopter Survey Results

The 2007 Colville River overflood limit derived from the helicopter-based mapping effort is shown in Figure 4-7. The photographs obtained during the overflight reconnaissance are included in Appendix B.

For much of the Colville River Delta, the overflood limit was readily apparent as the boundary between flooded, sediment-laden, or discolored ice on the inshore side, and relatively pristine white, blue, or snow-mottled ice on the offshore side. Strudel drainage also was evident in the overflood area. A representative example of a well-defined overflood limit in the eastern portion of the delta is shown in Figure 4-8.

As discussed in Section 3.1, the ice road constructed to support installation of the Oooguruk Development flowline effectively halted the eastward progression of the river overflood. The linear demarcation corresponding to the ice road is evident in Figure 4-7. At the offshore end of the road, water was observed flowing around the Oooguruk Drillsite (a 6.5-acre manmade island – Hall, 2008) toward the east. The overflood limit in this region did not change appreciably after June 4, when Coastal Frontiers personnel commenced mapping activities on behalf of Pioneer.

The extreme western portion of the overflood limit proved to be more difficult to map. In contrast to the situation described above, the western portion of the overflood area was characterized by relatively clear water and only slightly-stained ice. As a result, the seaward limit of the flood water was difficult to discern. It is speculated that the strong easterly winds described in Section 3.1 drove a thin layer of overflood water to the west after much of the suspended sediment had been deposited onto the sea ice. A representative example of a poorly-defined overflood limit in the western portion of the delta is shown in Figure 4-9.

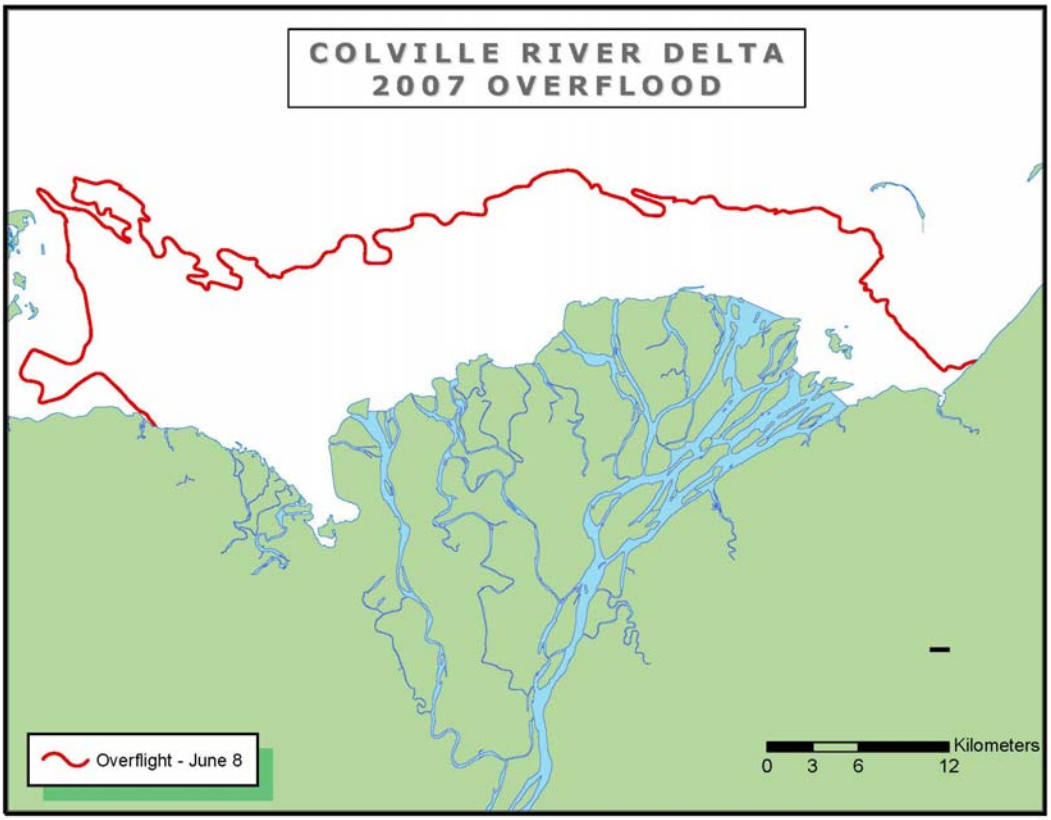

Figure 4-7. 2007 Overflood Limit Mapped During Helicopter Overflight

4.4.2 Satellite Mapping Results

As discussed above, the 2007 Colville River overflood limit was mapped with satellite imagery from five platforms: Landsat 7, MODIS, SPOT, ERS-2, and Radarsat. Figures 4-10 through 4-14 display a representative image and the interpreted overflood boundary for each satellite platform. Each figure also shows the overflood limit derived from the June 8 helicopter survey.

The overflood limits were easily-discernable in the Landsat 7, MODIS, ERS-2, and Radarsat images. In contrast, the seaward extent of the flood water was much less distinct on the SPOT image. As with the helicopter survey, the extreme western portion of the overflood boundary was difficult to interpret and map. As a result, the SPOT interpretation in this area differed significantly from those derived from the other satellite platforms and the field survey. It is speculated that the SPOT image in this area was impacted by a period of sustained gale force (30 kts+) easterly winds that appeared to drive the surface waters on the ice, potentially mixing the former overflood water and natural surface melt water without the characteristic gradation in surface sediment deposition. This situation was exacerbated by the fact that the SPOT image was obtained late in the overflood period (five days after the most recent image from the other satellite platforms and 2 days after the helicopter overflight).

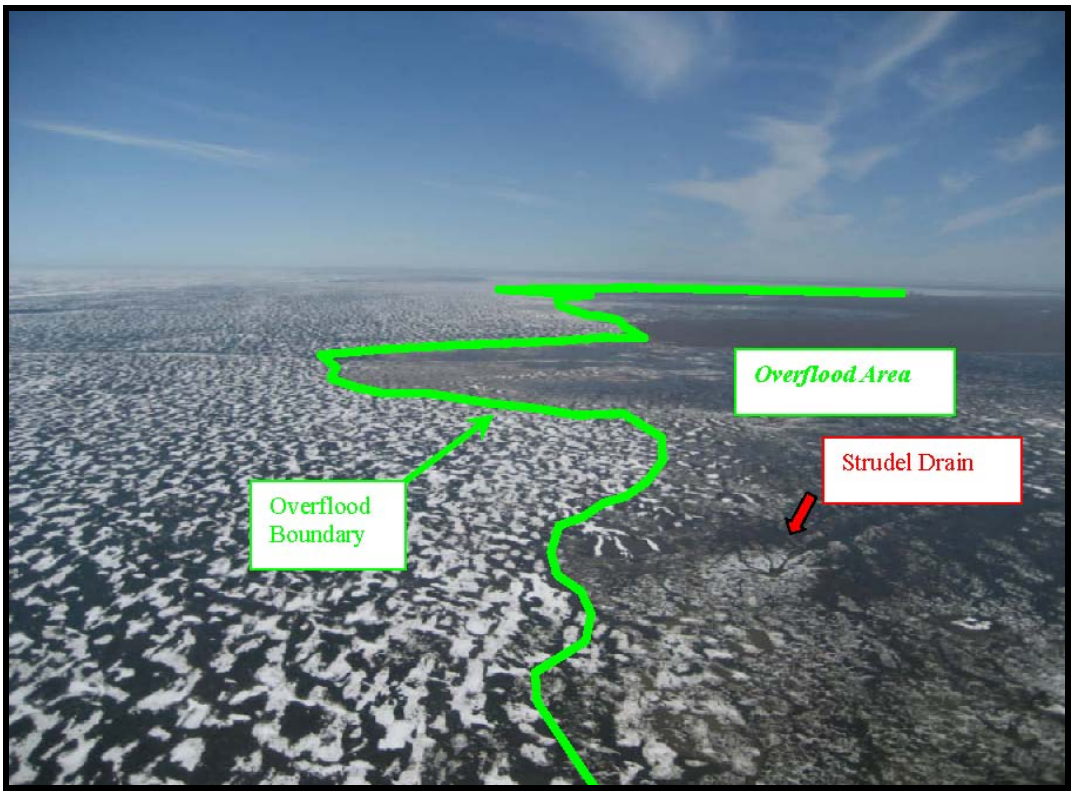

Figure 4-8. Well-Defined Overflood Limit on Eastern Portion of Colville River Delta

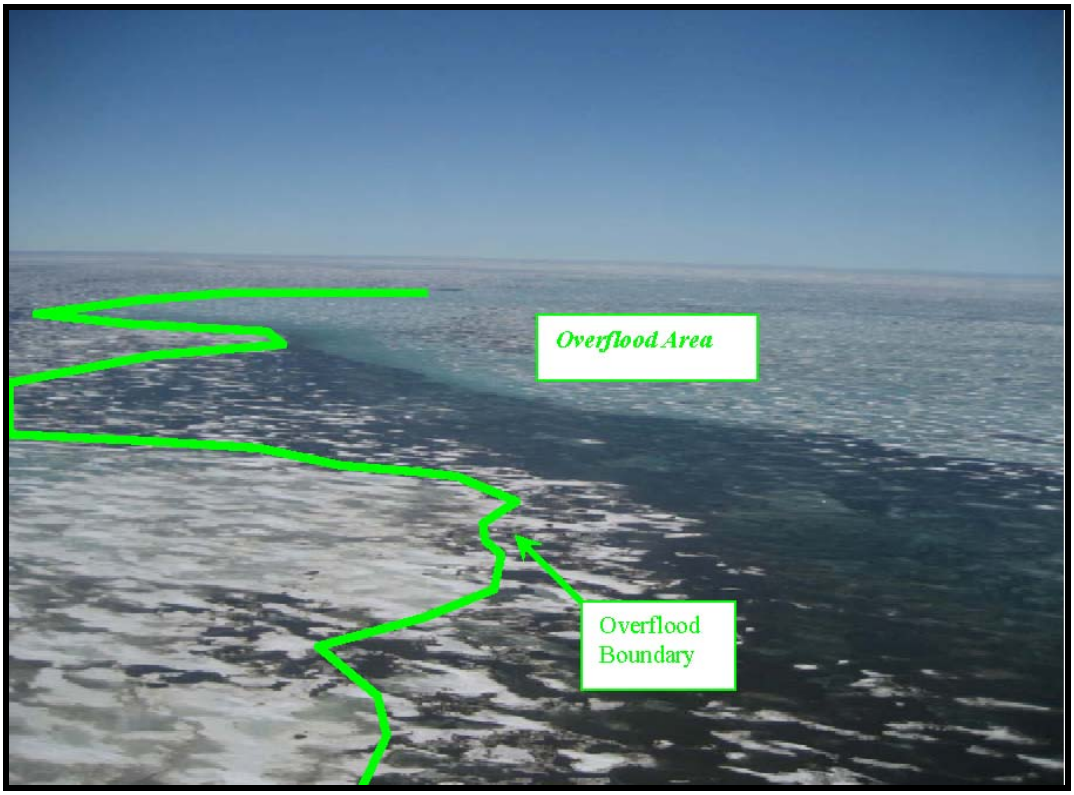

Figure 4-9. Poorly-Defined Overflood Limit on Extreme Western Portion of Colville River Delta

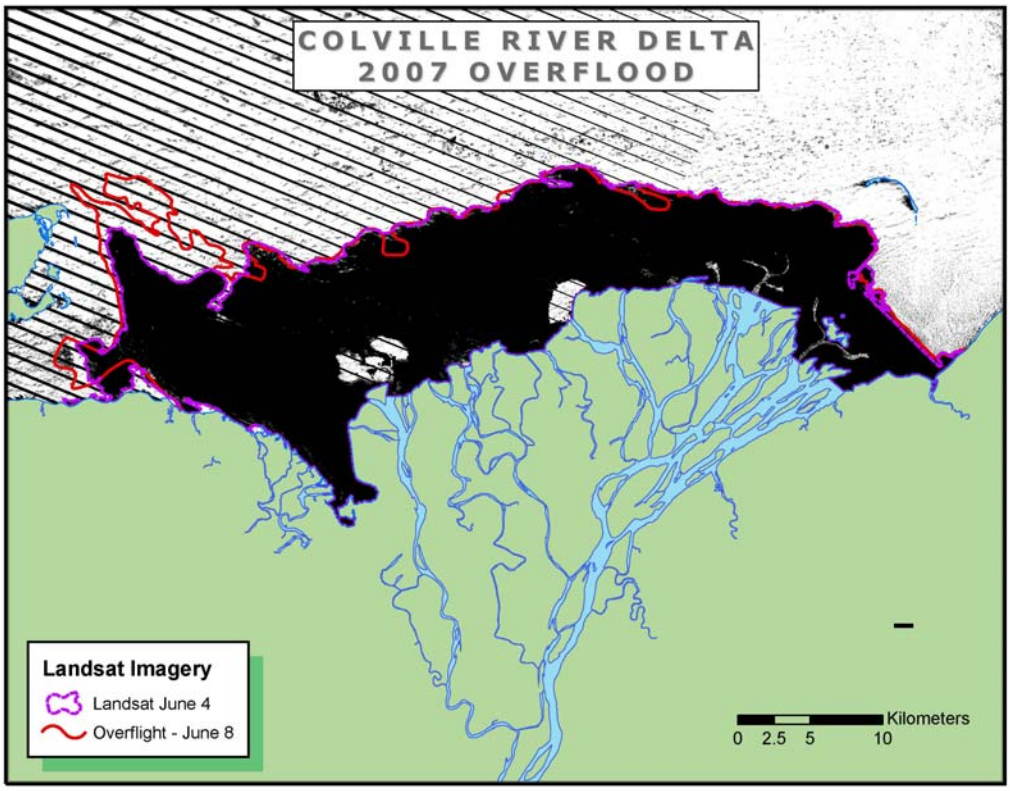

Figure 4-10. 2007 Overflood Limit Mapped Using Landsat Imagery

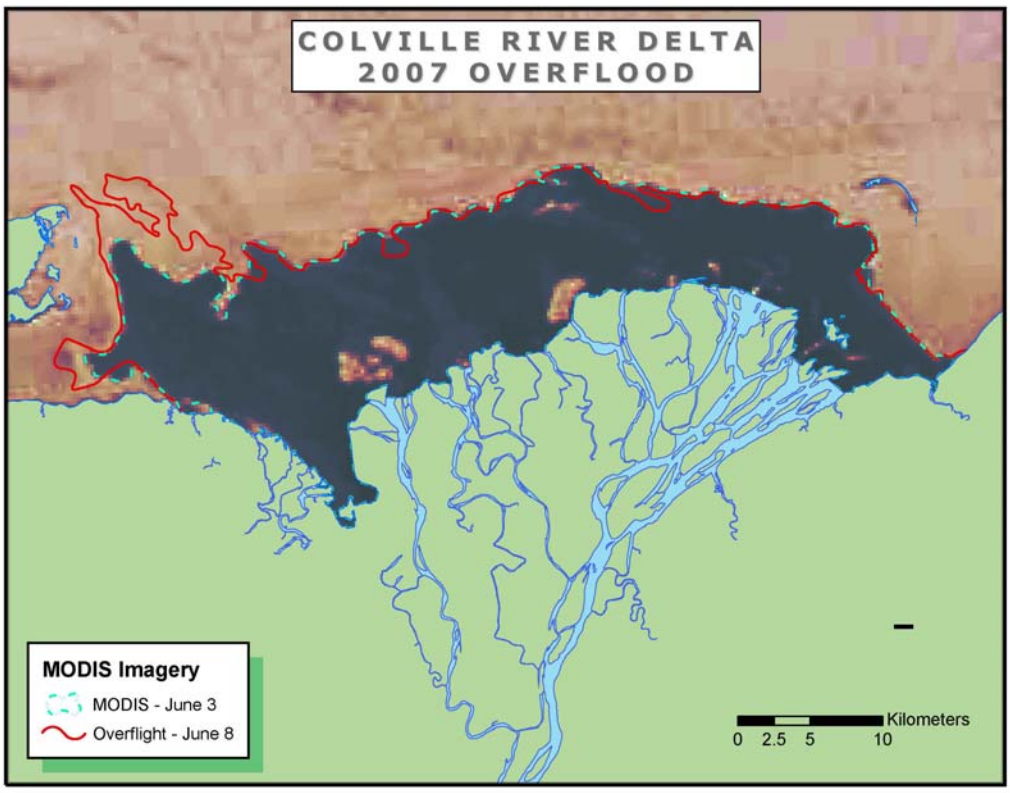

Figure 4-11. 2007 Overflood Limit Mapped Using MODIS Imagery

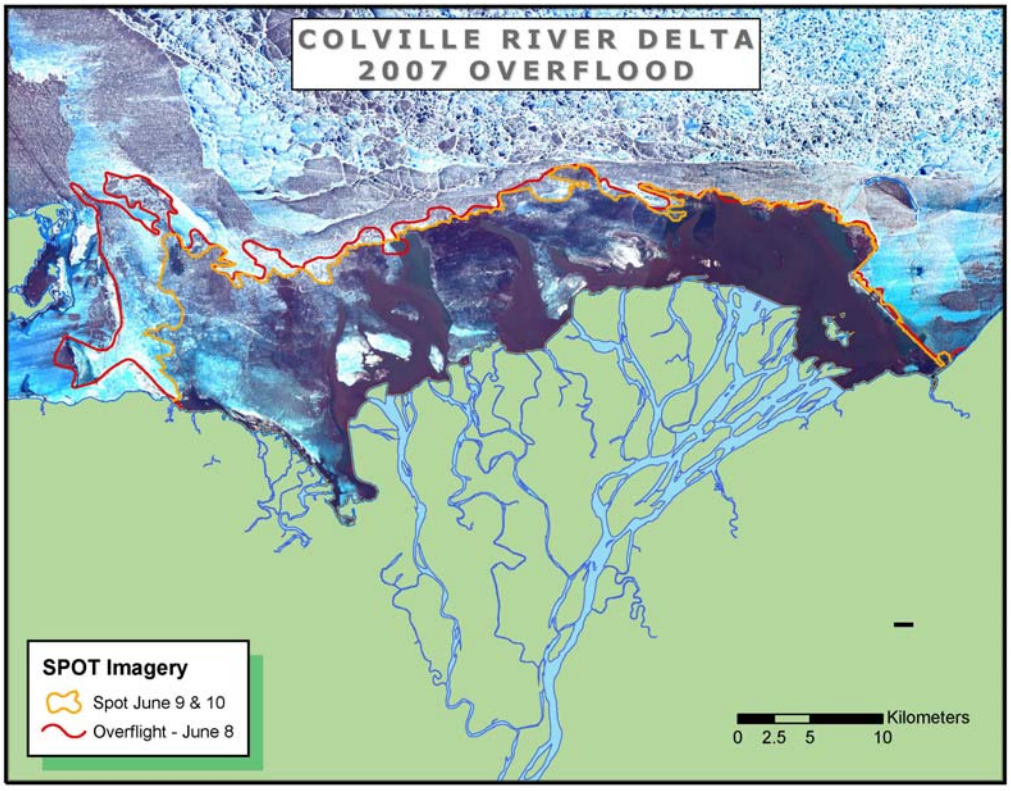

Figure 4-12. 2007 Overflood Limit Mapped Using SPOT Imagery

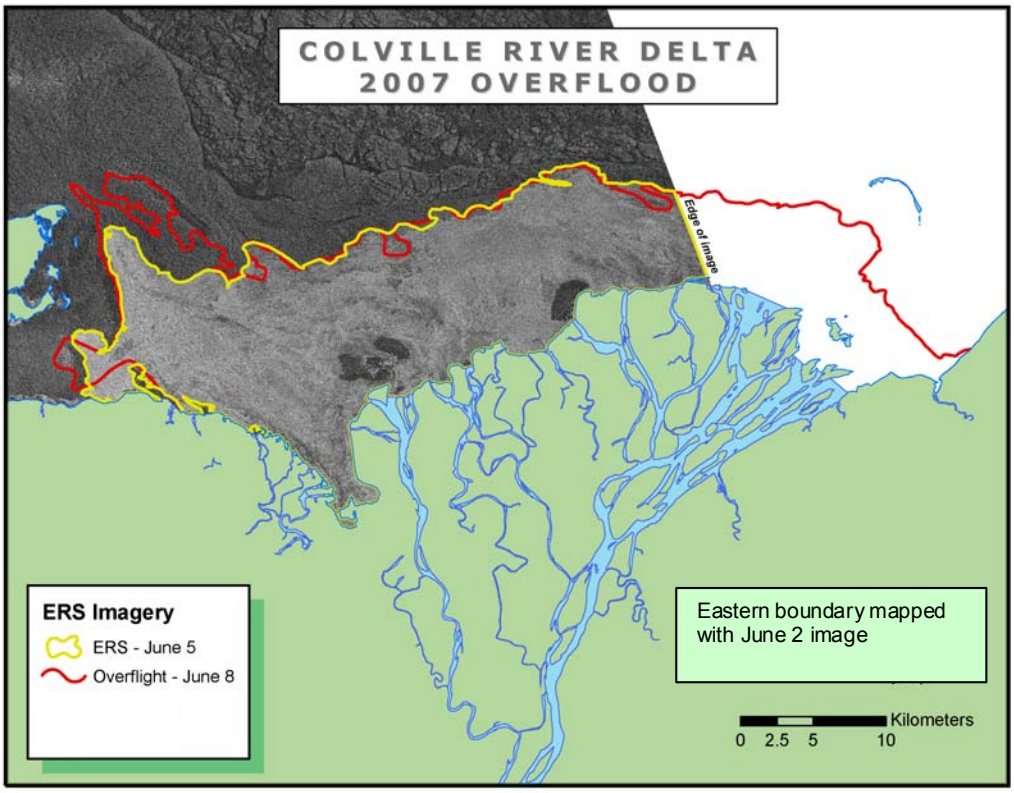

Figure 4-13. 2007 Overflood Limit Mapped Using ERS Imagery

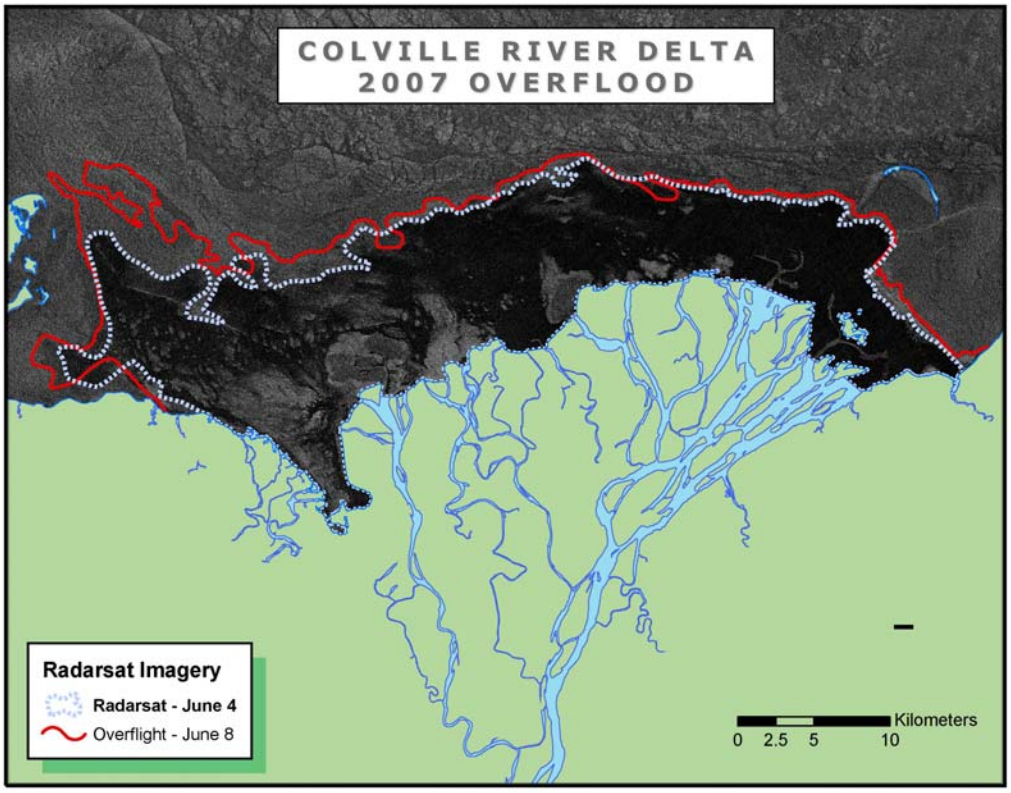

Figure 4-14. 2007 Overflood Limit Mapped Using Radarsat Imagery

4.4.3 Comparison of Helicopter- and Satellite-Mapped Overflood Boundaries

The overflood limit mapped during the helicopter overflight is compared with those derived from the satellite imagery in Figure 4-15. The figure also includes a 54-km baseline with stations at 2-km intervals. The overflood boundaries compare favorably over the majority of the river delta, between Stations 100+00 and 540+00. The greatest discrepancies occur in the western portion of the overflood, between Stations 0+00 and 80+00. Most notably, the western edge of the overflood limit derived from the SPOT imagery lies approximately 5 km to the east of the other limits. As discussed above, it was difficult to interpret this portion of the overflood boundary on the SPOT image.

A first-order comparison between the helicopter-derived overflood limit and the limits developed from each of the satellite platforms is provided by the overflood area computations shown in Table 4-4. The area encompassed by each of the overflood boundaries was calculated using GIS software. The greatest area (576 km^2) was associated with the overflood limit mapped during the helicopter overflight. The areas computed for the Landsat, MODIS, and ERS limits each fell within 10% of this value, while the areas for the SPOT and RadarSat limits were 16% and 14% lower, respectively.

The differences between the helicopter- and satellite-based limits at each of the baseline stations (Figure 4-15) are plotted in Figure 4-16. Table 4-5 provides the average difference and standard deviation relative to the helicopter limit for each of the satellite limits. As discussed above, the extreme western boundary of the overflood was difficult to map during the overflight and challenging to interpret on the SPOT and RadarSat images. Accordingly, Table 4-5 provides

comparisons both for the entire baseline and for those portions of the baseline identified as areas of high-confidence mapping (Stations 100+00 to 540+00) and low-confidence mapping (Stations 0+00 to 80+00).

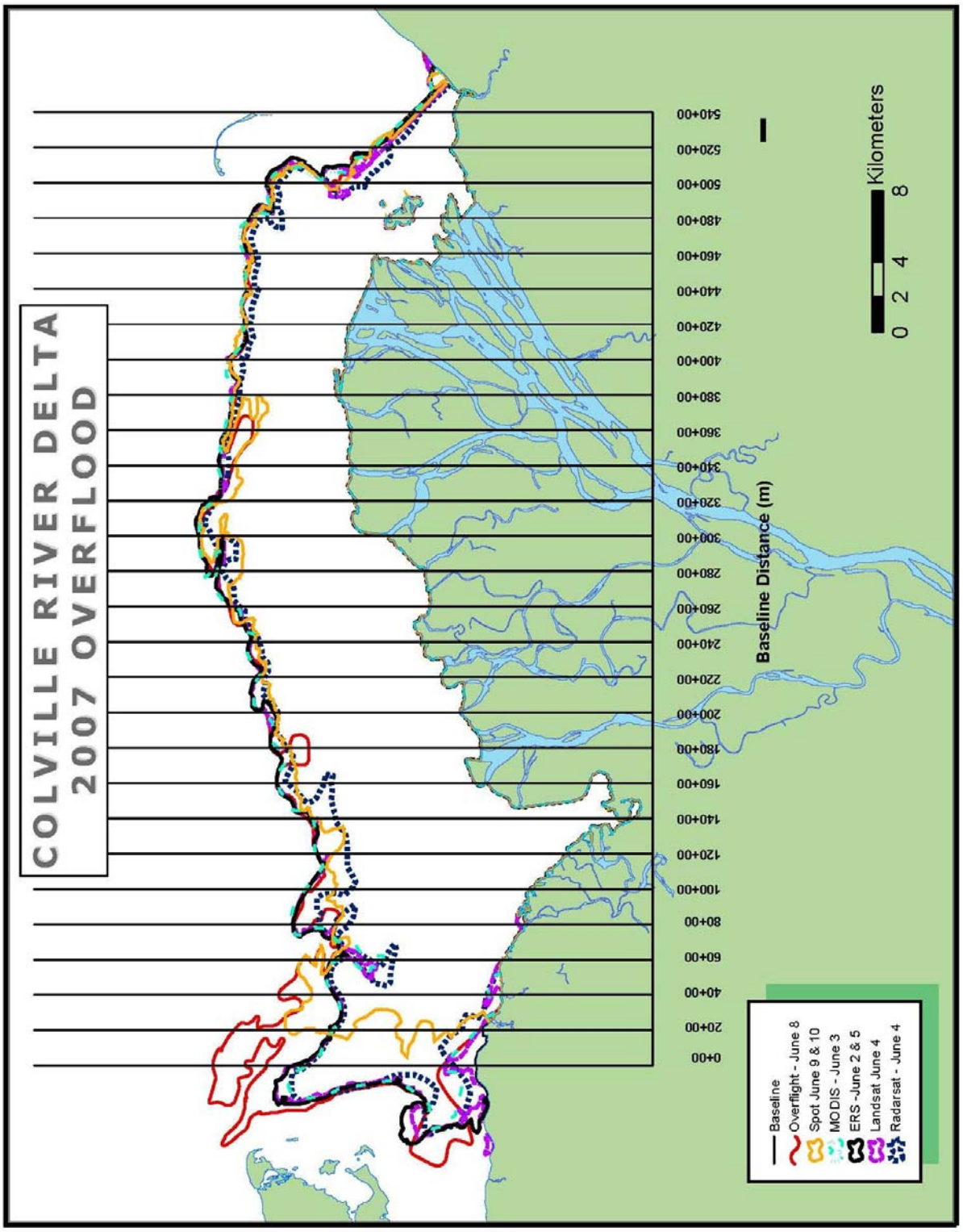

Figure 4-15. Comparison of 2007 Colville River Overflood Limits Derived from Helicopter Overflight and Satellite Imagery

Table 4-4. Overflood Limit Areas

Mapping Source	Date	Area (km^2)	Area Difference Relative to Helicopter Overflight (km^2)	% Difference Relative to Helicopter Overflight
Overflight	June 8	576	n/a	n/a
Landsat 7	June 4	547	-29	5%
MODIS	June 3	545	-31	6%
SPOT	June 9 & 10	490	-86	16%
ERS-2	June 2 & 5	559	-17	3%
RadarSat	June 4	497	-79	14%

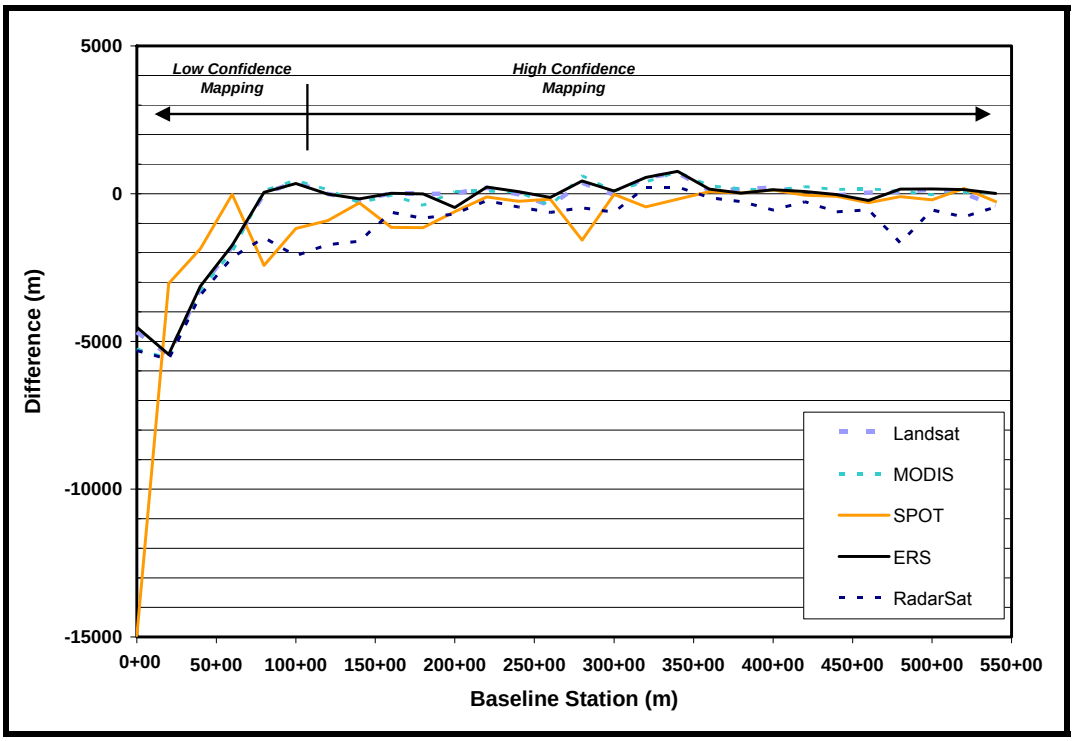

Figure 4-16. Differences between Helicopter-Based Overflood Limit and Satellite-Based Overflood Limits along a 54-km Baseline

The overflood boundaries compare favorably in the area of high-confidence mapping (Stations 100+00 through 540+00). In this region, the Landsat, MODIS and ERS limits were within 760 m of the helicopter limit at all stations. The average discrepancy ranged from 76 m for Landsat to 115 m for MODIS. The comparisons for the SPOT and RadarSat limits were less favorable, with discrepancies exceeding 1 km at several stations. The average differences in the area of high-confidence mapping for SPOT and RadarSat were -381 m and -671 m, respectively.

Table 4-5. Differences between Helicopter-Based Overflood Limit and Satellite-Based Overflood Limits along a 54-km Baseline

Mapping Source	Date	Entire Baseline (Sta. 0+00 to 540+00)		High Confidence (Sta. 100+00 to 540+00)		Low Confidence (Sta. 0+00 to 80+00)	
		Ave Diff. (m)	Std. Dev. (m)	Ave Diff. (m)	Std. Dev. (m)	Ave Diff. (m)	Std. Dev. (m)
Landsat 7	June 4	-480	1499	76	257	-3037	2204
MODIS	June 3	-475	1597	115	273	-3190	2366
SPOT	June 9, 10	-1110	2829	-381	481	-4464	5969
ERS-2	June 2, 5	-448	1478	98	258	-2959	2187
RadarSat	June 4	-1195	1446	-671	590	-3601	1840

Greater discrepancies occurred in the area of low-confidence mapping (Stations 0+00 through 80+00). The maximum differences for the Landsat, MODIS, ERS, and RadarSat limits exceeded 5 km. For the SPOT limit, the greatest difference was nearly 15 km (Station 0+00) because the overflood mapped using this imagery did not extend to the western end of the baseline. The average differences in this low-confidence region ranged from 2,959 m for ERS to 4,464 m for SPOT.

4.5 Discussion

The differences between the helicopter-based overflood limit and those developed from the satellite images may be explained by timing and interpretation of the images:

- Timing: Although the range of image dates (June 2 to June 10) encompassed the date of the helicopter survey (June 8), none of the satellite images corresponded exactly to the timing of the overflight (SPOT being closest).

  River overflood boundaries commonly are mapped after the floodwaters have began to recede. Evidence of the offshore extent of the overflood typically is easily identifiable from the helicopter. This approach provides high confidence that the maximum overflood boundary is documented. However, it is much more difficult to detect formerly flooded areas with the satellite images. This situation likely contributed to the difficulty interpreting the SPOT images, which were obtained late in the overflood period on June 9 and 10.

  Satellite images obtained early in the overflood period appear to be far less difficult to interpret due to the occurrence of the overflood water and sea ice that has yet to deteriorate. However, these images may not capture the fully developed overflood boundary. For example, Figure 4-3 illustrates drastic changes in the overflood boundary between May 30 and June 4. Due to the sensitivity in timing, there is no guarantee that even a sequence of satellite images obtained during the event will capture the fully

developed overflood (as evidenced in 2007 along the extreme western boundary off the Colville).

- Interpretation: As discussed previously, the extreme western portion of the overflood boundary was difficult to interpret during the helicopter overflight and on the SPOT and RadarSat images late in the flooding cycle. The mapping during the helicopter survey was complicated because the overflood area was characterized by relatively clear water and only slightly stained ice. It is speculated that strong easterly winds drove a thin layer of overflood water to this area after much of the suspended sediment had already been deposited onto the sea ice. The overflood mapping in this area was among the most challenging encountered by the field crew during the past decade.

  Each of the limits interpreted from the satellite images failed to match the helicopter derived boundary at the extreme northwest and southwest portion of the overflood area. In all cases, the helicopter mapped limit extended further west. It is possible, that the satellite images were not able to portray subtle changes associated with clear water or lightly sediment stained ice. As noted above, it also is possible that the helicopter survey misinterpreted the overflood boundary in this area. In the case of the SPOT image, interpretation may have been further complicated because the image was obtained even a few days later in the overflood period.

4.6 Conclusions

The following conclusions are suggested by the various boundaries derived for the 2007 Colville River overflood:

1. The most accurate depiction of river overflood limits is provided by helicopter-based mapping techniques. Landsat 7, MODIS, and ERS-2 performed equally well among the satellite platforms and provided the most accurate depiction of the overflood limit relative to the helicopter survey. The SPOT and Radarsat imagery provided the least accurate results. None of the satellite platforms investigated should be excluded from consideration when mapping historical overflood limits. This approach is necessary because the availability of multiple satellite platforms in a given year is rare. This situation did not occur for any of the other twelve years investigated (1995-2006) as part of the overall project.

2. Helicopter-based surveys can be used to map maximum annual overflood limits with high confidence under favorable conditions. Under unfavorable conditions, the survey crew has the opportunity to revisit areas where the edge of the flood water is difficult to discern, or to assign a level of uncertainly to these areas. Advantages of helicopter-based mapping include excellent resolution and the opportunity to make visual observations of unusual circumstances while the mapping is in progress. The obvious disadvantages are the high cost of helicopter operations, and the inability to acquire data on historical overflood events.

3. Under favorable conditions, satellite imagery can be used to derive overflood limits that approach the accuracy of helicopter-based limits. Late in the overflood period and under unfavorable conditions, overflood limits derived from satellite-based imagery can differ materially from those derived from helicopter-based mapping. Advantages of satellite

imagery include cost-effective overflood mapping over large areas (assuming that SAR imagery is readily available through research channels), and the ability to acquire data on historical events. Notable disadvantages include timing and availability of suitable images, and lower accuracy results relative to helicopter-based surveys.

4. While the discussion to this point has focused on mapping of overflood limits, it is important to recognize that river overflood is merely a facilitator of strudel drainage and associated sea floor scouring (an important pipeline design consideration). Helicopter-based surveys currently provide the most reliable means of comprehensively mapping strudel drainage features within the overflood boundary. Consequently, site specific investigations of strudel scour should employ helicopter-based surveys to acquire the drainage feature data necessary to subsequently locate and map scours during the open-water season.

5 OVERFLOOD MAPPING RESULTS, 1995-2007

The primary objective of the historical mapping component of the study was to derive the maximum observed annual overflood limits for all major rivers and streams in the study area (Figures 1-2 and 1-3) during the 13-year period between 1995 and 2007.

This chapter describes the 1995-2007 mapping task, summarizes the data coverage, presents the results, and discusses the findings. The overflood boundaries are presented as overall composite boundaries for all years and as annual maps in Appendix C. The associated ArcGIS database developed through this project contains the overflood areas as geo-referenced polygons along with related image files in MSAccess.

5.1 Helicopter Observations

Overflood boundaries derived from helicopter surveys constituted an important data source for several river systems. During portions of the 1995-2007 study period, overflood mapping surveys were conducted for the Kuparuk, Sagavanirktok, Kadleroshilik, Shaviovik, and Colville Rivers, as well as the local drainages in the Point Thomson area.

River overflood boundaries were obtained from industry studies conducted on behalf of BPXA's Northstar and Liberty Developments, Pioneer's Oooguruk Development, and Shell's Sivulliq Prospect. In each case, the study objectives consisted of mapping river overflood limits and strudel drains in the vicinity of proposed or existing subsea pipelines, and did not necessarily include mapping the entire overflood boundary for a given river. The studies are discussed in greater detail in Section 7. The available helicopter-derived overflood boundaries are summarized in Table 5-1. Access to this information granted by the industry sponsors is gratefully acknowledged.

The mapping methods for the industry studies were described previously in Section 3.1, and were comparable to those used for the 2007 Colville River overflood mapping effort. The overflood boundaries were mapped by recording successive positions with a survey grade GPS unit while flying over the observed boundary at typical altitudes of 30 to 200 m, and at a speed of approximately 60 knots. As discussed in Section 3, the survey accuracy varied from approximately 100 m for the surveys conducted prior to 2000 to up to 1 m for the surveys performed after 2003.

The geo-referenced overflood boundaries derived from the helicopter surveys were obtained in digital format as AutoCAD drawings. These data were imported into the ArcGIS database, and converted to closed polygons.

Table 5-1. Overflood Limits Mapped during Industry-Sponsored Studies

Year	Industry Study and Rivers Surveyed			
	Northstar	**Liberty**	**Oooguruk**	**Sivulliq**
	Kuparuk	*Sag / Kad / Shav*	*Colville*	*Pt. Thomson Area Local Drainage*
1996	✓	-	-	-
1997	✓	✓ / ✓ / ✓	-	-
1998	✓	✓ / ✓ / -	-	-
1999	-	-	-	-
2000	✓	✓ / ✓ / -	-	-
2001	✓	✓ / ✓ / -	-	-
2002	✓	-	-	-
2003	✓	✓ / ✓ / -	-	-
2004	✓	-	-	-
2005	✓	✓ / ✓ / ✓	✓	-
2006	✓	-	✓	✓
2007	✓	-	-	✓

Source: Coastal Frontiers, 1997, 1998a, 1998b, 1999a, 1999b, 2000a, 2000b, 2001a, 2002, 2003a, 2003b, 2004, 2005, 2006a, 2006b, 2007a, 2007b, 2007c, 2008a, 2008b

5.2 Satellite Imagery

Satellite imagery formed the key data source needed to develop the final mapped boundaries of peak overflood extent over the full 13-year time period. All applicable satellite imagery from 1995 to 2007 was accessed for as many river systems as possible in the study area from (Figure 1-1). The methods used to map the peak overflood seaward boundaries using satellite imagery are described fully in Section 3, and summarized below according to the main activities in chronological order:

Image Search and Acquisition: The historical archives of images with sufficient temporal and spatial coverage and resolution were searched for scenes obtained during the estimated overflood time window. Satellite platforms included Radarsat, ERS 1 and 2, Landsat 5 and 7, and MODIS. This process resulted in the acquisition of nearly 200 images (primarily Radarsat and ERS-1 and 2).

Image Screening: The images were screened by examining lower-resolution jpeg files to determine whether the image quality, timing and coverage area justified further interpretation.

Overflood Boundary Mapping: The image files were loaded into ArcGIS v. 9.1 and the overflood boundaries were digitized as closed polygons. An effort was made to map fine features along the overflood boundary, such as localized undulations.

Each image was assigned a quality ranking according to the levels of confidence that the image: (1) captured the peak overflood extent in terms of timing (neither too early to too late); and (2) displayed a clear seaward overflood boundary with sufficient discrimination from the surrounding, undisturbed sea ice.

A total of 64 images was used to carry out the 13-year historical mapping task: 21 Landsat, 38 Radarsat/ERS, 4 MODIS and 1 SPOT (2007 only). The image catalog is provided in Appendix F. Included in the catalog are the image resolution, river systems covered, and the image quality rankings.

5.3 Developing Composite Overflood Limits

The final mapped boundaries for each overflood were derived by integrating all of the polygons mapped from the satellite imagery with any available helicopter survey data. Specifically, the peak overflood limit at any longitudinal position was assumed to correspond to the most seaward mapped boundary regardless of the data source. In this manner, a final composite boundary could contain data from a number of different images and/or portions of a helicopter survey, depending on which source showed the floodwaters furthest from shore at any given point along the overflood front. Figure 4-15 from the previous section provides an extreme example of how multiple data sources (five satellite-derived boundaries and one helicopter-based boundary) were used to arrive at the maximum overflood extent. Throughout this process, no preference was given to one type of data over another such as: helicopter vs. satellite or ERS vs. Radarsat.

5.4 Mapping Results

Figure 5-1 provides a matrix identifying the composite overflood limits that were mapped for each major river and year from both the historical satellite imagery and helicopter surveys. (Refer to Figures 1-2 and 1-3 for river locations.) A blank cell in the matrix indicates that an overflood limit was not mapped because: (1) imagery and/or helicopter surveys were not available; or (2) the available imagery was either too early or late to capture the full extent of the overflood. Overflood limits were mapped for 129 out of 143 possible significant river and year combinations, resulting in a mapping success of 90%. This result exceeded expectations, and would not have been possible without having access to both the radar imagery and helicopter surveys.

Figures 5-2 and 5-3 show the combined composite overflood boundaries for the West and East Study areas (Figures 1-2 and 1-3, respectively) for the complete period of interest, 1995-2007. Appendix C contains the full polygon data set including smaller rivers and creeks tabulated according to maximum offshore and lateral extent (km) and area (km^2) together with the dates for peak extent as mapped in each of the 13 years.

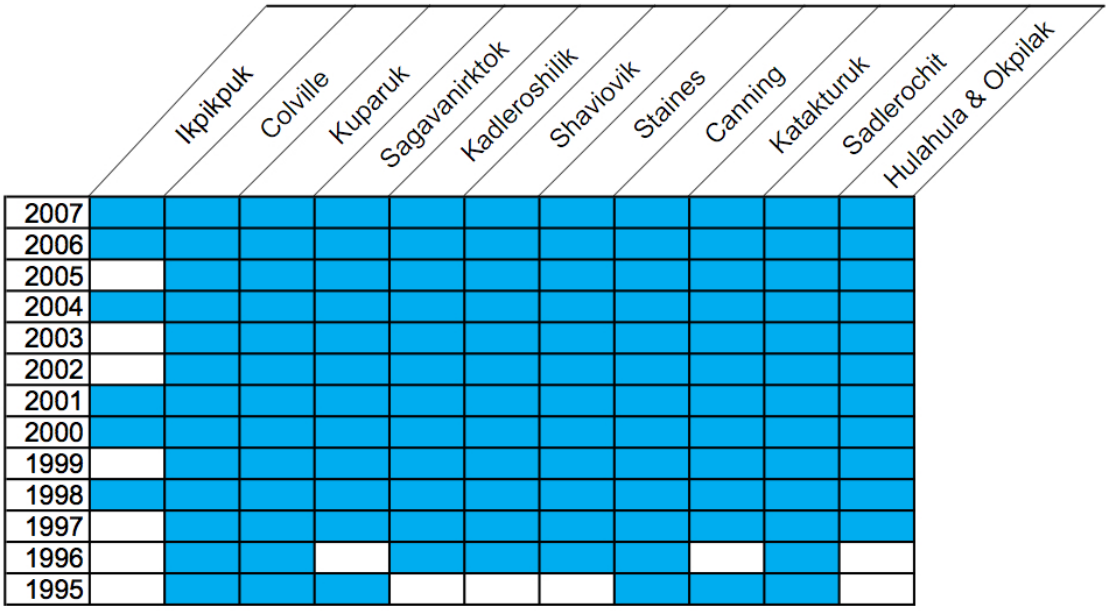

Figure 5-1. Matrix of Mapped Overflood Limits, 1995-2007

Note: *Blue shading indicates years in which the overflood boundaries of major rivers were mapped in this study. Figures 1-2 and 1-3 show the locations of all major rivers and numerous smaller watercourses covered in the full database.*

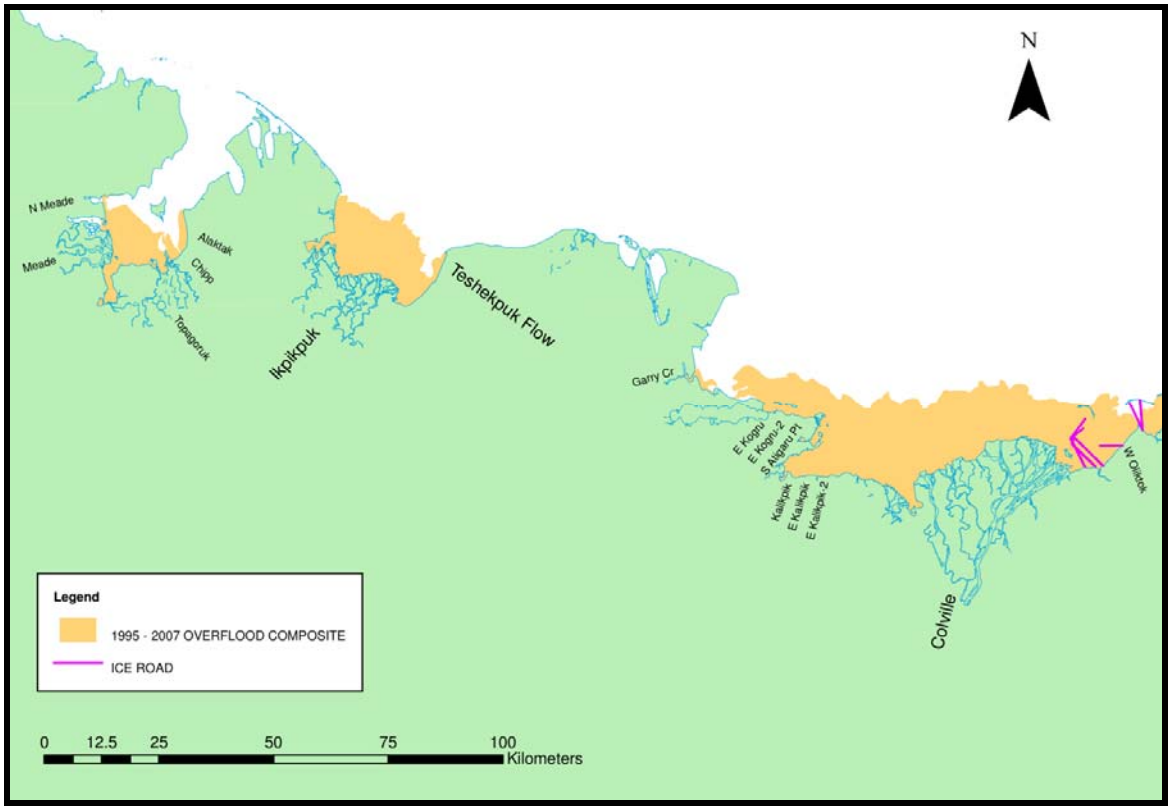

Figure 5-2. 1995-2007 Composite Overflood – West Study Region

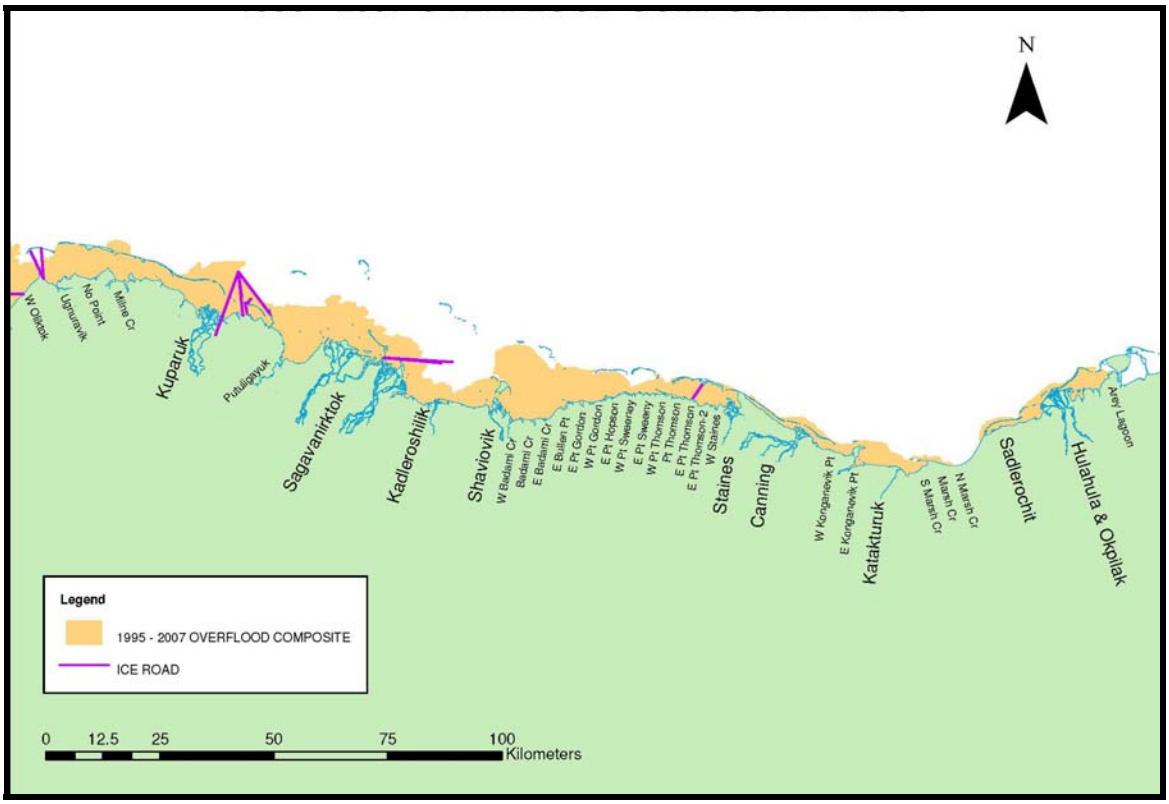

Figure 5-3. 1995-2007 Composite Overflood – East Study Region

5.5 Discussion

Figure 5-4 compares the overflood areas generated within the ArcGIS Database for the same 11 rivers used to display the data density in Figure 5-1. Although the results show that above- or below-average overfloods may occur in the same year for the three major rivers in the central study area (i.e., the Colville, Kuparuk and Sagavanirktok experienced above-average floods in 2004 and 2002, and below-average floods in 1997 and 1999), the correspondence is far from consistent. There are several examples where one river experienced an unusually small or large overflood without the adjacent rivers following suit. The comparison shows no clear temporal patterns in occurrence of minimum or maximum overflood between rivers in the East and West Study Regions.

The Shaviovik overflood area is relatively consistent from year to year but 2002 stands out with a mapped area close to double that in most other years. This explains why the Shaviovik overflood seaward boundary appears so far to the north (well beyond Tigvariak Island) in the combined composite of all years shown in Figure 5-3.

In terms of its contribution to the combined overflood area along the Alaskan Beaufort Sea Coast, the Colville River clearly dominates with an annual average of 717 km^2, more than three times larger than that of the second and third largest contributors, the Kuparuk and Sagavanirktok. None of the other sources of freshwater discharge generates a significant overflood relative to the Colville. Outside of the "top three" rivers, the individual overflood areas drop by a further order of magnitude. For example, the total average area for all 7 "major"

rivers east of the Sagavanirktok adds up to only 192 km^2, or just equal to the average for the Sagavanirktok itself. The Ikpikpuk overflood is not included in this comparison because of the relatively few years with data and lack of evidence that overflood in this area is an annual event.

	Overflood Areas in km^2										
	Ikpikpuk	Colville	Kuparuk	Sagavanirktok	Kadleroshilik	Shaviovik	Staines	Canning	Katakturuk	Sadlerochit	Hulahula & Okpilak
2007	94	603	98	178	20	85	86	16	9	15	31
2006	165	741	275	213	16	56	34	83	12	8	42
2005		771	240	137	16	64	11	27	8	5	26
2004	225	1011	263	247	11	64	36	33	13	13	22
2003		544	217	155	18	73	12	9	3	6	15
2002		909	262	233	25	109	23	40	4	5	38
2001	54	761	225	237	16	68	31	32	18	11	54
2000	284	858	142	177	19	69	20	20	14	16	61
1999		485	73	140	12	51	19	16	4	6	27
1998	11	792	158	260	18	59	36	16	2	5	19
1997		510	105	146	11	60	16	31	12	18	46
1996		598	96		4	28	15	26		5	
1995		735	90	209				29	13	9	
AVG	**139**	**717**	**173**	**194**	**16**	**66**	**28**	**29**	**9**	**9**	**35**

	Overflood areas substantially above average
	Overflood areas substantially below average

Figure 5-4. Comparison of Overflood Areas for Major Rivers – West to East

When reviewing the overflood boundaries developed for this study, it is important to consider the role that man-made features (such as ice roads and causeways) play in modifying or limiting the final distribution of the overflood. Table 5-2 summarizes the ice roads constructed in the project area between 1996 and 2007. Ice road locations were derived primarily from industry studies and reports, government agency publications, and personal communication with industry and construction representatives. During the 1995-2007 study period, 21 ice roads were constructed in support of industry projects. The year of construction, purpose, and geographic location of each road is incorporated into the ArcGIS database. The composite overflood maps contained in Appendix C include the locations of the ice roads present during each year to aid in interpreting the overflood limits.

Prior studies have noted the influence that man-made features can have on the overflood boundaries (Dickins, *et al*., 2001). In one example, Vaudrey commented that the Endicott Causeway, under construction in 1985, clearly influenced the overflood limits in northwestern Foggy Island Bay mapped in his helicopter survey on May 23 of that year (Vaudrey, 1986). Following completion of the causeway, it appeared that a greater "bulb" of water flowed out onto the ice between Point Brower and the old Duck 3 Island. Atwater (1991) also evaluated the effect of the causeway by comparing the timing of key overflood events pre- and post-construction based on an analysis of NOAA satellite imagery between 1983 and 1998.

Table 5-2. Ice Road History in the Project Area

Winter Season	BPXA *Northstar*	BPXA *Liberty*	Pioneer *Oooguruk*	ENI (Kerr McGee) *Nikaitchuq*	Savant *Kupcake*	Exxon *Pt. Thomson*
95-96	✓					
96-97		✓				
97-98						
98-99	✓					
99-00	✓					
00-01	✓					
01-02	✓					✓
02-03	✓		✓			
03-04	✓			✓		
04-05	✓			✓		
05-06	✓		✓			
06-07	✓		✓			
07-08	✓		✓	✓	✓	

Source: Brady, 2008; Brott, 2008; Coastal Frontiers, 2001b and 2007d; Market Wire, 2008; MMS, 2006; Northstar Project Team, 1996; Petroleum News, 2007; Sandwell Engineering, 2003; Smith, *et al.*, 2007; State of Alaska, Dept. of Natural Resources, 2006; US Army Corps of Engineers, 1998; Workman, 2008.

In a more recent example, during the construction of Northstar Island in June 2000, the combination of the enhanced freeboard of the ice road, snow and ice berms along the road, and the ice trench used for pipeline installation established an artificial barrier that effectively restricted further spreading to the east during the spring overflood from the Kuparuk River. The effect is shown dramatically in Figure 5-5 (extracted from Figure 3.8 in Section 3.2), and in the 2000 composite overflood map shown in Appendix C. The influence of Northstar project ice roads on the Kuparuk River overflood also is apparent in 2001 and 2002 (Appendix C).

More recently, in 2007, the ice road constructed along the Oooguruk flowline prevented the overflood waters from spreading farther east and created a sharp transition as shown below in Figure 5-6. This phenomenon was discussed in greater detail in Section 4.

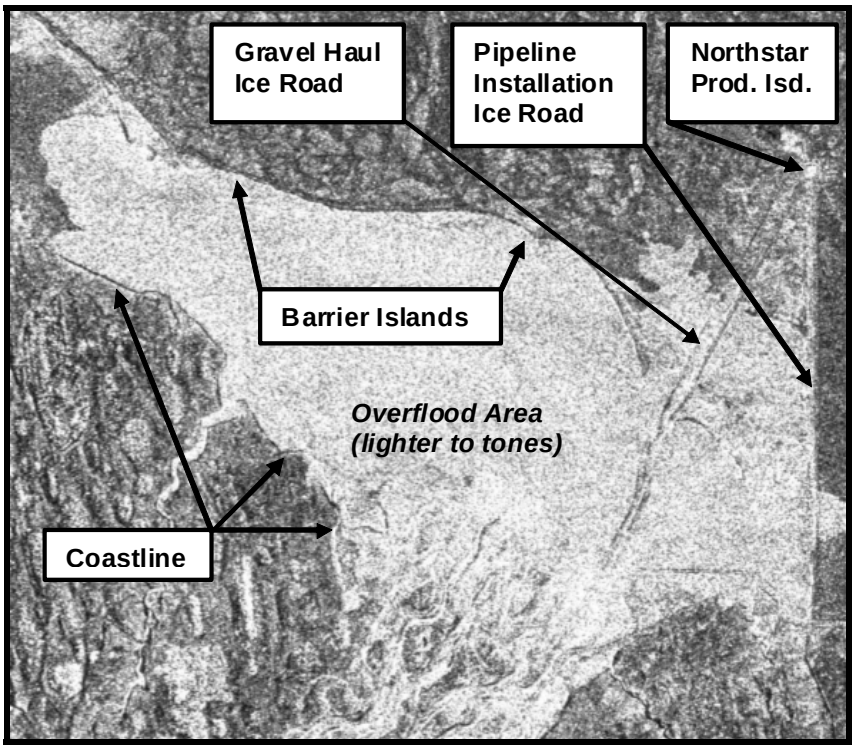

Figure 5-5. Radarsat Image of the Kuparuk Overflood on June 11, 2000

Note the impact of the Northstar ice road in containing the overflood waters.

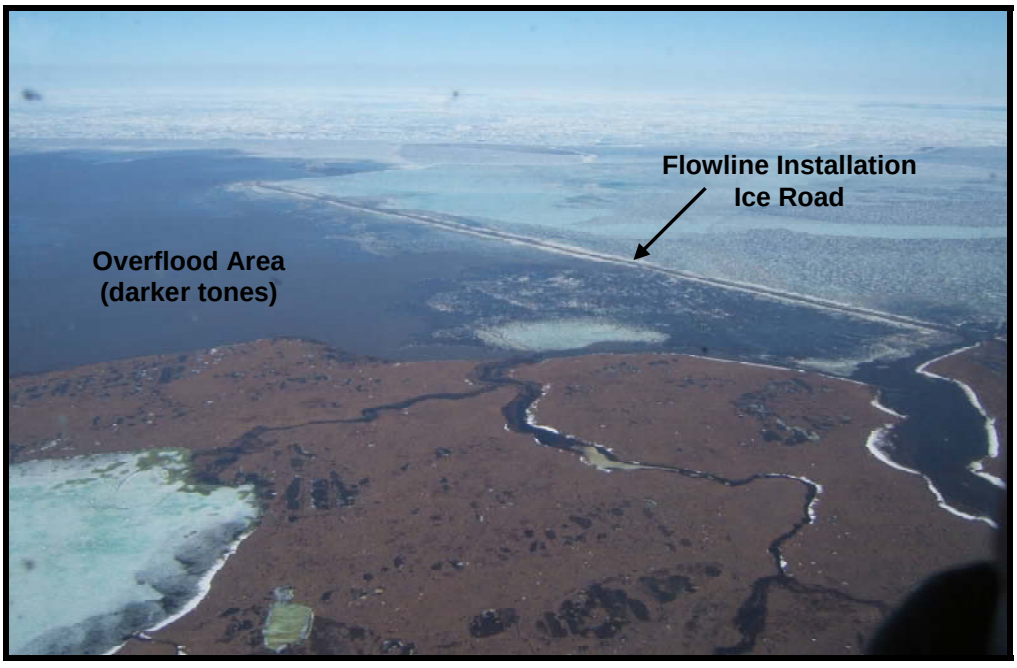

Figure 5-6. Aerial View of the Oooguruk Ice Road Blocking the Colville River Overflood, June 2007

6 ENVIRONMENTAL VARIABLES CORRELATION

River overflood on the sea ice is a complex phenomenon that likely is affected by the interaction of multiple variables including streamflow, precipitation, air temperature, snow depth on the ice sheet, tidal cracks and strudel drains, pressure ridges and other obstacles on the ice sheet, ice jams in river channels, freeze-back, wind, insulation, and man-made features such as ice roads. This section presents an analysis undertaken to fulfill two objectives:

1. Search for correlations between the suspected environmental driving forces to determine if one can be used as a proxy for others, or if two or more can be used interchangeably, and

2. Search for correlations between each suspected environmental driving force and overflood area to provide a means of predicting the severity of future overflood events.

Streamflow, precipitation, and air temperature were considered in the analysis. While the other factors listed above also may exert a significant influence, they are not addressed due to a lack of available data. The environmental variables were compared with the overflood areas derived for the Colville, Kuparuk and Sagavanirktok Rivers for the period from 1995 through 2007. These rivers were selected for investigation both because they produce the largest overfloods in the study area (Figure 5-4), and because at least five years of streamflow measurements are available for each river.

6.1 Environmental Variables

Table 6-1 summarizes the North Slope meteorological and streamflow monitoring stations used in this investigation. These monitoring stations were selected primarily on the basis of location, period of record, and availability of non-proprietary data. Other data sources were explored, but eliminated from further consideration because they were repetitive or did not encompass the period of interest.

It should be noted that data gaps exist in nearly all of the records. For the purposes of this study, additional variables were derived from the source data. The precipitation, air temperature, and streamflow characteristics for the 1995 to 2007 period are described below.

6.1.1 Streamflow

Daily streamflow data for the Colville, Kuparuk and Sagavanirktok Rivers were obtained from the US Geological Survey (USGS, 2008). Characteristics for each gauge are provided in Table 6-2. While the Kuparuk gauge is located near the coast, the Colville and Sagavanirktok gauges are located approximately 150 km inland.

Table 6-1. North Slope Meteorological and Streamflow Stations

Location	Period [1]	Data Type	Source [2]
Atigun Pass	1983-2007	Precipitation/Snowfall/Temp.	NRCS
Atigun Camp	1983-2007	Precipitation/Snowfall	NRCS
Imnaviat Creek	1982-2007	Precipitation/Snowfall	NRCS
Sagwon	1983-2007	Precipitation/Snowfall	NRCS
Prudhoe Bay	1979-2007	Precipitation/Snowfall	NRCS
Kuparuk	1982-2007	Temperature	WRCC
Colville Umiat	2003-2007	Streamflow	USGS
Kuparuk	1971-2007	Streamflow	USGS
Sagavanirktok	1983-2007	Streamflow	USGS

[1] Data gaps exist.
[2] National Resource Conservation Service (NRCS); Western Regional Climate Center (WRCC); United States Geological Service (USGS).

Table 6-2. USGS Streamflow Gauge Characteristics

Gauge	Location (NAD27)		Elevation (m)	Drainage Area (m^2)
	Latitude	Longitude		
Colville River (at Umiat)	69°21'38" N	152°07'18" W	84	35,800
Kuparuk River (near Deadhorse)	70°16'54" N	148°57'35" W	0	8,100
Sagavanirktok River (near Pump Sta. 3)	69°00'54" N	148°49'02"W	350	4,800

Streamflow hydrographs for the May-June period of each overflood year were generated for the three rivers. A flood threshold was selected for each river by inspecting the hydrographs. Using this value, the breakup period was defined as the day immediately prior to the streamflow rising above the threshold to the first day after the streamflow dropped below the threshold. Flood threshold values of 600 m^3/s, 225 m^3/s, and 150 m^3/s were chosen for the Colville, Kuparuk, and Sagavanirktok Rivers, respectively.

Four streamflow parameters were derived for each river using the hydrographs and the flood threshold values. The *peak discharge* (m^3/s) was defined as the highest daily streamflow value measured during the breakup period. The *average discharge* (m^3/s) was calculated as the mean of the daily streamflow values measured during the breakup period. The *total discharge volume* (m^3) during the breakup period was determined by measuring the area under the hydrograph for this period. The *flood intensity* (m^3/s/day), which provides an indication of how quickly the flood developed, was computed as the slope of the rising limb of the hydrograph.

The streamflow parameters are defined graphically in Figure 6-1, which shows the 2003 hydrograph for the Colville River.

The streamflow characteristics for the Colville, Kuparuk and Sagavanirktok Rivers are summarized in Tables 6-3, 6-4 and 6-5, respectively. The streamflow characteristics attain their highest values for the Colville River, while the lowest values are associated with the Kuparuk River. The greatest peak and average streamflow occurred in 2000 for the Kuparuk and Sagavanirktok Rivers (data not available prior to 2003 for the Colville).

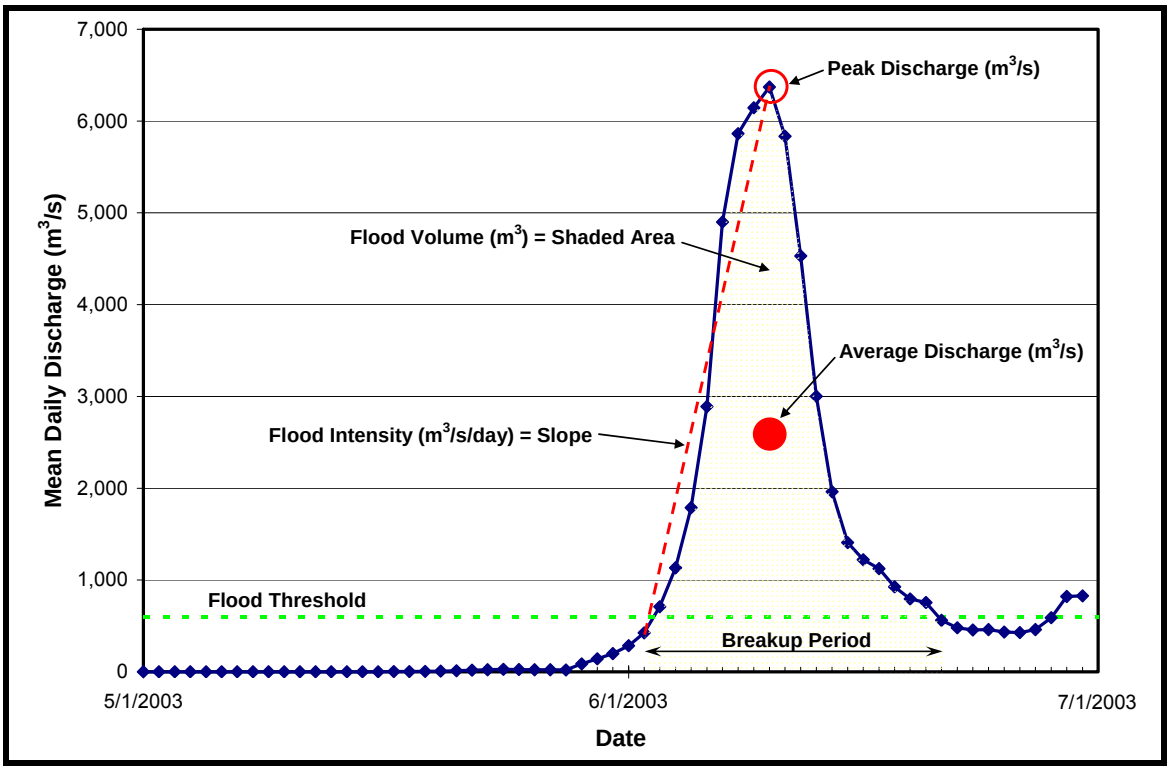

Figure 6-1. Streamflow Parameters (Colville River, 2003)

6.1.2 Precipitation

Accumulated precipitation data (snowpack size expressed as equivalent cm of water) were acquired from the National Resources Conservation Service (NRCS) for five stations: Atigun Pass, Atigun Camp, Imnaviat Creek, Sagwon, and Prudhoe Bay (NRCS, 2008). The stations are shown in Figure 6-2, with details provided in Table 6-6. Geographically, the stations range from the Brooks Range (Atigun Pass, elevation 1462 m) to the coast (Prudhoe Bay, elevation 9 m). These stations are believed to represent the best available precipitation indicators for the drainage basins in the study area. However, they provide neither comprehensive nor evenly-spaced coverage of the area of interest.

Table 6-3. Colville River Streamflow Characteristics during Break-up Period

Year	Peak Q (m^3/s)	Average Q (m^3/s)	Flood Volume (m^3)	Flood Intensity ($m^3/s/day$)
1995	-	-	-	-
1996	-	-	-	-
1997	-	-	-	-
1998	-	-	-	-
1999	-	-	-	-
2000	-	-	-	-
2001	-	-	-	-
2002	-	-	-	-
2003	6,372	2,617	4,521,775,104	661
2004	6,429	2,385	4,532,541,235	1,466
2005	4,843	2,247	6,212,791,757	269
2006	4,503	2,100	2,358,272,102	694
2007	5,098	2,276	2,949,675,264	566
Average	*5,449*	*2,325*	4,115,011,092	*731*
Maximum	*6,429*	*2,617*	6,212,791,757	*1,466*
Minimum	*4,503*	*2,100*	2,358,272,102	*269*

Table 6-4. Kuparuk River Streamflow Characteristics during Break-up Period

Year	Peak Q (m^3/s)	Average Q (m^3/s)	Flood Volume (m^3)	Flood Intensity ($m^3/s/day$)
1995	566	382	692,213,299	90
1996	1,529	673	930,120,330	283
1997	1,631	614	1,060,463,923	135
1998	1,272	546	566,151,690	157
1999	564	350	3,934,776,27	113
2000	2,209	784	1,015,833,416	363
2001	1,558	607	62,974,570	361
2002	1,416	699	483,228,012	425
2003	1,218	545	517,850,911	221
2004	850	524	814,506,762	71
2005	949	468	808,609,859	68
2006	850	401	623,603,681	159
2007	1,747	759	524,848,896	310
Average	1,258	566	747,127,909	212
Maximum	2,209	784	1,060,463,923	425
Minimum	564	350	62,974,570	68

Table 6-5. Sagavanirktok River Streamflow Characteristics during Break-up Period

Year	Peak Q (m^3/s)	Average Q (m^3/s)	Flood Volume (m^3)	Flood Intensity ($m^3/s/day$)
1995	286	197	119,161,498	63
1996	391	249	193,814,830	37
1997	351	225	389,440,328	49
1998	419	229	197,436,165	72
1999	221	179	138,980,966	16
2000	708	323	586,313,718	149
2001	309	206	195,429,750	35
2002	227	160	69,001,114	78
2003	397	255	462,576,614	50
2004	397	255	395,802,132	28
2005	229	181	125,400,960	15
2006	283	188	97,384,550	60
2007	283	191	148,499,205	24
Average	346	218	239,941,679	52
Maximum	708	323	586,313,718	149
Minimum	221	160	69,001,114	15

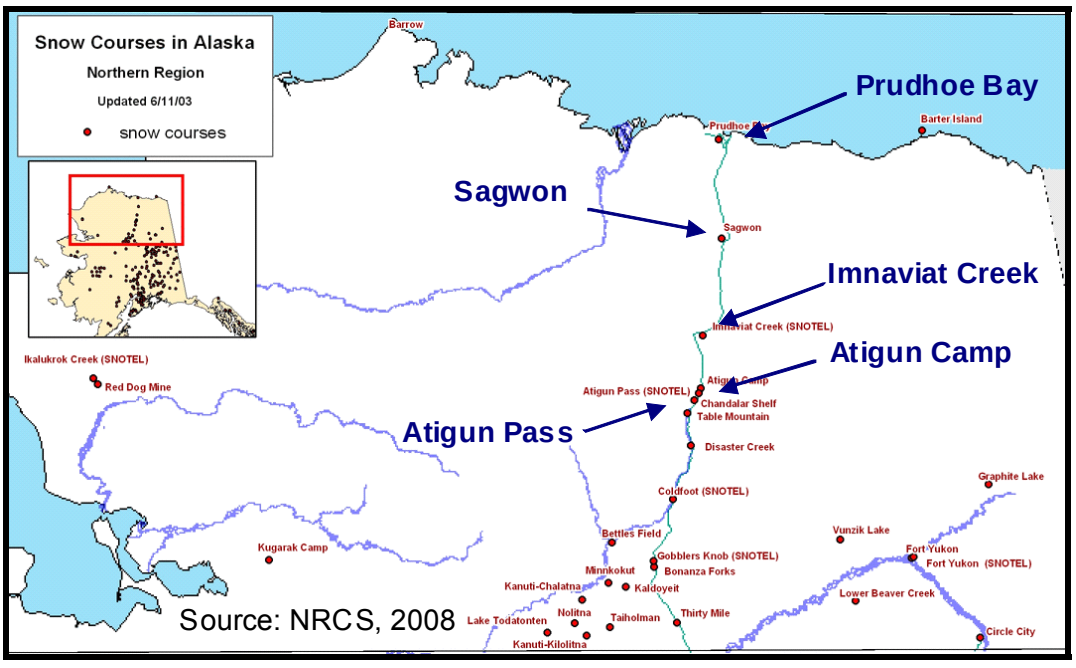

Figure 6-2. NRCS Snow Survey Sites Locations

Table 6-6. NRCS Snow Survey Site Characteristics

Site Name	Location (NAD83)		Elevation (m)	Hydrographic Unit
	Latitude	Longitude		
Atigun Pass	68° 08.00'N	149° 28.00'W	1462	Middle/North Fork Chandalar R.
Atigun Camp	68° 10.37'N	149° 25.88'W	1036	Atigun River
Imnaviat Creek	68° 37.00'N	149° 18.00'W	929	Kuparuk River
Sagwon	69° 25.43'N	148° 41.72'W	305	Sagavanirktok River
Prudhoe Bay	70° 15.00'N	148° 34.00'W	9	Sagavanirktok River

To provide an indication of the water available for river overflood in the spring, accumulated precipitation was tabulated at each station for the period October 1 to May 31. The results are provided in Table 6-7. The highest average precipitation occurred at Atigun Pass (21.6 cm), while the lowest occurred at Sagwon (8.3 cm). During the 13-year period of record, the highest precipitation occurred in 1995 (based on the three stations for which continuous data were available).

Table 6-7. Accumulated Precipitation at North Slope Monitoring Stations

Year	Accumulated Precipitation – October 1 to May 31 (cm)				
	Atigun Pass	Atigun Camp	Imnaviat	Sagwon	Prudhoe Bay
1995	28.7	14.0	-	10.2	-
1996	-	9.9	15.5	9.4	16.3
1997	19.1	10.2	8.1	-	10.9
1998	25.7	11.4	7.4	-	16.8
1999	16.0	8.9	7.1	-	10.7
2000	20.6	11.7	5.6	-	16.0
2001	20.6	7.6	6.9	-	12.7
2002	21.1	8.9	7.6	6.9	8.4
2003	26.9	10.7	20.6	7.9	11.2
2004	19.1	8.4	-	-	13.0
2005	22.9	8.9	9.1	8.9	11.7
2006	20.8	9.4	8.9	8.6	-
2007	18.3	7.9	9.9	6.6	10.7
Average	21.6	9.8	9.7	8.3	12.6
Maximum	28.7	14.0	20.6	10.2	16.8
Minimum	16.0	7.6	5.6	6.6	8.4

6.1.3 Temperature

Daily air temperature records were analyzed for two locations: Atigun Pass in the Brooks Range (NRCS, 2008) and Kuparuk near the coast (WRCC, 2008). While temperature data are available at other locations in the study area, these sites were selected to bracket the geographic

and climatological range of the region. The data for Atigun Pass consisted of daily measurements of the minimum, maximum, and average air temperature, while the records for Kuparuk contained only the daily minimum and maximum air temperature. The location of the Atigun Pass site was shown previously in Figure 6-2, with the site characteristics provided in Table 6-5. The Kuparuk site is located near the coast adjacent to the NRCS Prudhoe Bay station (Latitude 70° 19.00' N by Longitude 149° 35.00' W) at an elevation of approximately 20 meters.

"Thawing Degree Days" (TDD's) at each site were computed for the river overflood period as an indicator of the thermal impetus to river breakup. The calculation was performed in the following manner: (1) in the case of the Kuparuk data, a daily average temperature was computed as the mean of the daily maximum and minimum values (the average value was available in the Atigun Pass dataset); (2) if the daily average temperature was less than or equal to 32° F (the melting point of snow and freshwater ice), that day was excluded from further consideration; (3) if the daily average temperature exceeded 32° F, the difference between 32° F and the daily average temperature was recorded as the number of TDD's for that day; and (4) the cumulative number of TDD's was computed.

TDD's were accumulated for the period commencing on April 15 and ending on May 31. The results are displayed in Table 6-8. This period was selected as representative of the temperature changes during river breakup. The values of TDD for the April 15 - May 31 period ranged from 0 to 90 at Kuparuk and from 0 to 108 at Atigun Pass. The average TDD values were 89.5 and 108.0, respectively.

To gain insight into the timing of river overflood, TDD's also were accumulated from April 15 to the date of observed breakup for the Kuparuk and Sagavanirktok rivers. Breakup records for these rives have been maintained by FR Bell and Associates (2007) since 1980 (summarized previously in Table 4-2). The observed breakup date for the Kuparuk is based on the closure date for the Kuparuk River bridge, while the break-up date for the Sagavanirktok is based on observations of flow at the Sagavanirktok River Bridge. As shown in Table 6-9, the TDD's preceding the observed break-up dates at each river varied substantially from year to year, ranging from 0 to 170.

6.2 Correlation of River Overflood with Environmental Variables

The foregoing environmental variables -- streamflow, precipitation, and air temperature -- were compared with the overflood areas of the Colville, Kuparuk and Sagavanirktok Rivers for the 13-year period between 1995 and 2007. In addition, the influence of precipitation and air temperature on streamflow was investigated.

The degree of correlation was assessed by performing a linear regression analysis for each of the paired variables. A correlation coefficient (R^2) was derived for each comparison. The correlation coefficient is a statistical measure of the ability of one variable to predict the other, with values ranging from 0 (no correlation) to 1 (perfect correlation). The sections below summarize the overflood areas used in this assessment, and present the correlation results.

Table 6-8. Thawing Degree Days at Kuparuk and Atigun Pass, April 15 to May 31

Year	Thawing Degree Days (Apr 15 to May 31)	
	Kuparuk	Atigun Pass
1995	3	50
1996	90	-
1997	38	11
1998	89	79
1999	3	-
2000	0	0
2001	2	4
2002	63	96
2003	20	4
2004	16	42
2005	5	108
2006	42	-
2007	0	95
Average	*28*	*49*
Maximum	*90*	*108*
Minimum	*0*	*0*

Table 6-9. Thawing Degree Days at Kuparuk and Atigun Pass, April 15 to Break-up Date

Year	Sagavanirktok River			Kuparuk River		
	Observed Breakup Date	Atigun TDD	Kuparuk TDD	Observed Breakup Date	Atigun TDD	Kuparuk TDD
1995	May-10	4	1	May-13	4	1
1996	May-26	-	47	May-25	-	45
1997	May-17	4	0	May-22	4	22
1998	May-20	12	17	May-20	12	17
1999	May-27	40	0	May-26	33	0
2000	Jun-02	0	4	Jun-10	75	32
2001	Jun-03	13	9	Jun-07	26	15
2002	May-21	18	20	May-23	43	29
2003	Jun-01	9	20	Jun-02	20	22
2004	May-18	12	0	May-25	22	16
2005	May-08	32	0	May-24	59	0
2006	May-18	-	0	May-28	-	22
2007	May-26	50	0	Jun-06	170	19
Average	*May-22*	*18*	*9*	*May-27*	*43*	*18*
Maximum	*Jun-03*	*50*	*47*	*Jun-10*	*170*	*45*
Minimum	*May-08*	*0*	*0*	*May-13*	*4*	*0*

6.2.1 Overflood Areas

The area encompassed by the river overflood on the sea ice was derived for each of the rivers in the study area using the composite overflood limits described in Section 5. The overflood areas of the Colville, Kuparuk and Sagavanirktok Rivers for the period from 1995 through 2007 are listed in Table 6-10. These values were excerpted from Table 5-4. The greatest overflood areas were associated with the Colville River, while the smallest typically occurred at the Kuparuk River. The greatest variability during the 13-year period of interest occurred at the Kuparuk River, with the maximum and minimum values differing by a factor approaching 4.

Table 6-10. Overflood Areas of the Colville, Kuparuk and Sagavanirktok Rivers

Year	Overflood Area (km^2)		
	Colville	**Kuparuk**	**Sagavanirktok**
1995	735	90	209
1996	598	96	-
1997	510	105	146
1998	792	158	260
1999	485	73	140
2000	858	142	177
2001	761	225	237
2002	909	262	233
2003	544	217	155
2004	1012	263	247
2005	771	240	137
2006	741	275	213
2007	603	98	178
Average	717	173	194
Maximum	1,012	275	260
Minimum	485	73	137

6.2.2 Streamflow vs. Accumulated Precipitation and Temperature

Streamflow was judged to be the most promising parameter for the purpose of establishing a positive correlation with river overflood on the sea ice. As a point of beginning, the correlation between streamflow and precipitation and air temperature was assessed.

The average discharge during the breakup period for each of the three rivers was compared with the accumulated precipitation (October 1 to May 31) for each monitoring station. The accumulated precipitation during this period provides an indication of the water available for river overflood in the spring. As shown in Table 6-11, no significant correlation between streamflow and accumulated precipitation was identified. The average correlation coefficient (R^2) ranged from 0.1237 for the Kuparuk River to 0.1798 for the Colville River. The highest

reliable value of R^2 (0.5101) resulted from a comparison of the Kuparuk River average streamflow discharge and the accumulated precipitation at Sagwon. However, the trend indicates increasing discharge with decreasing precipitation.

Table 6-11. Correlation between Average River Discharge and Accumulated Precip.

River (Ave. Breakup Period Discharge)	Monitoring Station (Accumulated Precip., Oct 1-May 31)	Correlation Coeff (R^2)
Colville River	Atigun Pass	0.3786
	Atigun Camp	0.2645
	Imnaviat Creek	*
	Sagwon	0.0722
	Prudhoe Bay	0.0003
	Ave. =	***0.1798***
Kuparuk River	Atigun Pass	0.0467
	Atigun Camp	0.0342
	Imnaviat Creek	0.0005
	Sagwon	0.5101
	Prudhoe Bay	0.0269
	Ave. =	***0.1237***
Sagavanirktok River	Atigun Pass	0.0116
	Atigun Camp	0.1216
	Imnaviat Creek	0.0398
	Sagwon	0.0876
	Prudhoe Bay	0.4758
	Ave. =	***0.1473***

* Unreliable due to limited data points.

The flood intensity of each river (a measure of how quickly the floodwaters increased) was compared to TDD for locations on the coastal plain (Kuparuk) and the Brooks Range (Atigun Pass). April 15 - May 31 was selected as representative of the river break-up period. This comparison yielded no significant correlation (Table 6-12). The average correlation coefficient (R^2) ranged from 0.0169 for the Kuparuk River to 0.1541 for the Colville River. The comparison between the Colville River flood intensity and TDD at Atigun Pass yielded the highest R^2 value, which was only 0.2546.

6.2.3 Overflood Area vs. Streamflow

The overflood areas of the Colville, Kuparuk and Sagavanirktok Rivers were compared with the following measures of streamflow during the breakup period (October 1 to May 31): (1) the average discharge, (2) the peak discharge, (3) the flood volume, and (4) the flood intensity. The results are summarized in Table 6-13.

Table 6-12. Correlation between Flood Intensity and Thawing Degree Days

River (Breakup Flood Intensity)	Monitoring Station (TDD, Apr 15-May 31)	Correlation Coeff (R^2)
Colville River	Atigun Pass	0.2546
	Kuparuk	0.0536
	Ave. =	***0.1541***
Kuparuk River	Atigun Pass	0.0150
	Kuparuk	0.0187
	Ave. =	***0.0169***
Sagavanirktok River	Atigun Pass	0.1253
	Kuparuk	0.0125
	Ave. =	***0.0689***

Table 6-13. Correlation between Streamflow Characteristics and Overflood Area

Streamflow Characteristic during Breakup Period	River Overflood Area	Correlation Coeff (R^2)
Ave. Discharge	Colville	0.0702
	Kuparuk	0.0060
	Sagavanirktok	0.0000
	Ave. =	***0.0254***
Peak Discharge	Colville	0.0305
	Kuparuk	0.0169
	Sagavanirktok	0.0067
	Ave. =	***0.01803***
Flood Volume	Colville	0.0544
	Kuparuk	0.0190
	Sagavanirktok	0.0369
	Ave. =	***0.0368***
Flood Intensity	Colville	0.4731
	Kuparuk	0.0044
	Sagavanirktok	0.0451
	Ave. =	***0.1742***

Significant correlations between the various measures of streamflow and the overflood area were conspicuously absent. The correlation coefficients for average discharge, peak discharge, and flood volume all averaged less than 0.0400. While the average correlation coefficient for flood intensity was significantly larger (0.1742), it was still far too small to indicate a positive relationship. Furthermore, the R^2 value for the Colville River flood intensity comparison (nearly 0.5) is of questionable validity due to the limited number of data points available for comparison.

6.2.4 Overflood Area vs. Precipitation

The overflood area of each of the three rivers was compared with the accumulated precipitation (October 1 to May 31) at each monitoring station for which data were available. The results are summarized in Table 6-14.

Table 6-14. Correlation between Overflood Area and Accumulated Precipitation

River Overflood Area	Monitoring Station (Accumulated Precip., Oct 1-May 31)	Correlation Coeff (R^2)
Colville River	Atigun Pass	0.0113
	Atigun Camp	0.0007
	Imnaviat Creek	0.2154
	Sagwon	0.0038
	Prudhoe Bay	0.0333
	Ave. =	***0.0529***
Kuparuk River	Atigun Pass	0.0076
	Atigun Camp	0.1417
	Imnaviat Creek	0.0007
	Sagwon	0.0798
	Prudhoe Bay	0.0551
	Ave. =	***0.0570***
Sagavanirktok River	Atigun Pass	0.0408
	Atigun Camp	0.0000
	Imnaviat Creek	0.0950
	Sagwon	0.0054
	Prudhoe Bay	0.1233
	Ave. =	***0.0529***

As in the case of streamflow, no positive correlations were found between the overflood areas and the values of accumulated precipitation. The average correlation coefficient (R^2) was approximately 0.05 for each river. The highest R^2 value was only 0.2154, and resulted from a comparison between the Colville River overflood areas and the accumulated precipitation at Imnaviat Creek.

6.2.5 Overflood Area vs. Air Temperature

The overflood areas of the three rivers were compared with the TDD's (April 15 to May 31) for Kuparuk and Atigun Pass and assessed for correlation. The results are summarized in Table 6-15.

Once again, no meaningful correlations were identified. The average correlation coefficient (R^2) ranged from a miniscule 0.0091 for the Kuparuk River to 0.1289 for the Sagavanirktok River. The highest R^2 value was only 0.2460, and resulted from the comparison between the Sagavanirktok River overflood areas and the TDD values at Kuparuk.

Table 6-15. Correlation between Overflood Area and Thawing Degree Days

River Overflood Area	Monitoring Station (TDD, Apr 15 - May 31)	Correlation Coeff (R^2)
Colville River	Atigun Pass	0.0507
	Kuparuk	0.0016
	Ave. =	***0.0262***
Kuparuk River	Atigun Pass	0.0157
	Kuparuk	0.0024
	Ave. =	***0.0091***
Sagavanirktok River	Atigun Pass	0.0117
	Kuparuk	0.2460
	Ave. =	***0.1289***

6.2.6 Overflood Timing

The dates of break-up in the Kuparuk and Sagavanirktok Rivers were compared to the corresponding values of TDD from April 15 to the time of break-up (Table 6-9) in an attempt to determine whether air temperature could be used as a predictor of breakup. No trends were evident when the variables were compared. In several years, break-up occurred despite a zero value of TDD – a finding that indicates the absence of a minimum threshold below which break-up is unlikely to occur.

6.3 Conclusions

Despite the use of what was judged to represent the best environmental data available for the period 1995-2007, no meaningful correlations were identified between the annual overflood areas of the Colville, Kuparuk, and Sagavanirktok Rivers and the corresponding values of streamflow, precipitation, and temperature. Attempts to establish meaningful relationships between streamflow and either precipitation or temperature also proved to be fruitless.

The most important implication of these findings is that the extent of river overflood onto the sea ice cannot be predicted by any single environmental variable for which historical data currently exist. The overflood phenomenon appears to be governed by complex interactions between a number of environmental forces, some of which, such as ice jams in distributary channels, roughness and snow cover on the sea ice, and the density of drainage features on the sea ice, have not been quantified to date.

7 FACILITIES HAZARDS ASSESSMENT

This section discusses two potential hazards that river overflood on the sea ice poses to man-made facilities in the Alaskan Beaufort Sea: disturbance of subsea pipelines by strudel scouring, and interdiction of access to offshore facilities by on-ice flow. The two subsections that follow summarize the strudel drain and strudel scour data obtained from sources in the petroleum industry for this study, and describe the issues related to facilities access.

7.1 Strudel Scouring

Strudel scouring occurs when the overflood water drains through holes in the sea ice and impinges on the sea bottom. The resulting depressions can constitute significant design considerations for subsea pipelines (Lanan, *et al*., 2008). While ice gouges often govern the depth of pipeline burial in deeper waters, strudel scours tend to govern in nearshore areas adjacent to river and stream mouths. Strudel scour concerns have resulted in the burial of the two existing subsea pipelines in the Alaskan Beaufort Sea (BPXA's Northstar and Pioneer's Oooguruk). In the event that a strudel drain is located directly above a buried subsea pipeline, a sufficiently deep strudel scour may expose the pipeline and lead to an unsupported span. A strudel scour that forms directly over a buried pipeline also can remove the backfill material that is needed to prevent damage from ice keels and forestall upheaval buckling. An additional concern is that strudel drainage provides a mechanism to transport spilled oil below the ice sheet.

Strudel drain and strudel scour data were obtained from petroleum industry studies conducted on behalf of BPXA's Northstar Development, BPXA's Liberty Prospect, Pioneer's Oooguruk Development, and Shell's Sivulliq Prospect. The underlying studies tended to focus on mapping drains and scours in the vicinity of proposed or existing subsea pipelines, and did not necessarily attempt to locate all such features within the overflood boundaries of a specific river. The studies are summarized in Table 7-1. Access to the data granted by the industry sponsors is gratefully acknowledged.

Table 7-1. Industry-Sponsored Strudel Scour Studies

Project	Industry Sponsor	Rivers Included	Survey Dates
Northstar	BP Exploration (Alaska) Inc.	Kuparuk	1996-2007 [1]
Liberty	BP Exploration (Alaska) Inc.	Sagavanirktok Kadleroshilik Shaviovik	1997-2001, 2003, 2005 [1, 2]
Oooguruk	Pioneer Natural Resources	Colville	2005-2006
Sivulliq	Shell Exploration and Production	Local Drainages and Creeks	2006, 2007

[1] Strudel drains not mapped in 1999. [2] Strudel scours not mapped in 2000, 2001, 2003, or 2005.

Source: Coastal Frontiers, 1997, 1998a, 1998b, 1999a, 1999b, 2000a, 2000b, 2001a, 2002 2003a, 2003b, 2004, 2005, 2006a, 2006b, 2007a, 2007b, 2007c, 2008a, 2008b

7.1.1 Strudel Scour Formation

During the spring freshet, typically in late May or early June, flood waters pour out over the top of the sea ice. The overflood water can exceed a depth of 1 m and can spread several kilometers offshore. Figure 7-1 shows overflood water from the Kuparuk River progressing from Gwyder Bay to the region north of the barrier islands.

Figure 7-1. Kuparuk River Overflood, May 2006

Initially, the overflood waters pass over the region of bottomfast ice (typically extending to a water depth approaching 2 m). Farther offshore, in water depths greater than about 2 m (the floating landfast ice region), the overflood waters drain through holes and discontinuities in the ice sheet caused by tidal cracks, thermal cracks, stress cracks, and seal breathing holes. When the drainage rate is high, powerful strudel jets or whirlpools can develop at the drain sites and create large scour depressions on the sea floor. Figure 7-2 shows a circular drainage feature that probably originated from a seal breathing hole, while Figure 7-3 shows a crack drain resulting from a tidal crack.

Early in the overflood period, strudel drainage is precluded in the bottomfast ice region by the lack of a flow path to the ocean, even if discontinuities are present in the ice sheet. As the overflood period progresses, the bottomfast ice sheet breaks free and rises to the surface, allowing strudel drainage to commence (Reimnitz, *et al.*, 1974). However, the drainage tends to be less vigorous in this region because it occurs late in the overflood period after the peak river discharge has subsided. As a result, the scouring tends to be milder than that which occurs farther offshore. In both cases, however, strudel drainage provides a pathway to transport spilled oil below the ice sheet.

Figure 7-2. Representative Circular Strudel Drain

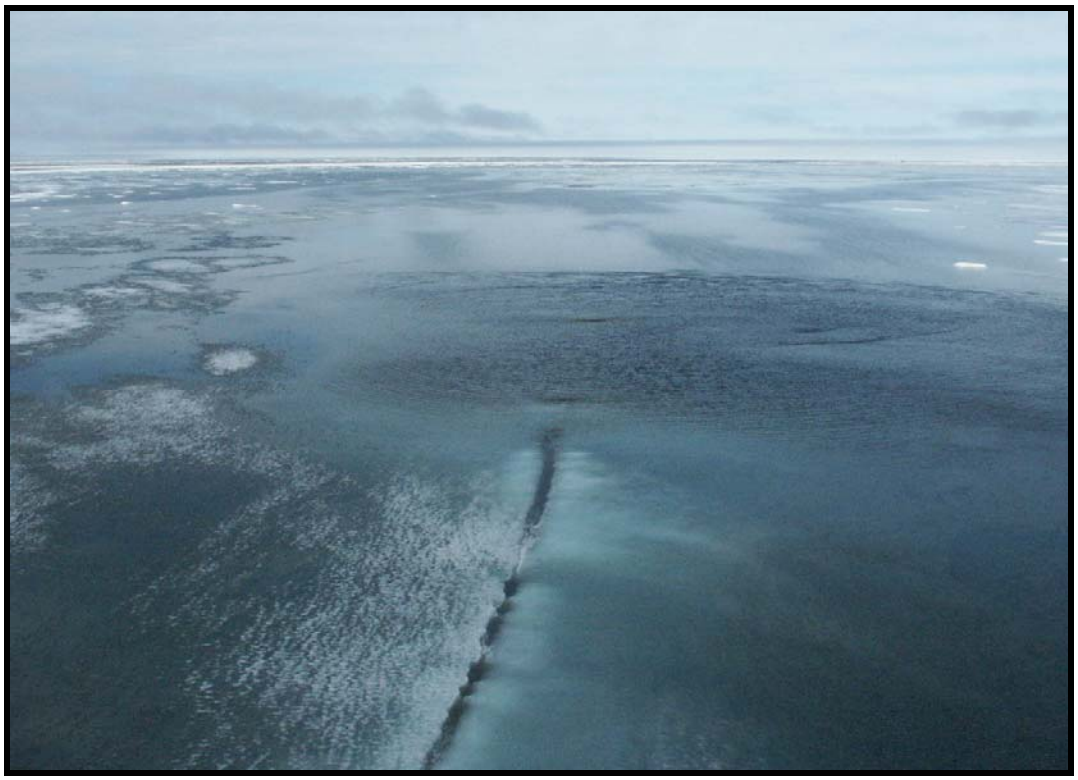

Figure 7-3. Representative Crack Drain

7.1.2 Strudel Scour Zonality

Based on the strudel formation process described above and an assessment of strudel scour data obtained for the Northstar Development, Leidersdorf, et al. (2007), classified the zone of bottomfast ice as the "Secondary Strudel Zone" and the zone of floating fast ice immediately seaward of the Secondary Strudel Zone as the "Primary Strudel Zone". The Primary Strudel Zone was defined as the region between the 1.5-m and 6-m isobaths, with the Secondary Strudel Zone located landward of the 1.5-m isobath. Based on the recognition that the potential for strudel scour formation diminishes in water depths beyond approximately 6 m, a third zone (the "Tertiary Strudel Zone") was defined for the purposes of this study as the region offshore of the Primary Strudel Zone. The strudel scour formation and zonation are illustrated in Figure 7-4.

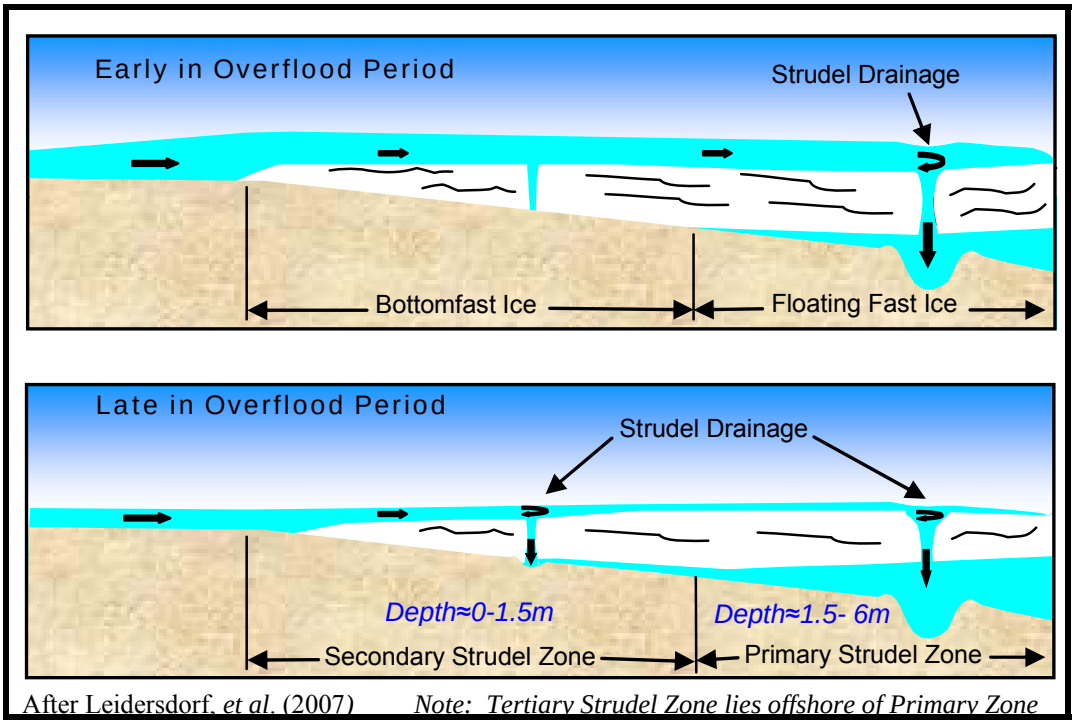

Figure 7-4. Strudel Process and Zonation

Using the Northstar Development strudel scour data acquired during the first four years after pipeline startup (2002 – 2005), Leidersdorf, *et al.* (2007), found that both the frequency and severity of scouring were greatest in the Primary Strudel Zone. The peak scour depths and diameters were found in water depths ranging from 2 to 5 m. A maximum scour depth of 4.3 m was reported. In contrast, the frequency and severity of scouring were found to be significantly lower in Secondary Strudel Zone. The maximum scour depth in this zone was 0.6 m.

For the purposes of this study, the bathymetric contours developed by the National Oceanic and Atmospheric Administration (NOAA) from a survey conducted in the late 1940's and early 1950's were used to define the boundaries of the three strudel zones. While imperfect, the NOAA data offer the only comprehensive bathymetric mapping of the entire study area. The overflood region from the shoreline to the 1.5-m (5-ft) isobath was defined as the Secondary Strudel Zone, while the region between the 1.5-m and 6.1–m (20-ft) isobaths was defined as the

Primary Strudel Zone. The region from the 6.1-m isobath to the offshore boundary of the overflood was defined as the Tertiary Strudel Zone.

The strudel scour potential in the study area was assessed by segregating the composite overflood limits presented in Section 5 into the aforementioned three zones based on the NOAA contours. The strudel scour zones developed for the western portion of the study area for 2001 are shown in Figure 7-5 as an example. Analogous maps for each year from 1995 through 2007 are presented in Appendix D. The area of each strudel zone at each river was computed, and also appears in Appendix D. The intent is to provide a database that can be used to assess the risk to prospective pipeline routes posed by strudel scouring.

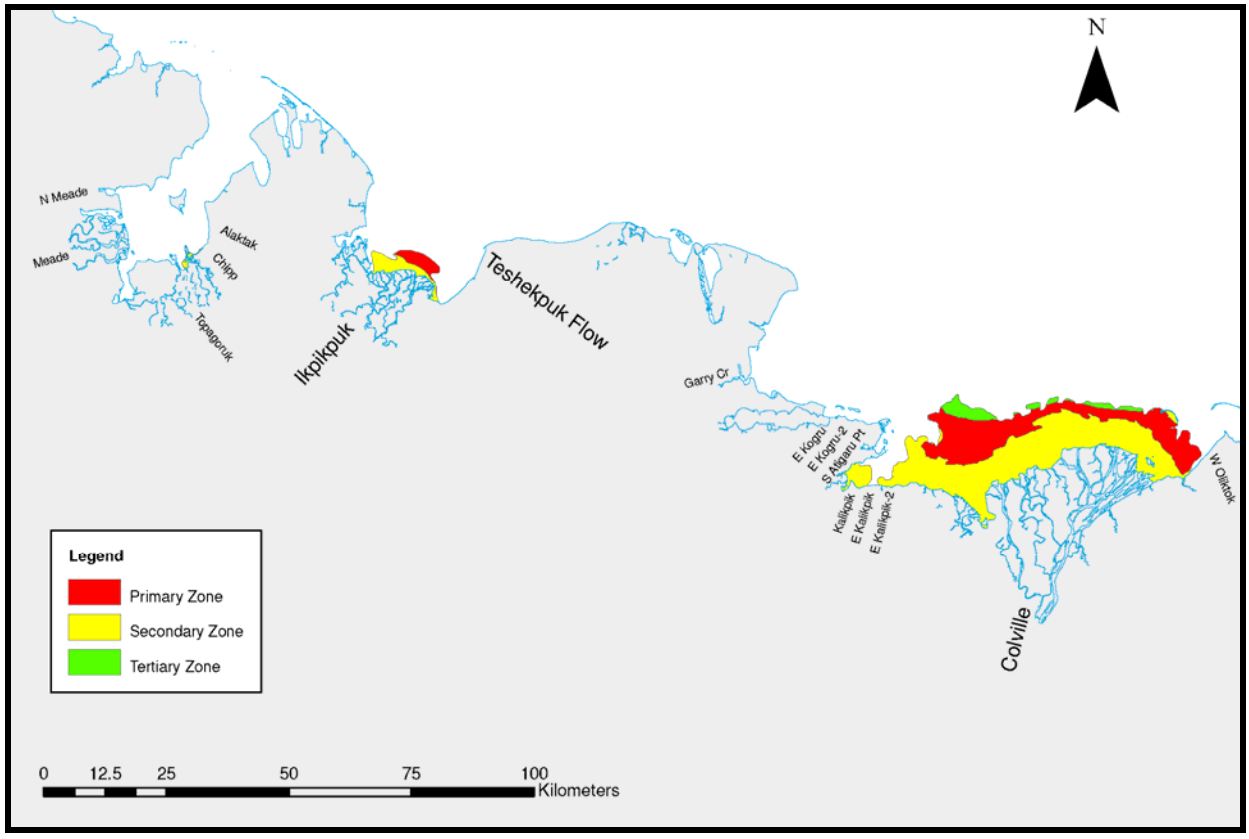

Figure 7-5. 2001 Strudel Zones in Western Portion of the Study Area

Table 7-2 summarizes the strudel zone areas for three of the largest rivers in the study area: the Colville, Kuparuk, and Sagavanirktok. The Secondary Zone accounts for the majority of the average overflood area of each river. The variability of the Secondary Zone area is low for the Colville and Sagavanirktok Rivers, suggesting that the sea ice is inundated at least as far offshore as the 6.1-m isobath in most years. The higher variability in this zone for Kuparuk River is attributable to large interannual differences in the lateral overflood extent within the barrier islands west of the river mouth (Appendix D). On average, the Primary Strudel Zone constitutes 31% of the Colville River overflood area, 47% of the Kuparuk River overflood area, and 36% of the Sagavanirktok River overflood area. The overflood reached the Tertiary Strudel Zone approximately 50% of the time at the Colville and Kuparuk Rivers, and on only one occasion at the Sagavanirktok River. Accordingly, the Tertiary Zone accounts for only a small fraction of the average overflood area for each river.

Table 7-2. Strudel Zone Areas for the Colville, Kuparuk and Sagavanirktok Rivers

Year	Colville			Kuparuk			Sagavanirktok		
	Strudel Zone Area (km^2)			Strudel Zone Area (km^2)			Strudel Zone Area (km^2))		
	Secondary	Primary	Tertiary	Secondary	Primary	Tertiary	Secondary	Primary	Tertiary
1995	470	253	12	53	37	0	121	87	0
1996	407	184	7	62	34	0			
1997	391	120	0	70	35	0	111	35	0
1998	529	262	1	82	67	9	148	112	0
1999	386	99	0	54	20	0	104	36	0
2000	533	304	21	75	65	2	126	51	0
2001	450	268	43	104	94	18	149	88	0
2002	503	300	105	106	115	41	117	115	2
2003	437	107	0	104	109	3	113	42	0
2004	589	409	14	110	152	1	140	108	0
2005	528	243	0	106	133	1	100	37	0
2006	534	207	0	120	155	0	139	74	0
2007	460	143	0	68	29	0	126	52	0
Average	478	223	16	86	80	6	124	70	0
Maximum	589	409	105	120	155	41	149	115	2
Minimum	386	99	0	53	20	0	100	35	0

The strudel zone areas for the eleven major river systems located between the Colville and Okpilak Rivers are compared in Figure 7-6. The Secondary Strudel Zone accounts for the greatest portion of the overflood, representing, on average, 66% of the total overflood area. The Primary Strudel Zone accounts for 32%, while the Tertiary Zone accounts for a mere 2%.

7.1.3 Strudel Drains

During each study listed in Table 7-1, drainage features in the sea ice were identified while performing a helicopter-based reconnaissance of the target overflood area. The studies typically focused on mapping strudel drains in the vicinity of proposed or existing subsea pipelines. As a result, all drains within the overflood boundary of a specific river typically were not mapped. Appendix E provides a series of maps showing the strudel drain search areas and individual drainage features mapped during each of these studies.

Individual strudel drains were mapped by hovering over each feature while recording multiple position fixes with a GPS unit. Prior to 2004, the surveys were conducted with the GPS unit operated in autonomous mode, resulting in a position accuracy of approximately 100 m. In 2000, the U.S. Government discontinued Selective Availability, thereby increasing the accuracy of autonomous positions to approximately 7 m (Milbert, 2001). Commencing in 2004,

differential corrections broadcast in real time via the Wide Area Augmentation System (WAAS) were used. Equipment manufacturers Trimble and Magellan report an accuracy of 1 to 3 m for WAAS corrected positions in the Continental U.S. (Lewis, 2001; Magellan, 2001).

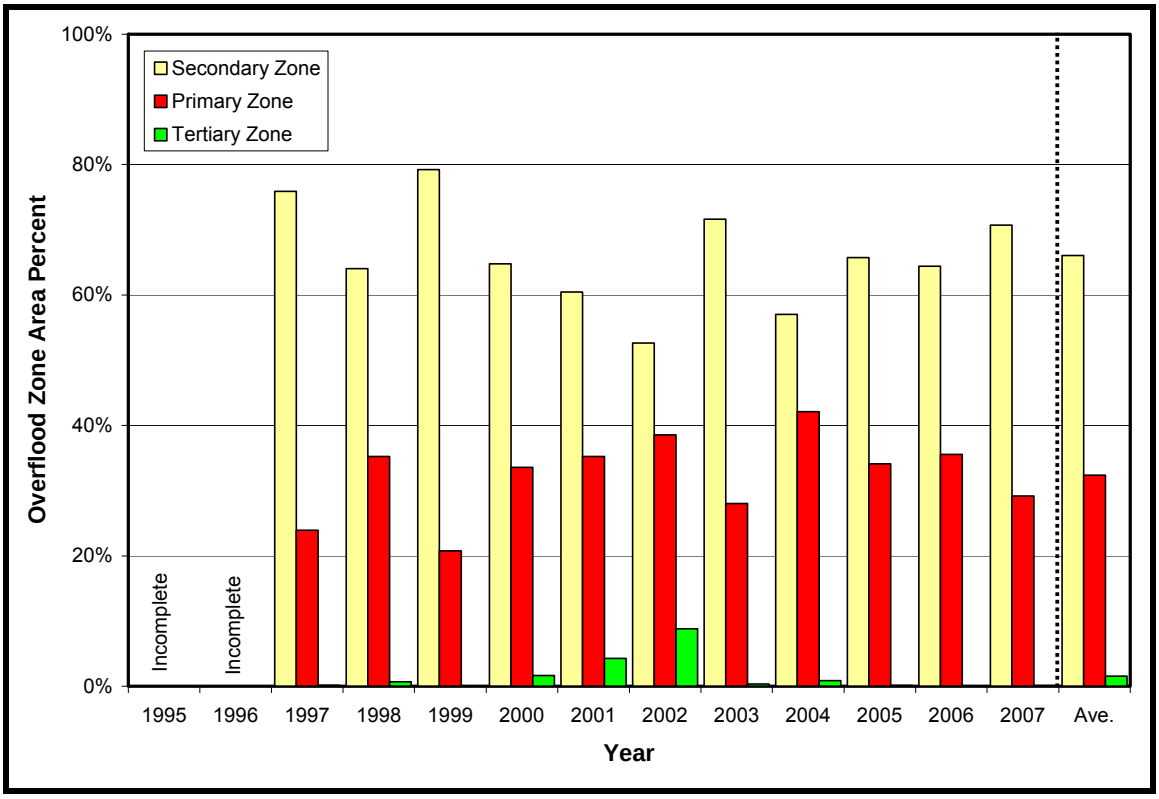

Figure 7-6. Strudel Zone Area Comparison for Major River Systems

The geographic location and observed characteristics (when available) of each drainage feature are included in the ArcGIS database. Both circular drains and linear crack drains were identified. The drains also were segregated into the three zones described previously in Section 7.1.2. A summary of the drainage features mapped during each of the studies is provided in Table 7-3, while Figures 7-7 through 7-10 show the locations of all of the drains.

As shown in Table 7-4, the density of strudel drains (number of drains per square kilometer of area searched) varies substantially from river to river in any given year, and from year to year off any given river. At the Kuparuk River, the drain density ranged from 0.6 to 7.1 drains/km^2. In contrast, the range in the Foggy Island Bay area (comprised of the Sagavanirktok or Sag, Kadleroshilik or Kad, and Shaviovik or Shav Rivers) was relatively narrow at 0.7 to 2.6 drains/km^2. The small streams and creeks near the Sivulliq Prospect yielded drain densities of 1.0 and 1.7 drains/km^2 for the two years investigated. The greatest density (8.7 drains/km^2) occurred at the Colville River in 2006.

As in the case of river overflood itself, the factors that influence the occurrence and distribution of strudel drains are complex and poorly-understood. Accordingly, the drain densities shown in Table 7-4 are applicable only to those areas from which they were derived, and should not be used to infer such densities for other portions of the overflood area of the associated river, or for the overflood areas of other rivers.

Table 7-3. Strudel Drains Mapped During Industry-Sponsored Studies

Year	Number of Strudel Drains Mapped			
	Northstar	**Liberty**	**Oooguruk**	**Sivulliq**
	Kuparuk	*Sag / Kad / Shav*	*Colville*	*Pt. Thomson Area Local Drainage*
1996	46	-	-	-
1997	47	141 / 30 / 7	-	-
1998	73	10 / 64 / -	-	-
1999	-	-	-	-
2000	63	30 / 32 / -	-	-
2001	72	40 / 69 / -	-	-
2002	116	-	-	-
2003	98	54 / 2 / -	-	-
2004	62	-	-	-
2005	20	56 / 155 / 168	99	-
2006	47	-	238	18
2007	8	-	-	14

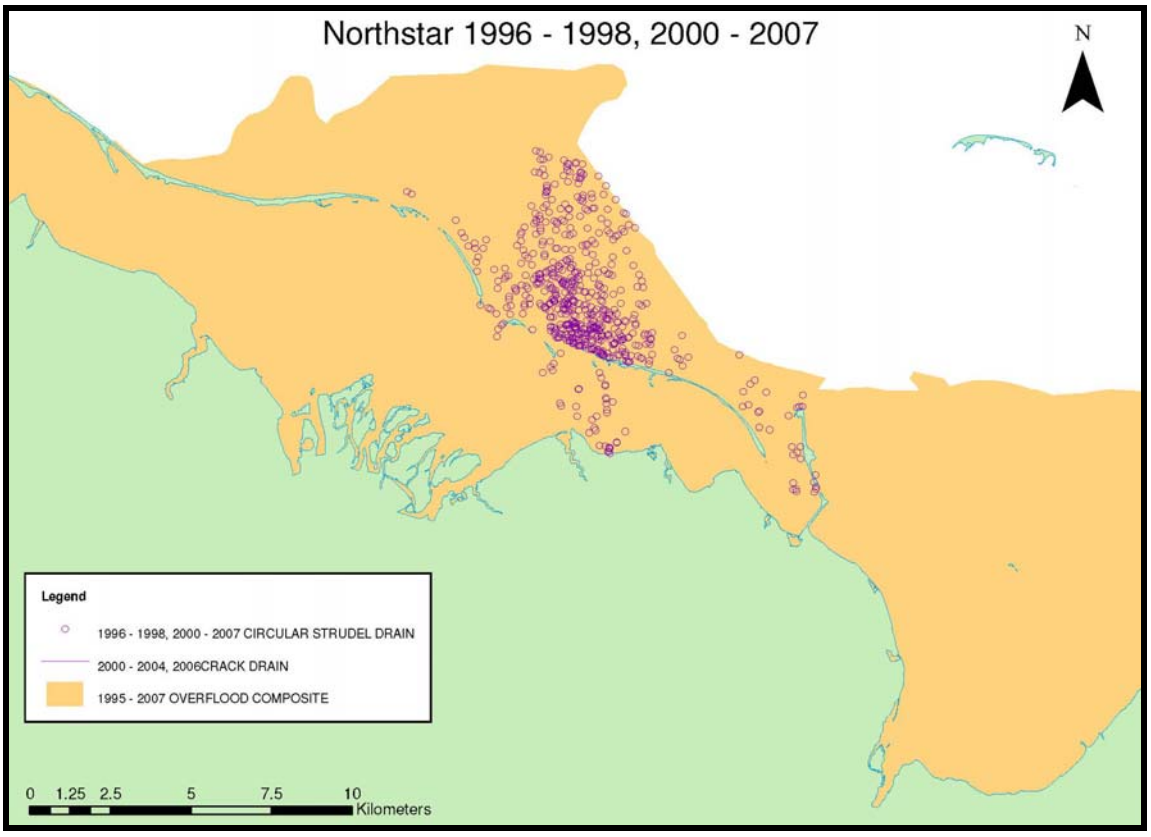

Figure 7-7. Strudel Drains Mapped on behalf of Northstar Development

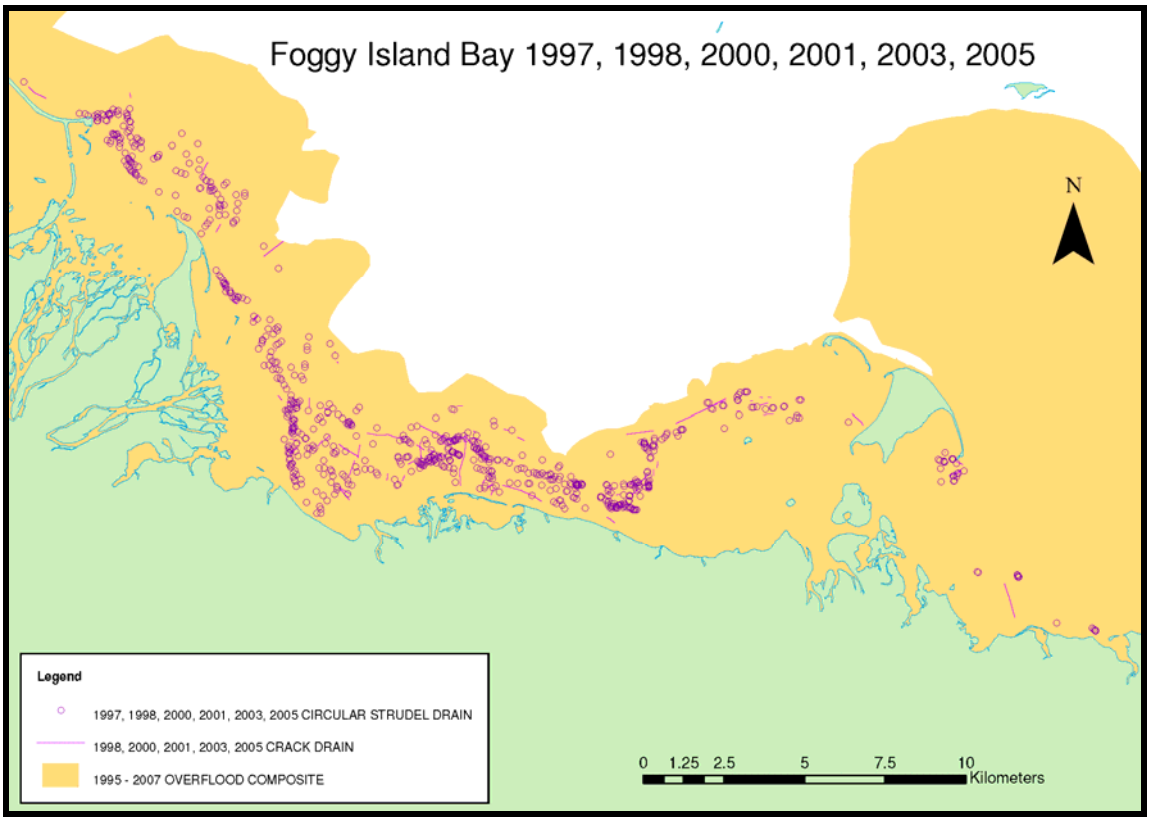

Figure 7-8. Strudel Drains Mapped on behalf of Liberty Prospect

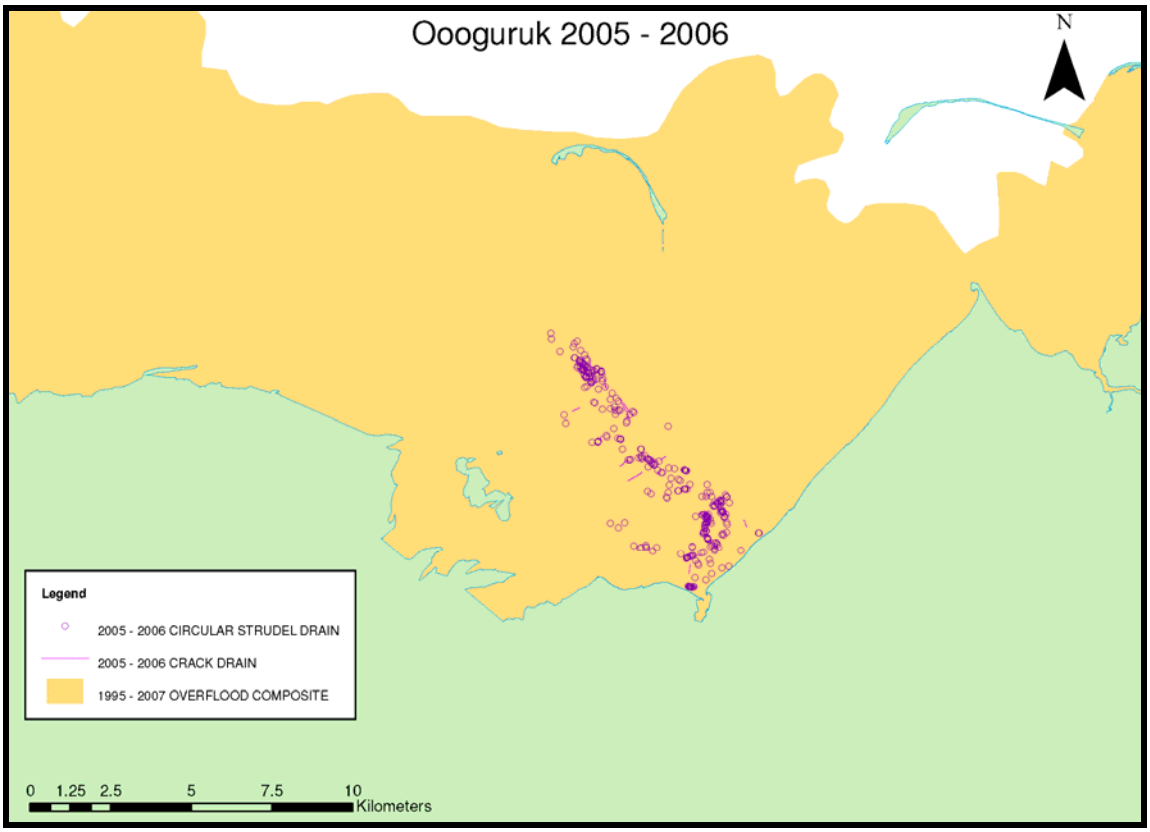

Figure 7-9. Strudel Drains Mapped on behalf of Oooguruk Development

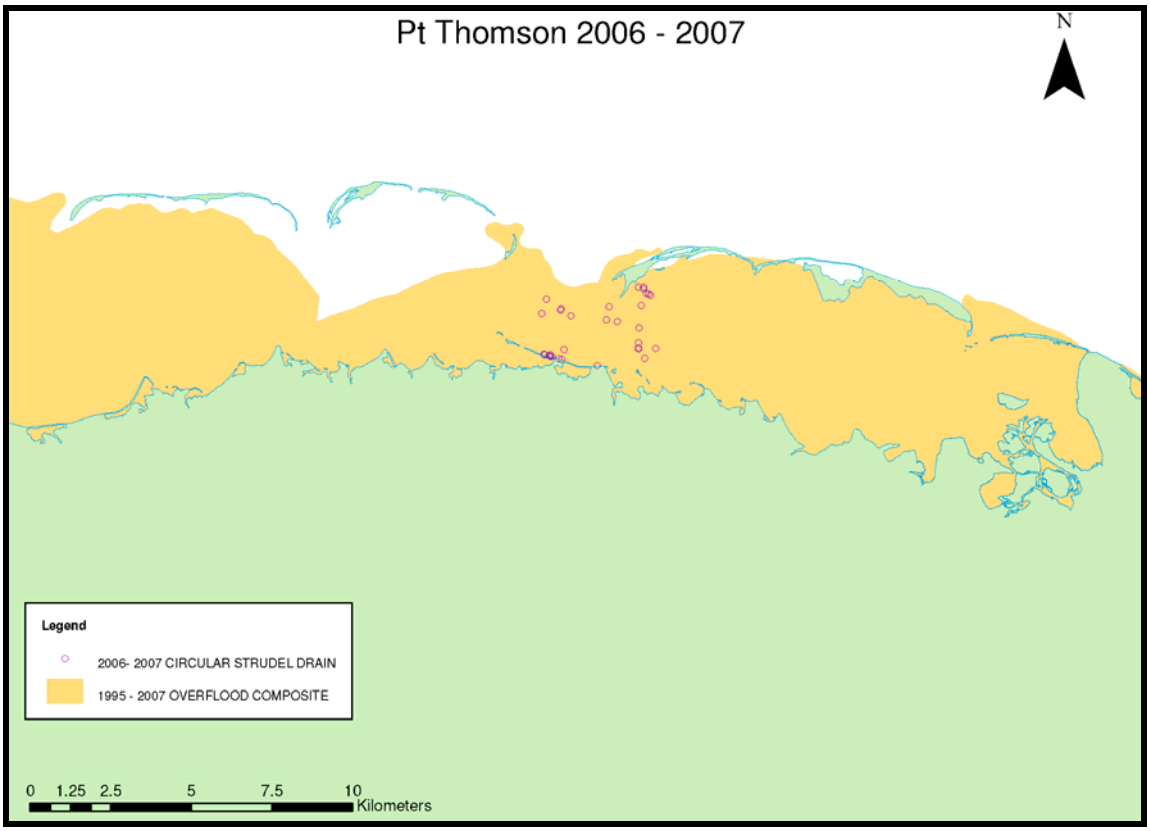

Figure 7-10. Strudel Drains Mapped on behalf of Sivulliq Prospect

Table 7-4. Strudel Drain Densities from Industry-Sponsored Studies

Year	Strudel Drain Density (Drains/km^2)			
	Northstar	**Liberty**	**Oooguruk**	**Sivulliq**
	Kuparuk	*Sag / Kad / Shav*	*Colville*	*Local Drainage*
1996	0.6	-	-	-
1997	1.5	1.5	-	-
1998	1.4	1.0	-	-
1999	-	-	-	-
2000	7.1	0.7	-	-
2001	4.4	1.2	-	-
2002	4.4	-	-	-
2003	4.5	0.7	-	-
2004	3.8	-	-	-
2005	1.2	2.6	3.1	-
2006	5.7	-	8.7	1.7
2007	1.1	-	-	1.0

Figure 7-11 provides the distribution of drains among the Primary, Secondary, and Tertiary Zones for the six rivers and streams addressed in the industry studies. In keeping with the findings in the Northstar Development, most of the drains were located in the Primary Zone. Drains were found in the Secondary Zone at each of the six sites, but only at the Kuparuk River

were drains mapped in the Tertiary Zone. This situation arose, at least in part, because the flood waters from the other rivers did not extend to the 6.1-m isobath for any of the survey years.

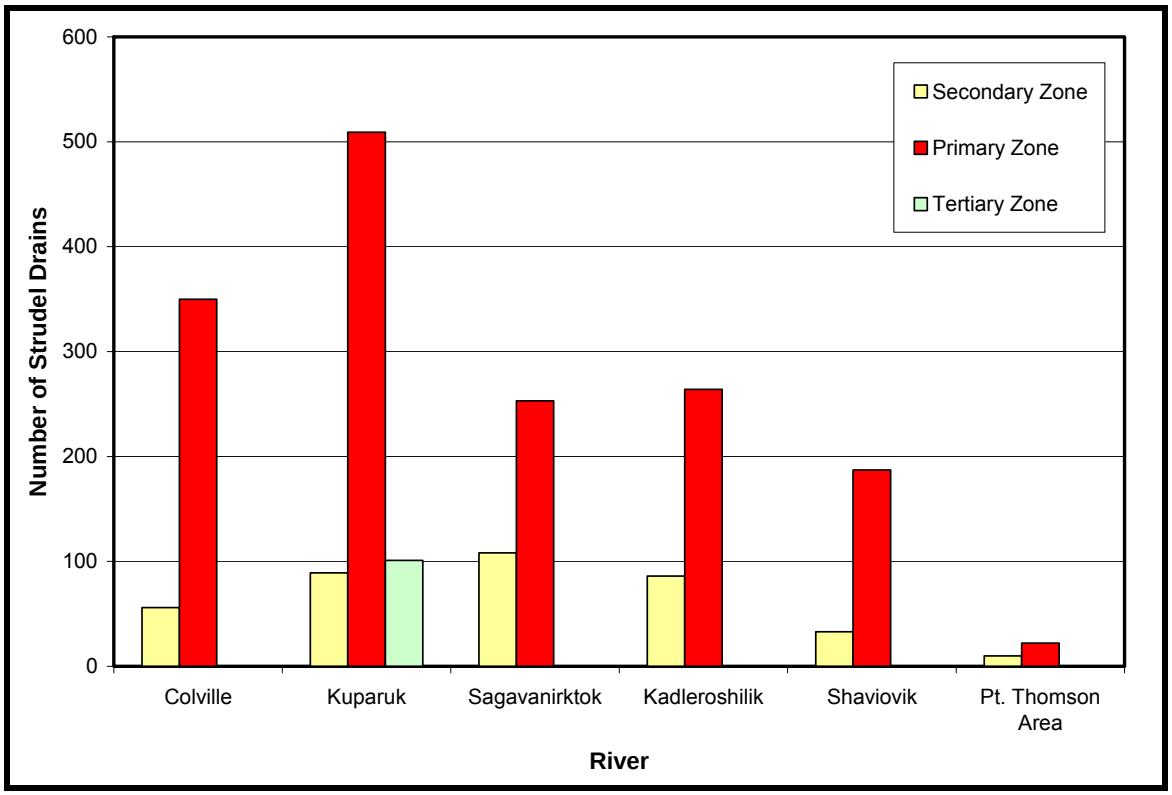

Figure 7-11. Drains Mapped in each Strudel Zone

7.1.4 Strudel Scours

The drainage of overflood water through holes and discontinuities in the ice sheet can create powerful strudel jets that erode large scour depressions in the sea floor. The drainage and associated strudel scouring typically are more severe in the Primary Strudel Zone. In the shallower waters of the bottomfast ice region (Secondary Strudel Zone), both drainage and scouring tend to be less pronounced. While occasional strudel drains have been mapped in the Tertiary Strudel Zone (water depths greater than about 6 m), few strudel scours have been discovered in this region.

Most strudel scours are circular in plan form. Linear scours, which are formed by drainage through elongated cracks, also have been documented. Additional details regarding strudel types are provided by Vaudrey (1996).

Prior to the mid-1990's, measurements of strudel scour characteristics were sparse. The USGS documented three scour depressions off of the Kuparuk River and one in the Sagavanirktok River delta during studies conducted in 1974 (Reimnitz, *et al*., 1974) and 1978-80 (Reimnitz and Kempema, 1982). The scours were found in water depths of approximately 3.0 m, with scour depths ranging from 1.0 to 4.5 m. McClelland Engineers (1982, as reported in Coastal Frontiers, 1997) detected 613 scours in the Sagavanirktok River delta during a 1982 study conducted in support of the Endicott Development. A maximum scour

depth of 6.7 m was documented, and four additional scours with depths in excess of 4.5 m also were found. In 1985, Harding Lawson Associates (1986, as reported in Coastal Frontiers, 1997) discovered 46 scours in water depths of 2.1 to 8.1 m off of the Kuparuk River. Scour depths (measured for only six of the features) ranged from 0.1 to 1.7 m. Coastal Frontiers Corporation (1996) noted seven scours near Resolution Island (located in the Sagavanirktok River delta in a water depth of approximately 2 m) between 1985 and 1995. The greatest scour depth was 2.8 m.

The strudel scour data assembled for this study were derived from the industry studies described above (Table 7-1). In each case, the locations of drainage features found during the spring helicopter reconnaissance were searched during a vessel-based summer survey. A strudel scour found on the sea floor at one of the drainage sites was assumed to have been formed that year. Scours also were discovered at some locations where drainage features had not been mapped during the spring reconnaissance. These scours were either relic features formed during a prior overflood event or created by a drainage feature that escaped detection during the overflight.

The characteristics of each scour were measured using multi-beam sonar, single-beam sonar, side scan sonar, or with a combination of these tools. When possible, the location, water depth, scour depth, maximum horizontal dimension at the elevation of the surrounding sea bottom, and type (circular or linear) of each feature was recorded. The geographic location and measured characteristics of each strudel scour are included in the ArcGIS database to the extent that they are available. The scours also were segregated into the three zones described previously in Section 7.1.2. A summary of the strudel scours detected during each of the studies is provided in Table 7-5, while Figures 7-12 through 7-15 show the locations of all of the scours.

Table 7-5. Strudel Scours Mapped During Industry-Sponsored Studies

Year	Number of Strudel Scours Mapped			
	Northstar	**Liberty**	**Oooguruk**	**Sivulliq**
	Kuparuk	*Sag / Kad / Shav*	*Colville*	*Pt. Thomson Area Local Drainage*
1996	99	-	-	-
1997	86	114 / 30 / 47	-	-
1998	10	14 / 16 / -	-	-
1999	7	0 / 3/ -	-	-
2000	77	-	-	-
2001	38	-	-	-
2002	50	-	-	-
2003	56	-	-	-
2004	49	-	-	-
2005	7	-	119	12
2006	26	-	223	2
2007	6	-	-	-

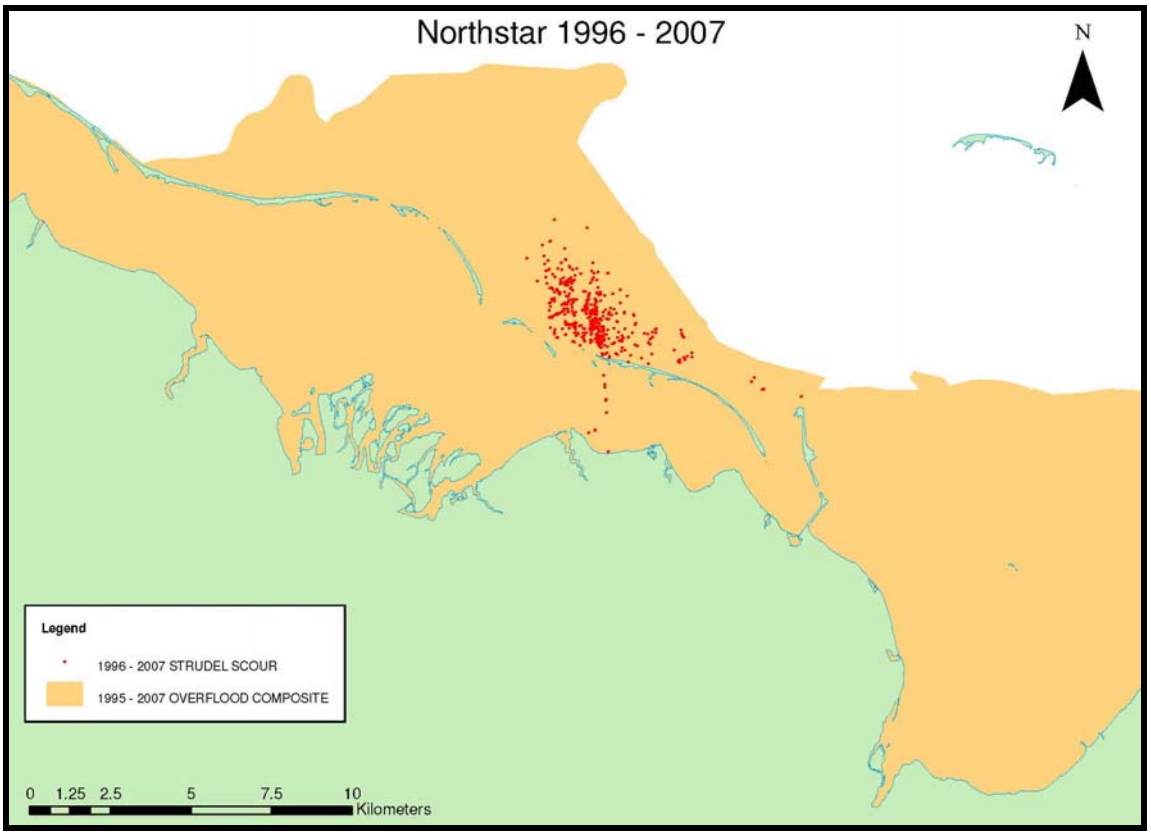

Figure 7-12. Strudel Scours Mapped on behalf of Northstar Development

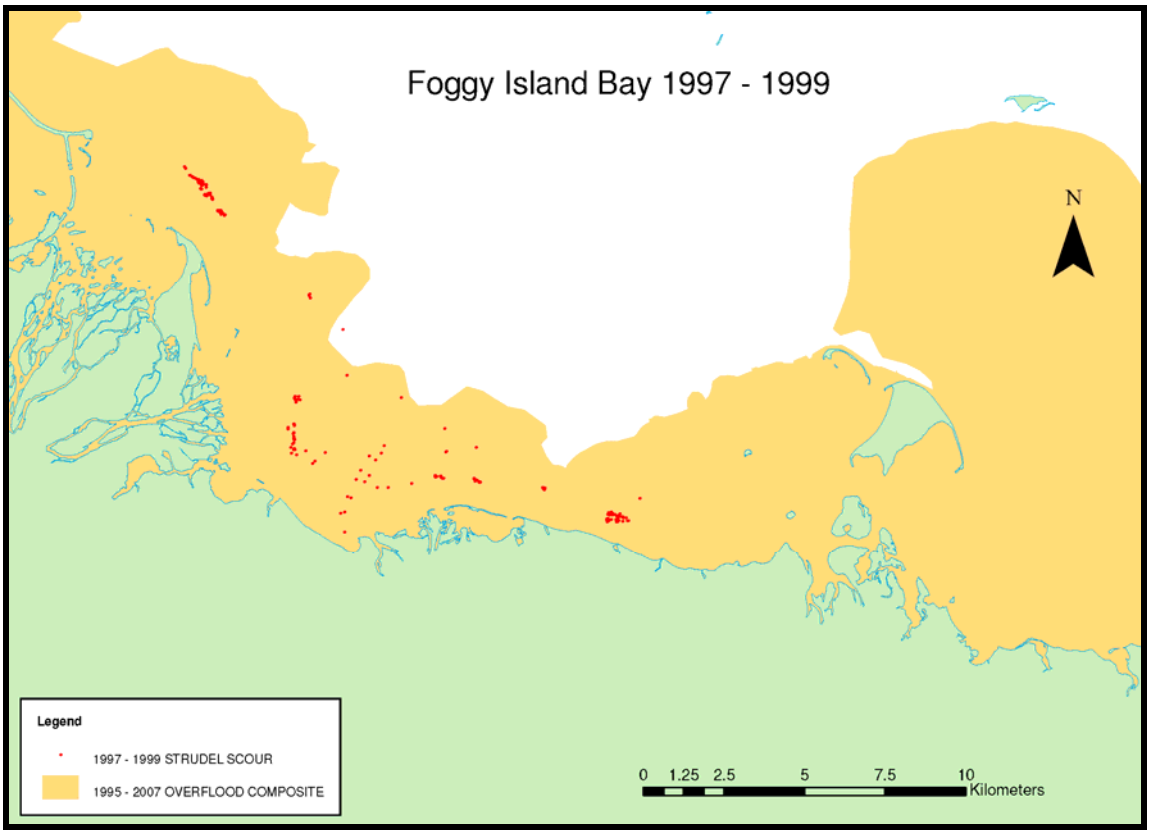

Figure 7-13. Strudel Scours Mapped on behalf of Liberty Prospect

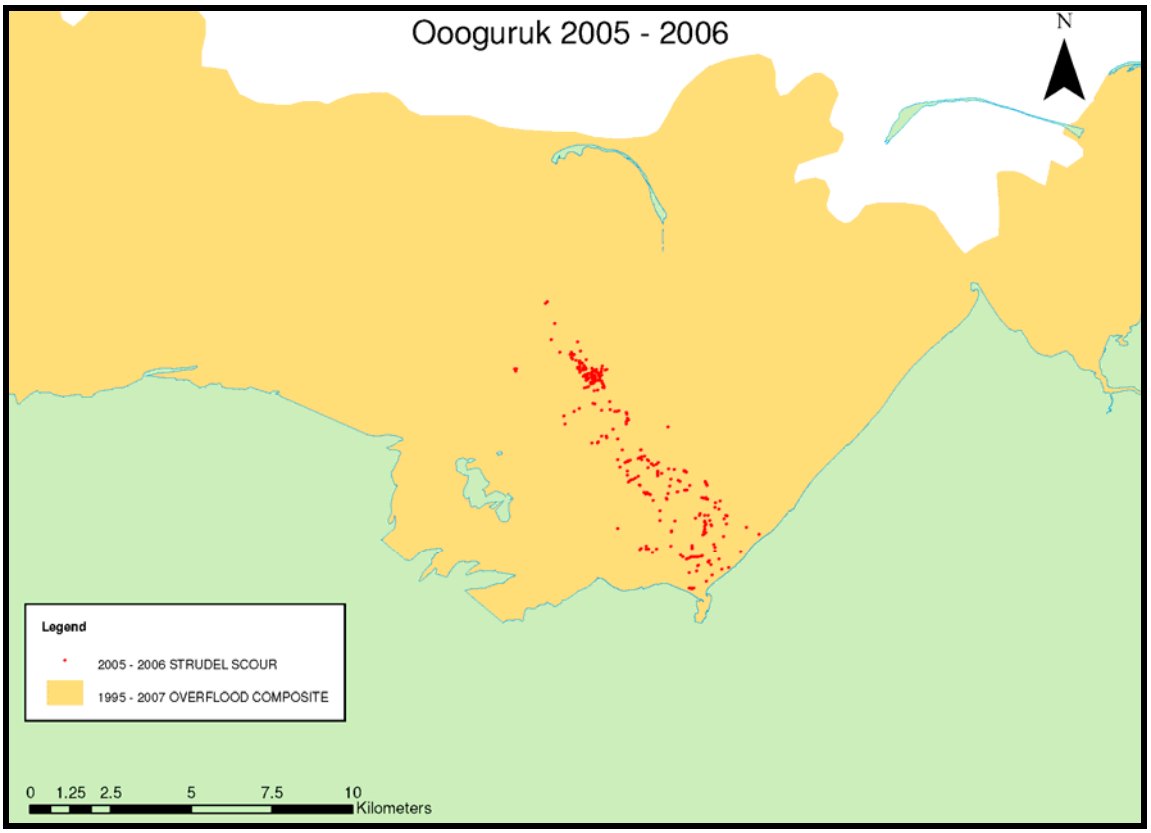

Figure 7-14. Strudel Scours Mapped on behalf of Oooguruk Development

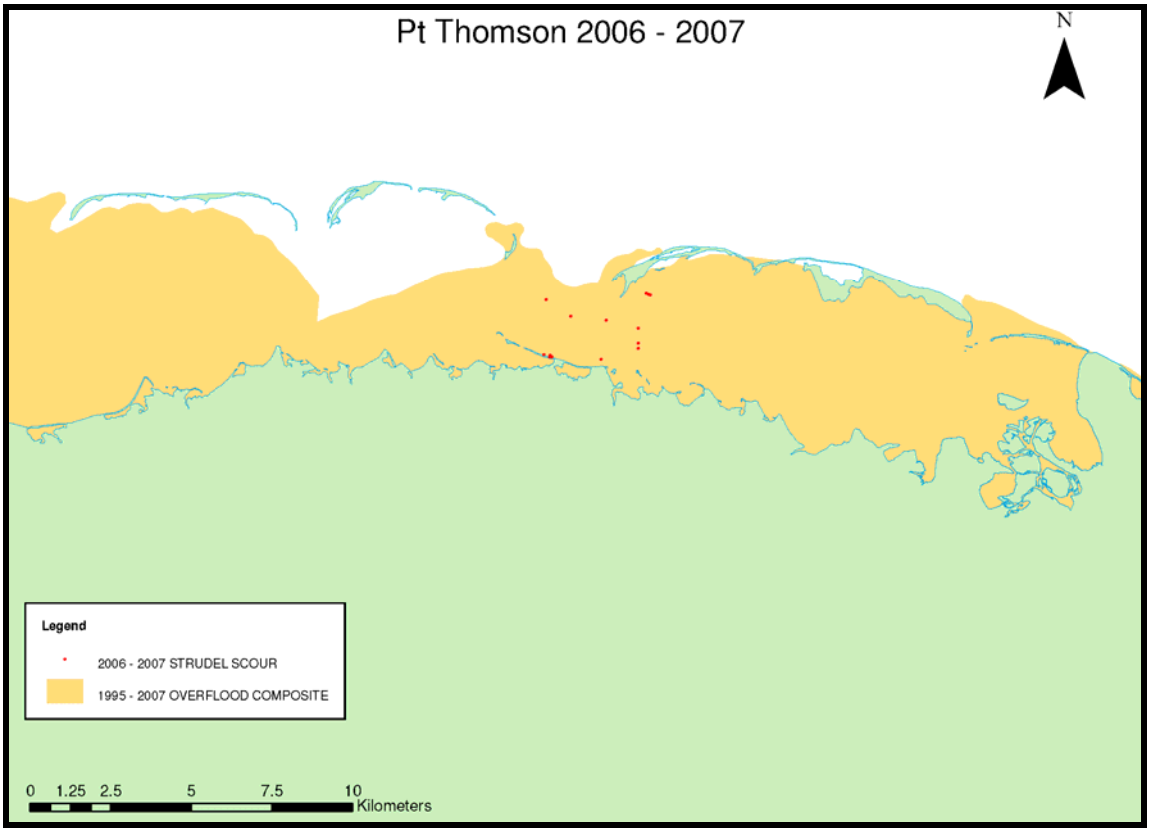

Figure 7-15. Strudel Scours Mapped on behalf of Sivulliq Prospect

As indicated in Figure 7-16, the majority of the scours was located in the Primary Zone (ranging from 64% of the total number of scours in the Pt. Thomson Area to 100% in the Shaviovik River). Strudel scours were found in the Secondary Zone of each river except for the Shaviovik. Two scours were mapped in the Tertiary Zone of the Kuparuk River, while no scours were located in this zone in the other overflood areas. It is noteworthy that although 101 drainage features were mapped in the Tertiary Zone of the Kuparuk River overflood (Figure 7-11), only two strudel scours were discovered in this region.

Tables 7-6 through 7-11 present statistical characterizations of the scours mapped in each of the river overflood areas. A summary of the maximum strudel characteristics is provided on Table 7-12. The scour populations are segregated by zone (Secondary, Primary, and Tertiary). Because the characteristics of circular and linear scours are distinctly different, statistics are provided according to scour type. In the case of circular scours, the term "maximum horizontal dimension" refers to the largest horizontal extent measured at the elevation of the surrounding sea bottom (*i.e.*, the diameter of a perfectly circular scour or the major axis of an oblong scour). In the case of linear scours, the "maximum horizontal dimension" represents the length measured parallel to the scour orientation. The "scour depth" is measured as distance from surrounding sea bottom to the deepest point in the scour depression. As indicated previously, the characteristics of each individual scour are provided in the ArcGIS database.

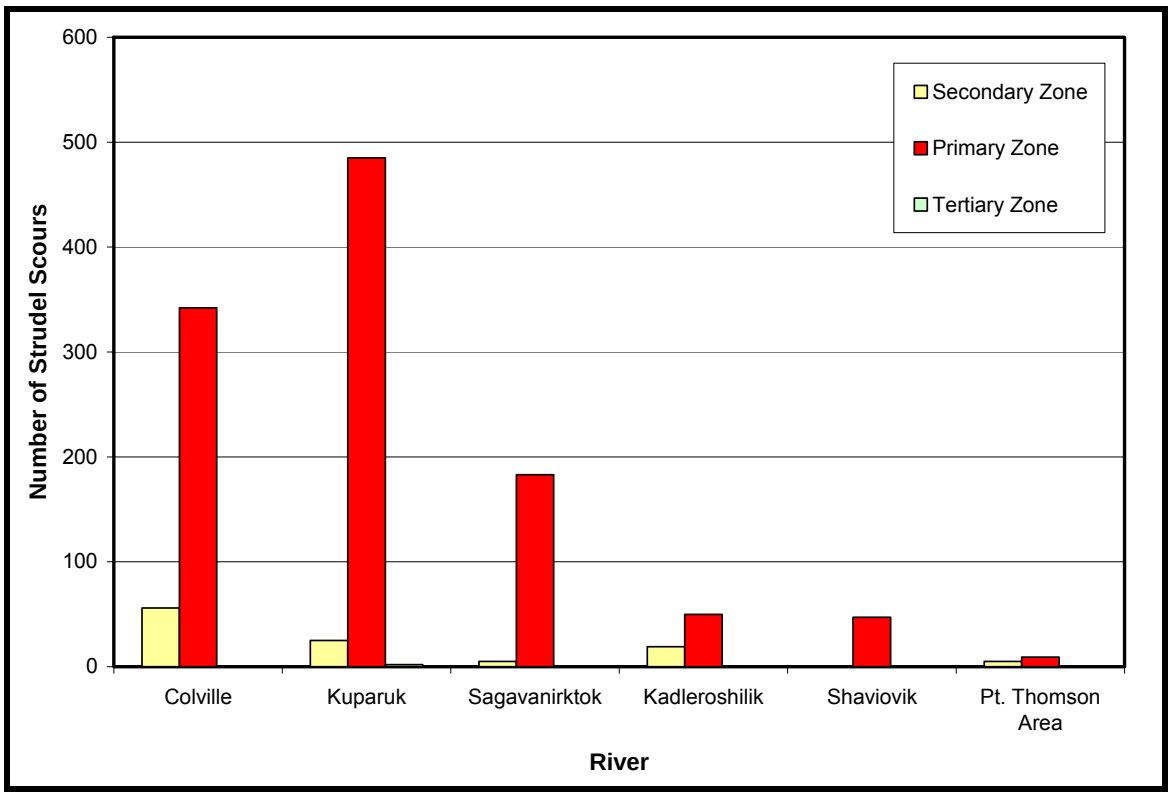

Figure 7-16. Strudel Scours Mapped in each Strudel Zone

Table 7-6. Strudel Scour Characteristics Measured off the Colville River in 2005 and 2006 on behalf of the Oooguruk Development

Strudel Scour Characteristic	Secondary Zone			Primary Zone			Tertiary Zone		
	Data Points	Mean (m)	Range (m)	Data Points	Mean (m)	Range (m)	Data Points	Mean (m)	Range (m)
Circular Scours									
Scour Depth	55	0.40	0.90-2.29	282	0.27	0.09-2.07	-	-	-
Max. Horiz. Dim.	55	17.9	3.4-50.3	282	17.3	3.4-70.4	-	-	-
Water Depth	55	1.43	0.80-1.93	282	2.12	1.50-2.57	-	-	-
Linear Scours									
Scour Depth	1	0.70	n/a	4	0.21	0.18-0.24	-	-	-
Max. Horiz. Dim.	1	63.4	n/a	4	26.5	20.7-35.7	-	-	-
Water Depth	1	1.2	n/a	4	2.05	1.87-2.48	-	-	-

Table 7-7. Strudel Scour Characteristics Measured off the Kuparuk River between 1996 and 2007 on behalf of the Northstar Development

Strudel Scour Characteristic	Secondary Zone			Primary Zone			Tertiary Zone		
	Data Points	Mean (m)	Range (m)	Data Points	Mean (m)	Range (m)	Data Points	Mean (m)	Range (m)
Circular Scours									
Scour Depth	24	0.41	0.12-1.16	322	0.62	0.09-4.27	2	0.38	0.37-0.40
Max. Horiz. Dim.	25	6.7	1.5-17.4	459	9.5	1.5-40.6	2	5.2	4.0-6.4
Water Depth	25	1.61	0.61-3.41	459	3.60	1.62-6.07	2	6.31	5.98-6.65
Linear Scours									
Scour Depth	-	-	-	16	0.51	0.12-1.90	-	-	-
Max. Horiz. Dim.	-	-	-	14	63.2	7.0-280.5	-	-	-
Water Depth	-	-	-	26	3.83	2.59-4.66	-	-	-

Table 7-8. Strudel Scour Characteristics Measured off the Sagavanirktok River in 1997, 1998 and 1999 on behalf of the Liberty Prospect

Strudel Scour Characteristic	Secondary Zone			Primary Zone			Tertiary Zone		
	Data Points	Mean (m)	Range (m)	Data Points	Mean (m)	Range (m)	Data Points	Mean (m)	Range (m)
Circular Scours									
Scour Depth	3	0.23	0.12-0.34	30	0.86	0.12-2.38	-	-	-
Max. Horiz. Dim.	4	7.8	5.5-10.1	178	7.4	1.5-39.6	-	-	-
Water Depth	4	1.41	1.25-1.74	178	3.13	1.71-4.57	-	-	-
Linear Scours									
Scour Depth	0	n/a	n/a	2	1.31	0.15-2.47	-	-	-
Max. Horiz. Dim.	1	29.3	n/a	5	32.1	18.3-62.5	-	-	-
Water Depth	1	1.49	n/a	5	2.26	1.77-3.54	-	-	-

Table 7-9. Strudel Scour Characteristics Measured off the Kadleroshilik River in 1997, 1998 and 1999 on behalf of the Liberty Prospect

Strudel Scour Characteristic	Secondary Zone			Primary Zone			Tertiary Zone		
	Data Points	Mean (m)	Range (m)	Data Points	Mean (m)	Range (m)	Data Points	Mean (m)	Range (m)
Circular Scours									
Scour Depth	12	0.49	0.09-0.98	8	0.58	0.15-1.01	-	-	-
Max. Horiz. Dim.	18	13.7	2.7-30.2	29	11.6	3.4-31.7	-	-	-
Water Depth	18	1.68	1.19-2.01	29	2.14	1.74-3.29	-	-	-
Linear Scours									
Scour Depth	1	0.24	n/a	0	n/a	n/a	-	-	-
Max. Horiz. Dim.	0	n/a	n/a	2	42.2	15.2-69.2	-	-	-
Water Depth	1	1.28	n/a	2	2.71	2.68-2.74	-	-	-

Table 7-10. Strudel Scour Characteristics Measured off the Shaviovik River during 1997, 1998 and 1999 on behalf of the Liberty Prospect

Strudel Scour Characteristic	Secondary Zone			Primary Zone			Tertiary Zone		
	Data Points	Mean (m)	Range (m)	Data Points	Mean (m)	Range (m)	Data Points	Mean (m)	Range (m)
Circular Scours									
Scour Depth	-	-	-	5	0.47	0.24-0.73	-	-	-
Max. Horiz. Dim.	-	-	-	47	9.8	2.4-28.4	-	-	-
Water Depth	-	-	-	47	2.56	2.01-2.99	-	-	-
Linear Scours									
Scour Depth	-	-	-	-	-	-	-	-	-
Max. Horiz. Dim.	-	-	-	-	-	-	-	-	-
Water Depth	-	-	-	-	-	-	-	-	-

Table 7-11. Strudel Scour Characteristics Measured off Local Drainages and Creeks during 2006 and 2007 on behalf of the Sivulliq Prospect

Strudel Scour Characteristic	Secondary Zone			Primary Zone			Tertiary Zone		
	Data Points	Mean (m)	Range (m)	Data Points	Mean (m)	Range (m)	Data Points	Mean (m)	Range (m)
Circular Scours									
Scour Depth	5	0.24	0.13-0.32	9	0.55	0.22-1.18	-	-	-
Max. Horiz. Dim.	5	4.7	3.3-6.2	9	7.1	3.1-10.0	-	-	-
Water Depth	5	1.92	1.76-2.15	9	2.44	1.31-3.12	-	-	-
Linear Scours									
Scour Depth	-	-	-	-	-	-	-	-	-
Max. Horiz. Dim.	-	-	-	-	-	-	-	-	-
Water Depth	-	-	-	-	-	-	-	-	-

Table 7-12. Summary of all Maximum Strudel Scour Dimensions Measured during Industry Studies, 1996-2007

Strudel Scour Characteristic	Secondary Zone	Primary Zone	Tertiary Zone
	Dimension (River) [1]	Dimension (River)	Dimension (River)
Circular Scours			
Scour Depth (m)	0.34 (Sag) – 2.29 (Col)	0.73 (Shav) – 4.27 (Kup)	0.40 (Kup)
Max. Horiz. Dim (m).	10.1 (Sag) – 50.3 (Col)	10.0 (Pt Thm) – 70.4 (Col)	6.4 (Kup)
Linear Scours			
Scour Depth (m)	0.24 (Kad) – 0.70 (Col)	0.24 (Col) – 2.47 (Sag)	
Max. Horiz. Dim. (m)	29.63 (Sag) – 63.4 (Col)	37.5 (Col) – 280.5 (Kup)	

[1] Colville=Col; Kuparuk=Kup; Sagavanirktok=Sag; Kadleroshilik=Kad; Shaviovik=Shav; Pt. Thom. Area=Pt Thm

The frequency and severity of strudel scouring tend to be highest in the Primary Zone. The maximum scour depths recorded for circular features ranged from a minimum of 0.73 m off the Shaviovik River to a maximum of 4.27 m off the Kuparuk. The greatest maximum horizontal dimensions for circular scours varied from 10.0 m in the Pt. Thomson area to 70.4 m off the Colville River. The maximum scour depths for linear features were more modest, ranging from 0.24 m off the Colville River to 2.47 m off the Sagavanirktok. Not surprisingly, the maximum horizontal dimensions for linear scours exceeded those of their circular counterparts, with the maximum lengths varying between 37.5 m off the Colville River and 280.5 m off the Kuparuk.

Strudel scours occur less frequently in the Secondary Zone than in the Primary Zone, and tend to be less severe. The maximum scour depths for circular features varied from 0.34 m off the Sagavanirktok River to 2.29 m off the Colville. Similarly, the greatest maximum horizontal dimensions for circular scours in Secondary Zone were less than those in the Primary Zone, ranging from 10.1 m off the Sagavanirktok River area to 50.3 m off the Colville River. Of the three linear scours mapped in the Secondary Zone, the greatest scour depth was 0.70 m and the greatest maximum horizontal dimension was 63.4 m (both characteristics belonging to a feature found off the Colville River).

Only two scours were mapped in the Tertiary Zone, both circular in plan form and found off the Kuparuk River. The scour depths were 0.37 and 0.40 m, while the maximum horizontal dimensions were 4.0 and 6.4 m. The scours were located in water depths up to 6.65 m.

Scatter plots of scour depth versus water depth, scour maximum horizontal dimension versus water depth, and scour maximum horizontal dimension versus scour depth are presented for the circular scours mapped off each river in Figures 7-17, 7-18, and 7-19. Because of their distinctly different nature, linear scours are excluded.

Figures 7-17 and 7-18 indicate that the highest frequency of scours occurs in water depths between 2 and 5 m (within the Primary Strudel Zone). The greatest scour depths tend to occur in water depths of 2 to 4 m (Figure 7-17). The envelope of maximum horizontal dimensions also peaks in this range of water depths before tailing off gradually with increasing depth (Figure 7-18). Despite significant scatter, the strudel scour maximum horizontal dimensions appear to increase with increasing scour depth (Figure 7-19).

The correlations between strudel scour characteristics were assessed by performing a linear regression analysis for each of the paired variables. A correlation coefficient (R^2), which is a statistical measure of the ability of one variable to predict the other, was derived for each comparison. By definition, the values of R^2 can range from 0 (no correlation) to 1 (perfect correlation). The results are summarized in Table 7-13.

No significant correlation between strudel scour depth and water depth was identified for any of the river data sets investigated. The correlation coefficients (R^2) ranged from 0.0211 for the Colville River to 0.2524 for the Shaviovik. The analysis of strudel scour maximum horizontal dimensions and water depths also yielded no significant correlation. The correlation coefficient (R^2) varied from 0.0002 for the Colville River to 0.0984 for the Sagavanirktok. Comparing strudel scour maximum horizontal dimensions and strudel scour depths yielded correlation coefficients (R^2) ranging from 0.0134 for the Kadleroshilik River to 0.4451 for the Pt. Thomson area features.

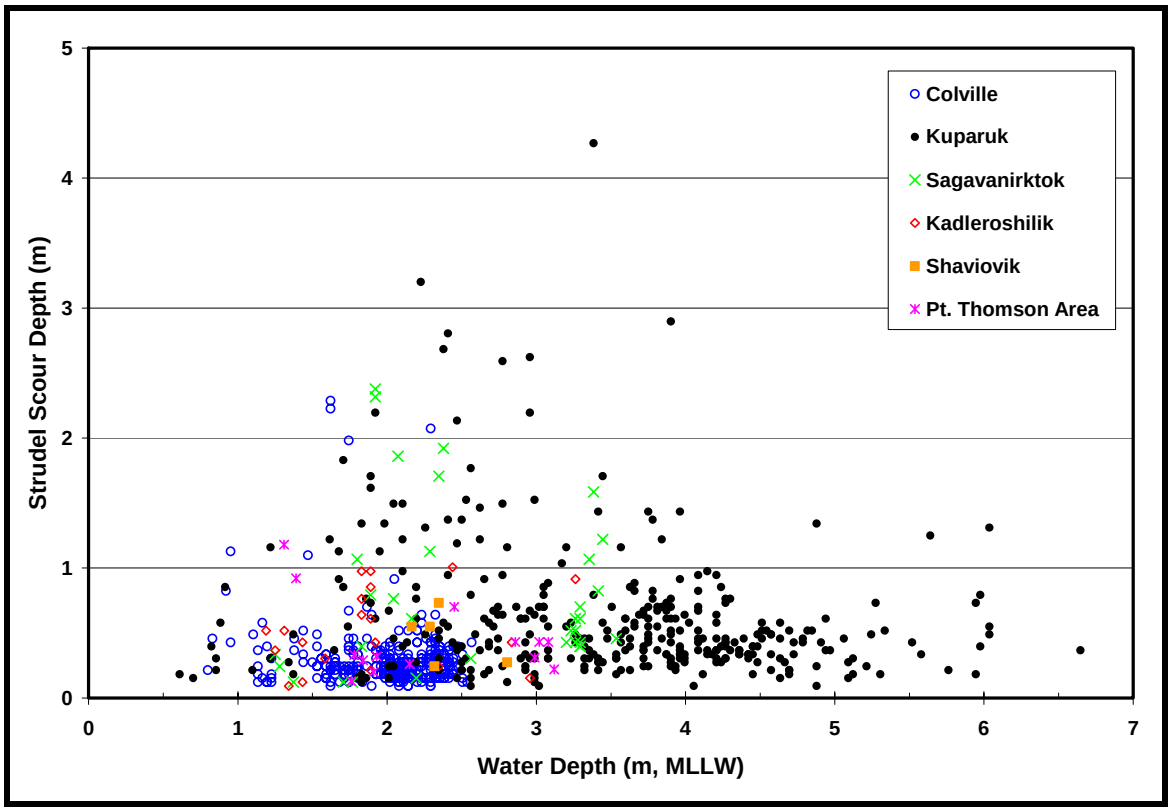

Figure 7-17. Strudel Scour Depth vs. Water Depth for Circular Scours

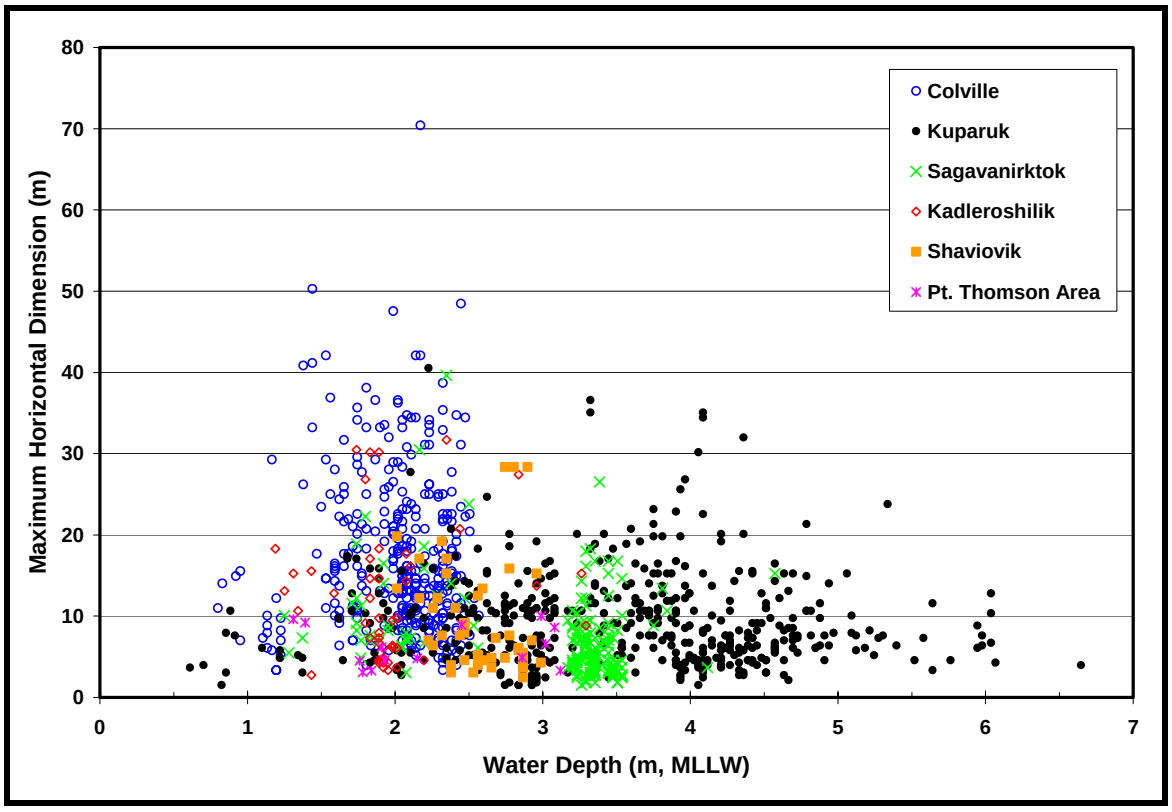

Figure 7-18. Strudel Scour Max Horiz. Dimension vs. Water Depth for Circular Scours

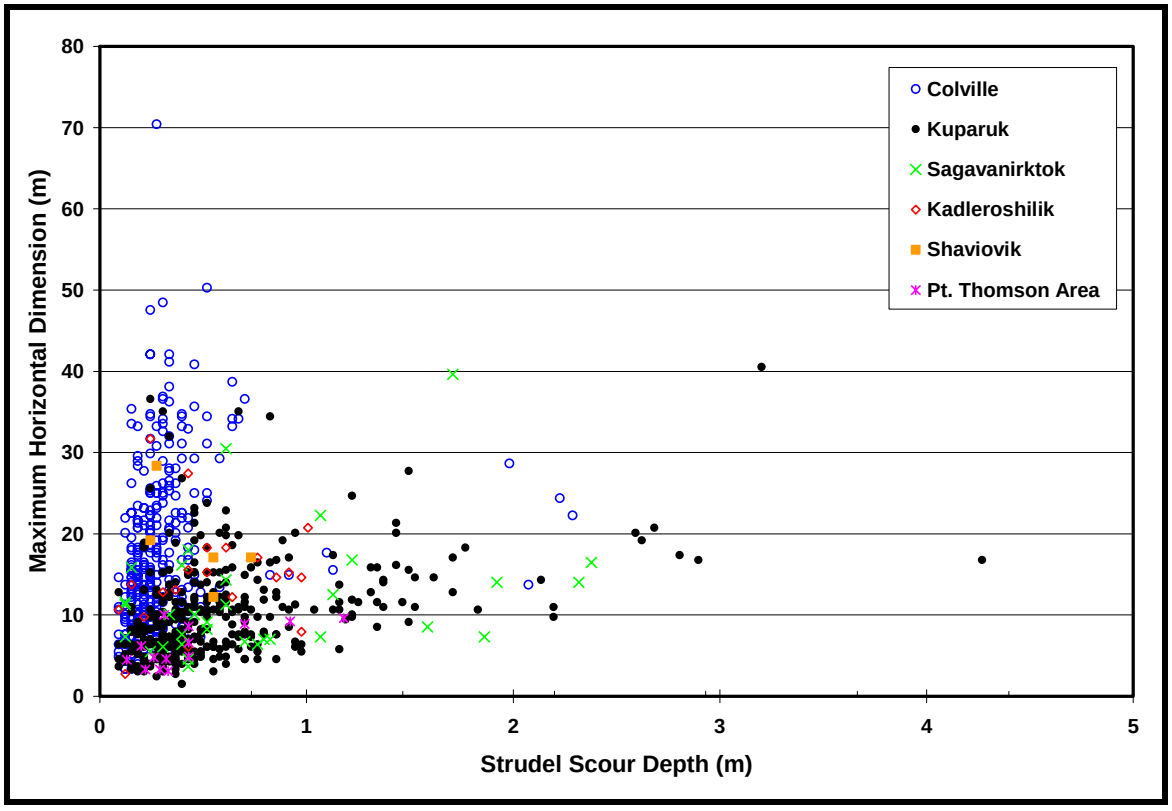

Figure 7-19. Strudel Scour Max Horiz. Dimension vs. Scour Depth for Circular Scours

Table 7-13. Correlations between Strudel Scour Characteristics

Variables	River	Correlation Coeff (R^2)
Scour Depth vs. Water Depth	Colville	0.0211
	Kuparuk	0.0349
	Sagavanirktok	0.0010
	Kadleroshilik	0.0527
	Shaviovik	0.2524
	Pt. Thomson Area	0.1477
Max Horiz. Dim. vs. Water Depth	Colville	0.0002
	Kuparuk	0.0003
	Sagavanirktok	0.0984
	Kadleroshilik	0.0079
	Shaviovik	0.0227
	Pt. Thomson Area	0.0010
Max Horiz. Dim. vs. Water Depth	Colville	0.0516
	Kuparuk	0.1458
	Sagavanirktok	0.0976
	Kadleroshilik	0.0134
	Shaviovik	0.3923
	Pt. Thomson Area	0.4451

7.1.5 Case History: The Northstar Development Pipelines

The Northstar Development pipelines provide a unique opportunity to assess the impact of strudel scours on live subsea pipelines. Leidersdorf, *et al.* (2007), presented an analysis covering the four year period between 2002 and 2005. The assessment presented in this section is a derivative of that work incorporating two additional years of strudel scour data (2006 and 2007).

Twin 273-mm pipelines convey gas to Northstar Production Island and oil to shore. The pipelines were trenched into the sea bottom in Spring 2000. The trench then was backfilled with native sediments to fulfill the permit condition of maintaining a 1.8 m minimum depth of cover over the pipelines. Pipeline operation commenced in October 2001 with the introduction of hot oil to the sales line.

The 9.6-km long pipelines extend south from a water depth of approximately 11.5 m at the production island through the barrier islands, and across Gwyder Bay to a shore crossing near Point Storkersen. Approximately 3.1 km of the pipeline alignment lies within the Secondary Strudel Zone, extending from the shoreline to the 1.5-m isobath (just north of the barrier islands). The Primary Strudel Zone (from the 1.5-m isobath to the 6-m isobath) encompasses 3.6 km of the pipeline length. The remaining 2.9 km, from the 6-m isobath to the production island, lies in the Tertiary Strudel Zone.

A monitoring program has been conducted each year since pipeline installation in 2000. The program consists of a helicopter-based reconnaissance of river overflood and strudel

drainage features during the break-up season followed by a sea bottom survey of the pipeline alignment and drainage sites during the open-water season. During the first six years of the program (2000 to 2005), the investigation of drains and scours was limited to a 3048-m wide corridor centered on the pipeline alignment. In 2006, the corridor width was reduced to 1,524 m. The program constitutes one of the industry studies shown in Table 7-1 and described previously.

Based on the finding that the introduction of hot oil materially altered the scour regime (Leidersdorf, *et al.*, 2007), this investigation is restricted to the six year period between 2002 and 2007. The assessment of drains and scours is limited to those features found within the 1,524-m corridor common to each of the survey years. Relict scours (those that were formed in years prior to the year of discovery) also are excluded, because their characteristics may have been altered by sediment in-filling prior to mensuration. It should be noted that the segregation of features by strudel zone is based on the precise water depth measured at the location of each scour rather than on the more generalized NOAA bathymetry described in Section 7.1.2.

Table 7-14 summarizes the occurrence of strudel drains and scours in the 1,524-m corridor from 2002 to 2007. The data show significant interannual variability in the numbers of both drains and scours, and also evidence a preponderance of circular scours relative to linear scours. On average, slightly more than half of the drains produced scour depressions.

A statistical characterization of the scours mapped in the corridor between 2002 and 2007 is presented in Table 7-15. The scour populations are segregated by zone (Secondary, Primary, and Tertiary), and according to scour type. The percent sea floor disturbance for circular scours was computed as the combined area of all such features in a given year (based on scour diameter) divided by the total area of the strudel zone. A corresponding value was not calculated for the linear features due to insufficient information regarding scour area.

Table 7-14. Strudel Drain and Scour Occurrence within Pipeline Corridor, 2002-2007

Feature	Frequency of Occurrence (number per year)		
	Mean	Minimum	Maximum
Strudel Drains	34	8	62
Strudel Scours			
Circular	18	3	34
Linear	1	0	4

Circular scours (109) greatly outnumbered linear scours (4). Most of the circular scours (84%) and all of the linear scours were located in the Primary Zone. Twelve circular scours were mapped in the Secondary Zone, while only five were found in the Tertiary Zone. Scour severity was highest in the Primary Zone, with scour depths for circular features ranging from 0.09 to 2.90 m (0.64-m average) and scour diameters from 3.1 to 26.8 m (9.3-m average). The mean scour depth was 0.42 m in the Secondary Zone and 0.68 m in the Tertiary Zone. The maximum values in these zones were 1.16 and 1.31 m, respectively. The scour diameters varied from 1.5 to 10.7 m (5.3-m average) in the Secondary Zone, while those in the Tertiary Zone ranged from 4.0 to 12.8 m (7.6-m average).

All four linear scours were confined to the Primary Zone. The dimensions were modest, with a maximum scour depth of 0.55 m and a maximum length of 40.5 m.

Figures 7-20 and 7-21 present scatter plots of scour depth versus water depth and scour maximum horizontal dimension versus water depth for the circular scours mapped within the pipeline corridor between 2002 and 2007. Because of their distinctly different nature, linear scours were excluded. The greatest scour depths were found in water depths of 1.5 to 4 m, while the greatest scour diameters occurred in water depths of 2.5 to 5.5 m.

The average annual disturbance of the sea floor attributable to strudel scours was modest, ranging from 0.001% in the Secondary Zone to 0.026% in the Primary Zone. Given the low area of sea floor disturbance, the formation of nine scours directly over the pipelines between 2002 and 2007 was surprising (Table 7-16). Three of these encounters occurred in the Primary Strudel Zone, while six occurred in the Secondary Zone. The latter number is particularly noteworthy in that it represents half of all scours found in the Secondary Zone.

Leidersdorf, *et al*. (2007), postulated that the high encounter frequency in the Secondary Zone was attributable to radiant heat from the pipelines propagating through the backfill and degrading the overlying ice cover. This premature melting promoted early strudel drainage and preferential scour formation over the pipelines, a phenomenon termed the "strudel magnet" effect. Support for this theory is provided in Figure 7-22, which shows a distinct thermal signature in the bottomfast ice sheet along the pipeline alignment. Fortunately, as discussed above, the intensity of scouring in the Secondary Zone tends to be mild. As a result, these six encounters did not pose a significant threat to the integrity of the pipelines.

Table 7-15. Strudel Scour Characteristics within Pipeline Corridor, 2002-2007

Strudel Scour Characteristic	Secondary Zone			Primary Zone			Tertiary Zone		
	Ave.	Min	Max	Ave.	Min	Max	Ave.	Min	Max
Circular Scours	*12 Scours*			*92 Scours*			5 Scours		
Quantity (per yr)	2	1	5	15	1	29	1	0	3
Scour Depth (m)	0.42	0.15	1.16	0.64	0.09	2.90	0.68	0.37	1.31
Scour Diameter (m)	5.3	1.5	10.7	9.3	3.1	26.8	7.6	4.0	12.8
Water Depth (m)	0.99	0.61	1.37	3.38	1.62	5.94	6.16	6.03	6.64
% Sea Floor Disturbance	0.001	0.000	0.004	0.026	0.001	0.045	0.001	0.000	0.003
Linear Scours	*0 Scours*			*4 Scours*			*0 Scours*		
Quantity (per yr)	-	-	-	1	0	4	-	-	-
Scour Depth (m)	-	-	-	0.40	0.24	0.55	-	-	-
Scour Diameter (m)	-	-	-	18.9	7.0	40.5	-	-	-
Water Depth (m)	-	-	-	3.69	2.62	4.11	-	-	-

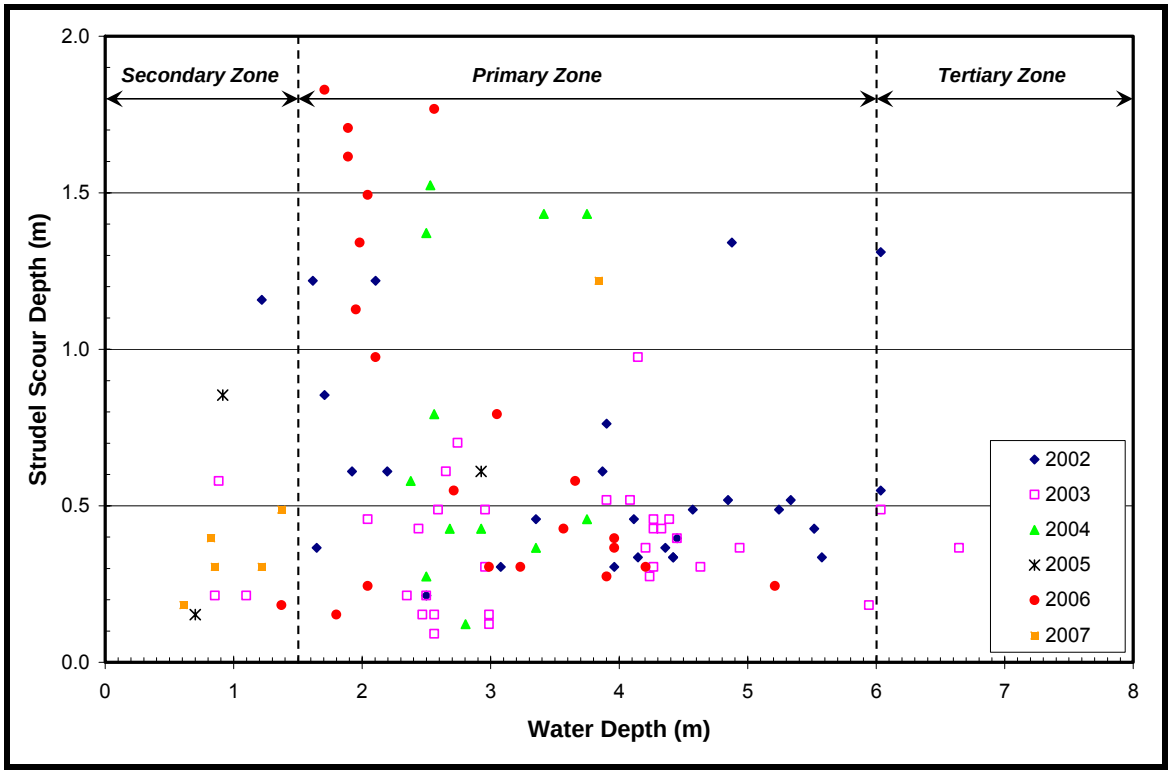

Figure 7-20. Strudel Scour Depth vs. Water Depth for Circular Scours within Northstar Development Pipeline Corridor, 2002-2007

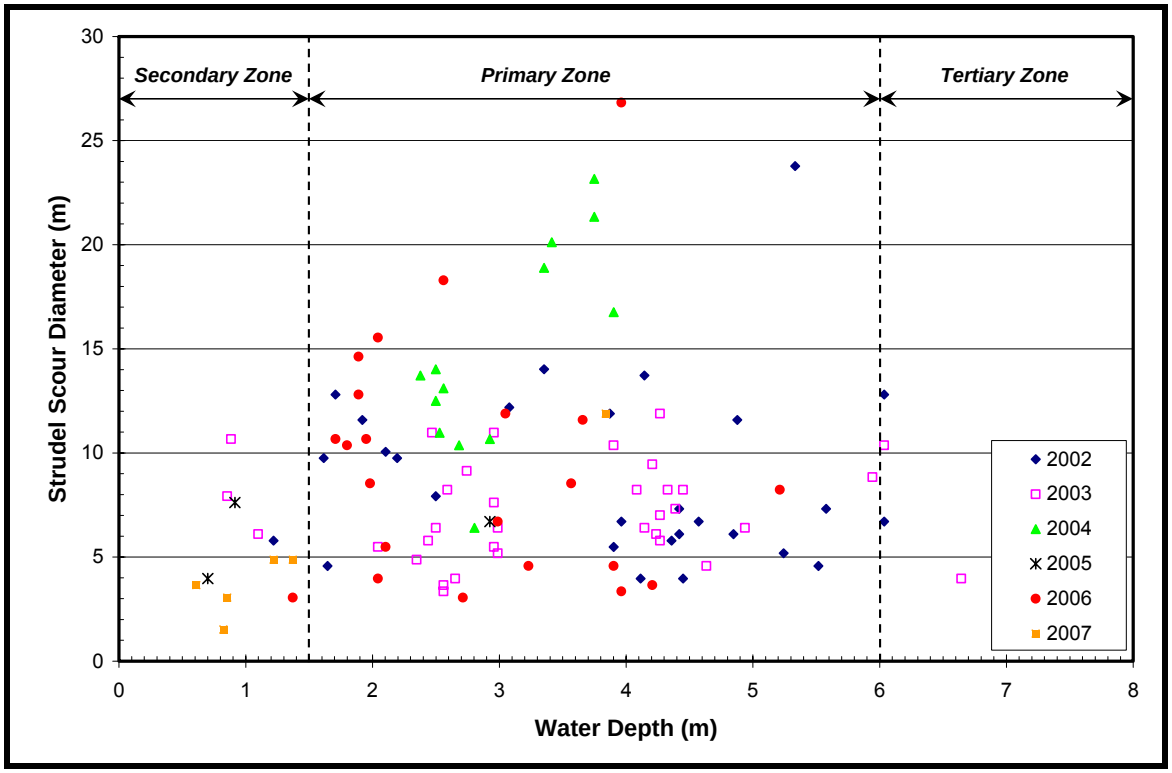

Figure 7-21. Strudel Scour Diameter vs. Water Depth for Circular Scours within Northstar Development Pipeline Corridor, 2002-2007

Table 7-16. Strudel Scour Encounters with Northstar Pipelines, 2002-2007

Strudel Scour Encounters	Secondary Zone	Primary Zone	Tertiary Zone
2002	0	0	0
2003	3	0	0
2004	0	1	0
2005	1	1	0
2006	0	1	0
2007	2	0	0
Total	*6*	*3*	*0*
Frequency	*1.0 /year*	*0.5 /year*	*0.0 /year*

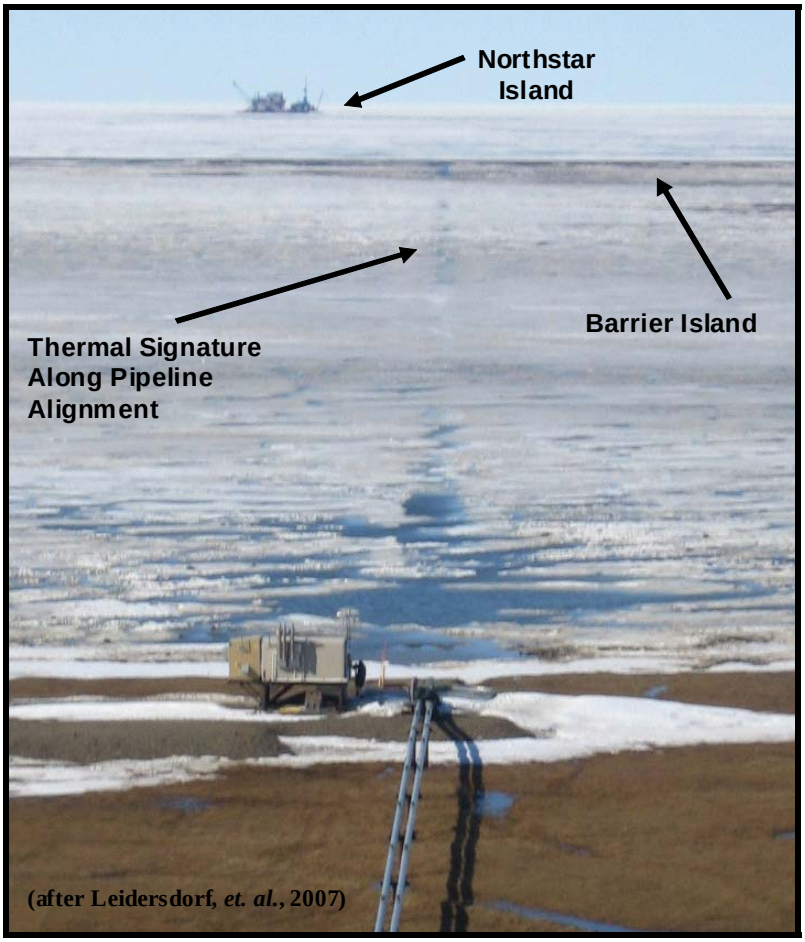

Figure 7-22. Thermal Signature of Northstar Pipelines

A thermal signature similar to that shown in Figure 7-22 was conspicuously absent in the Primary Zone, where the ice is floating rather than bottomfast. However, the occurrence of three strudel scours directly over the pipelines suggested that the lines may be influencing scour processes in this region as well. To understand if the presence of the pipelines was increasing the encounter frequency in the Primary Zone, the probability of one or more scours impacting the pipelines in a given year in absence of the strudel magnet effect was computed as described below and illustrated in Figure 7-23.

$$P = n\left(\frac{2d}{w}\right) \qquad (1)$$

where: P = encounter probability for one or more scours in one year
n = average number of scours/year (15)
d = average scour diameter (9.3 m)
w = corridor width (1,524 m)

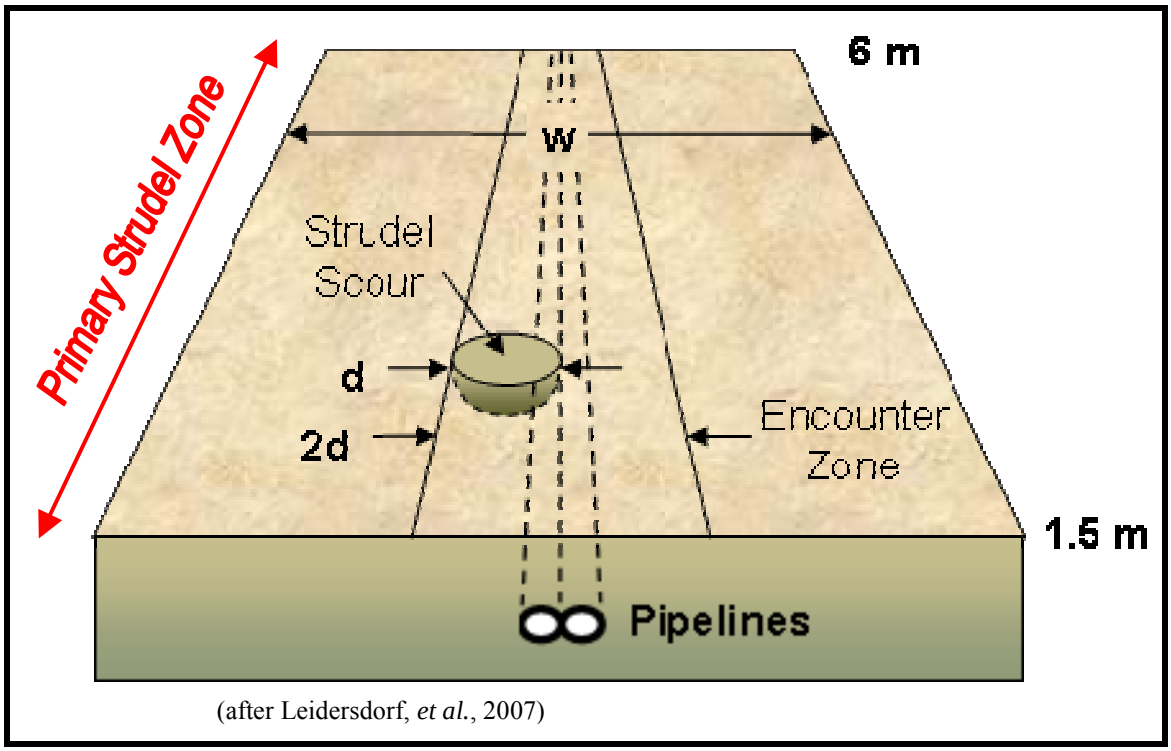

(after Leidersdorf, *et al.*, 2007)

Figure 7-23. Strudel Scour Encounter Probability Conceptual Model

The probability of one or more scours impacting the pipelines in multiple years was determined by considering the possible combination of events:

$$p_i = \left\{\frac{N!}{[i!(N-i)!]}\right\} P^i (1-P)^{(N-i)} \qquad (2)$$

where: p_i = encounter probability for one or more scours in i years
N = number of years under consideration
i = number of years out of N years with at least one encounter

Applying Equation 1 with the circular strudel scour characteristics shown in Table 7-14 yields an encounter probability of 19% for one year. The probability of encounters during a six-year period (Equation 2) is shown in Table 7-17. The probability of three scour depressions forming over the pipelines (as occurred between 2002 and 2007) is only 7%. The low encounter probability suggests that the pipelines have increased the frequency of scour formation in the Primary Zone. While radiant heat from the pipelines is a likely explanation for the high encounter frequency, it is not known whether the impact is direct (degradation of the ice sheet), indirect (increased biological activity in the warmer water), or a combination of the two (Leidersdorf, *et al.,* 2007).

As indicated in Table 7-15, the severity of strudel scouring is greatest in the Primary Zone. Hence the potential consequences of scour depressions forming over the pipelines are more severe in the Primary Zone than in the Secondary Zone. Fortunately, the deepest scour to form over the Northstar Pipelines to date (2.9-m scour depth) did not expose the lines because the center of the depression was offset to one side. Sufficient data do not exist to evaluate the encounter frequency in the Tertiary Zone.

Table 7-17. Strudel Scour Encounter Probability for One or More Scours in the Primary Zone During a Six-year Period

Years with at Least One Encounter	Encounter Probability
0	28.8%
1	39.8%
2	22.9%
3	7.0%
4	1.2%
5	0.1%

7.2 Facilities Access

In addition to the threat posed to subsea pipelines by strudel scour, sea ice overflood also can impact nearshore ice roads. Seasonal ice roads are used to support construction, drilling, and resupply operations at offshore sites. Ice roads located within the zone of river overflood can be rendered impassable due to rapid deterioration of the ice sheet. Portions of ice roads located beyond the overflood boundary typically are capable of supporting substantial vehicle and equipment loads into June (Coastal Frontiers, 2001b). However, premature ice road closure can be precipitated by the impacts of flooding.

Oil spill response operations may be hampered by limiting the options to access and control an accidental spill with conventional surface vehicles (*e.g.*, Rolligon, snow machine, Snow Cat etc.). Amphibious vehicles such as hovercraft and air boats are required to travel through the overflood areas. Provisions are made for these alternate means of access in the Alaska Clean Seas Technical Manual (ACS, 2006).

Another concern is the possibility that any oil present on the overflood surface could potentially spread through wind action to cover large areas before the flood waters drain. Hence, the overflood phenomenon could significantly alter the characteristics and clean-up of any accidental spill, including areal extent, film thickness, oil weathering, emulsification and recovery. Possible implications of an oil spill/overflood interaction are discussed further in Dickins and Owens (2002).

8 SUMMARY AND CONCLUSIONS

1. *Field Survey Program and Satellite Image Validation*: Helicopter-based mapping techniques provide the most accurate depiction of river overflood limits. The helicopter-derived 2007 Colville River overflood boundary was compared to the boundaries mapped using images from three visible spectrum satellite platforms (Landsat 7, SPOT, and MODIS) and two SAR satellite platforms (ERS-2 and Radarsat) to gain an understanding of the accuracy and limitations of various image platforms. Landsat 7, MODIS, and ERS-2 performed equally well among the satellite platforms and provided the most accurate depiction of the overflood limit relative to the helicopter survey. The SPOT and Radarsat imagery provided the least accurate results. The findings suggest that satellite imagery can be used to derive overflood limits that approach the accuracy of helicopter-based results under favorable conditions. However, late in the overflood period and under unfavorable conditions, overflood boundaries derived from satellite-based imagery can differ materially from those derived from helicopter-based mapping. Because the availability of images from multiple satellite platforms in a given year is rare, however, none of the satellite platforms investigated should be excluded from consideration when mapping historical overflood limits.

2. *Historical Overflood Boundary Mapping*: River overflood boundaries were mapped for all major rivers and streams in the study area for the 13-year period between 1995 and 2007 using a combination of historical helicopter surveys and satellite images. Satellite imagery, and particularly radar satellite imagery, formed the key data source needed to develop the final mapped boundaries. To increase the probability of capturing the peak overflood, a maximum composite overflood limit was developed for each watercourse by integrating all of the mapped overflood limits for a given year. When the 11 major river systems in the study are considered, overflood limits were mapped for 129 out of 143 possible river and year combinations, resulting in a mapping success of 90%. This result exceeded expectations, and would not have been possible without having access to both the radar imagery and helicopter surveys.

3. *Correlation of River Overflood with Environmental Variables*: No meaningful correlations were identified between annual overflood areas and the corresponding values of streamflow, precipitation, and temperature. Attempts to correlate streamflow with either precipitation or temperature also proved to be fruitless. The most important implication of these findings is that the extent of river overflood onto the sea ice cannot be predicted by any single environmental variable for which historical data currently exist. The overflood phenomenon appears to be governed by complex interactions between a number of environmental forces, some of which, such as ice jams in distributary channels, roughness and snow cover on the sea ice, and the density of drainage features on the sea ice, have not been quantified to date.

4. *Hazards Related to Strudel Scours*: Strudel scouring can constitute a significant design consideration for subsea pipelines in nearshore areas adjacent to river and stream mouths. Strudel scour concerns have resulted in the burial of the two existing subsea pipelines in the Alaskan Beaufort Sea (BPXA's Northstar and Pioneer's Oooguruk). In the event that

a strudel drain is located directly above a buried subsea pipeline, a sufficiently deep strudel scour may expose the pipeline and lead to an unsupported span. A strudel scour that forms directly over a buried pipeline also can remove the backfill material that is needed to prevent damage from ice keels and forestall upheaval buckling. An additional concern is that strudel drainage provides a potential mechanism to transport spilled oil below the ice sheet.

5. *Strudel Scour Zonation*: Strudel scour frequency and severity can be segregated into zones according to water depth. Strudel scouring typically is most common and severe in the Primary Strudel Zone, which extends offshore from the bottomfast ice edge to approximately 6 m water depth. In the zone of bottomfast ice (the "Secondary Strudel Zone") and offshore of the Primary Zone (the "Tertiary Strudel Zone"), scouring tends to be more modest and occur less frequently. When the major rivers in this region were considered, the Secondary Strudel Zone accounted for the greatest portion of the overflood area in any given year. On average, this zone encompassed 66% of the total average overflood area. The Primary Strudel Zone accounted for 32% of the total average overflood area, while the Tertiary Zone accounted for a mere 2%. Strudel zone information should be used to assess the risk to prospective pipeline routes posed by strudel scouring in different coastal areas.

6. *Strudel Scour Pipeline Encounter Frequency*: A case study of strudel scours in the vicinity of the BPXA Northstar Development suggests that the presence of the operational pipeline materially altered the scour regime, and has led to a substantially higher than expected scour encounter frequency with the pipelines. This phenomena is most prominent in the Secondary Zone, and is believed to be attributable to radiant heat from the pipelines propagating through the backfill and degrading the overlying ice cover. While less pronounced, a statistical analysis of strudel occurrence also indicates an increased encounter frequency in the Primary Zone. Radiant heat from the pipelines also may explain the high encounter frequency in this zone. However, it is not known whether the impact is direct (degradation of the ice sheet), indirect (increased biological activity in the warmer water), or a combination of the two. Because scouring is more severe in the Primary Zone, the potential consequences of scour depressions forming over the pipelines are greater in this zone than in the Secondary Zone.

7. *Hazards Related to Facilities Access*: Rapid deterioration of the ice sheet can render ice roads impassable within the zone of river overflood, impacting both facilities access and oil spill response.

9 REFERENCES

ACS (Alaska Clean Seas) Technical Manual. Vol. 1. 2006 Rev. Prudhoe Bay, AK.

Alexander, M. 2007. Michael Baker Jr. Inc. personal communication by e-mail.

Atwater, S.G. 1991. Ice Break-up and Freeze-up. In *1989 Endicott Environmental Monitoring Program Final Report*, prepared by SAIC for the U.S. Army Corps of Engineers, Anchorage AK.

Barber, D.G., Papakyriakou, T.N., LeDrew, E.F., Shokr, M.E. 1995. An Examination of the Relation Between the Spring Period Evolution of the Scattering Coefficient and Radiative Fluxes over Landfast Sea-ice. *Int. J. Remote Sens. 16, 3343-3363.*

Barnes P., and E. Reimnitz. 1974. Flooding of Sea Ice by the Rivers of Northern Alaska. U.S.G.S. Professional Paper 929, Menlo Park, CA, p.356-359.

Barry, R.G., R.E. Moritz and J.C. Rogers. 1979. The Fast Ice Regimes of the Beaufort and Chukchi Sea Coasts, Alaska. *Cold Regions Science and Technology, 1.*

Brady, M. 2008. Personal Communication, Nanuq Construction, Inc.

Brott, L. 2008. Personal Communication, Northstar Project Operations, BPXA.

Canada Centre for Remote Sensing (CCRS). 2008. Tutorial: Fundamentals of Remote Sensing Microwave remote sensing. http://www.ccrs.nrcan.gc.ca/resource/tutor/fundam/chapter3/05_e.php

Carlson, R.F. 1977. Effects of Seasonability and Variability of Streamflow on Nearshore Coastal Areas, in *Environmental Assessment of the Alaskan Continental Shelf, Vol. XIV - Transport*, NOAA, Boulder CO.

Coastal Frontiers Corporation, 1996, 1995 Resolution Island Inspection Program, Chatsworth, CA, 51 pp.+ appen.

Coastal Frontiers Corporation. 1997. Northstar Development 1996 Pipeline Route Survey. Chatsworth, CA: BPXA. 72 pp. + appen.

Coastal Frontiers Corporation. 1998a. Northstar Development 1997 Pipeline Route Survey. Chatsworth, CA: BPXA. 56 pp. + appen.

Coastal Frontiers Corporation. 1998b. Liberty Development 1997 Pipeline Route Survey. Chatsworth, CA: BPXA, 62 pp + appen.

Coastal Frontiers Corporation. 1999a. Northstar Development 1998 Pipeline Route Survey. Chatsworth, CA: BPXA. 56 pp. + appen.

Coastal Frontiers Corporation. 1999b. Liberty Development 1998 Pipeline Route Survey. Chatsworth, CA: BPXA, 54 pp + appen.

Coastal Frontiers Corporation. 2000a. Northstar Development 1999 Pipeline Route Survey. Chatsworth, CA: BPXA. 26 pp. + appen.

Coastal Frontiers Corporation. 2000b. Liberty Development 1999 Pipeline Route Survey. Chatsworth, CA: BPXA, 18 pp + appen.

Coastal Frontiers Corporation. 2001a. Northstar Development 2000 Pipeline Route Monitoring Program. Chatsworth, CA: BPXA. 48 pp. + appen.

Coastal Frontiers Corporation. 2001b. Northstar Pipeline Trench Backfill Program, Winter 2001. Chatsworth, CA: BPXA.

Coastal Frontiers Corporation. 2002. Northstar Development 2001 Pipeline Route Monitoring Program. Chatsworth, CA: BPXA. 45 pp. + appen.

Coastal Frontiers Corporation. 2003a. Northstar Development 2002 Pipeline Route Monitoring Program. Chatsworth, CA: BPXA. 55 pp. + appen.

Coastal Frontiers Corporation. 2003b. 2003 Liberty Development River Overflood Reconnaissance. Memorandum Dated July 18, 2003. Chatsworth, CA: BPXA.

Coastal Frontiers Corporation. 2004. Northstar Development 2003 Pipeline Route Monitoring Program. Chatsworth, CA: BPXA. 49 pp. + appen.

Coastal Frontiers Corporation. 2005. Northstar Development 2004 Pipeline Route Monitoring Program. Chatsworth, CA: BPXA. 51 pp. + appen.

Coastal Frontiers Corporation. 2006a. Northstar Development 2005 Pipeline Route Monitoring Program. Chatsworth, CA: BPXA. 51 pp. + appen.

Coastal Frontiers Corporation. 2006b. Oooguruk Development 2005 Bathymetric Survey Program. Chatsworth, CA: Pioneer Natural Resources, 30 pp + appen.

Coastal Frontiers Corporation. 2007a. Northstar Development 2006 Pipeline Route Monitoring Program. Chatsworth, CA: BPXA. 62 pp. + appen.

Coastal Frontiers Corporation. 2007b. Oooguruk Development 2006 Bathymetric Survey Program. Chatsworth, CA: Pioneer Natural Resources, 44 pp + appen.

Coastal Frontiers Corporation. 2007c. Sivulliq Development 2006 Nearshore Survey Program. Chatsworth, CA: Shell Exploration and Production: Houston, TX. 40 pp. + appen.

Coastal Frontiers Corporation. 2007d. Map of Oooguruk Flowline Survey, Summer 2007. For Pioneer Natural Resources.

Coastal Frontiers Corporation. 2008a. Northstar Development 2007 Pipeline Route Monitoring Program. Chatsworth, CA: BPXA. 73 pp. + appen.

Coastal Frontiers Corporation. 2008b. Sivulliq Development 2007 Nearshore Survey Program. Chatsworth, CA: Shell Exploration and Production: Houston, TX. 37 pp. + appen.

Curtis, J., B. Hartmann, and G. Wendler. 2003. Climate variability for Arctic Alaska. In: AMS Proceedings of the Seventh Conference on Polar Meteorology and Oceanography of High Latitude Climate Variations, Hyannis, Mass.: 16 pp.

Dickins (DF Associates) and OASIS Environmental. 2006. North Slope Nearshore and Offshore Breakup Study. Report prepared for the Alaska Department of Environmental Conservation, Anchorage AK. 19 pp.

Dickins, D.F. and E.H. Owens. 2002. Annual Ice Cycle at the Mouth of the Colville River and Implications for Oil Transport. Proceedings 2002 Arctic and Marine Oil Spill Conference (published with permission of ConocoPhillips Alaska based on a previous study completed in 1999 – proprietary).

DF Dickins, Vaudrey & Associates and Coastal Frontiers. 1999. Sea Ice Overflood Limits Affecting the Liberty Pipeline Route: Results of a Literature Search and Satellite Image Analysis. For BP Exploration (Alaska), Anchorage (proprietary – see published summary – Dickins *et al*. 2001).

Dickins, D.F., Hearon G. and K. Vaudrey. 2001. Sea Ice Overflood in Stefansson Sound, Alaskan Beaufort Sea. In Proceedings 16th International Conference on Port and Ocean Engineering Under Arctic Conditions, Ottawa, pp. 193-202.

Fetterer, F. *et. al.*. 1994. Sea ice type maps from Alaska Synthetic Aperture Radar Facility imagery: An assessment. *JGR*, Vol. 99, No. C11, pp. 22443-22458.

FR Bell and Associates. 2007. Chronology of River Break-up Dates, provided as an MS Excel Spreadsheet.

Hall, J.D. 2008. Oooguruk Project Field Development Concept and Execution. Proc., 2008 Offshore Technology Conference, OTC-19526.

Harding Lawson Associates. 1986. North Star Project Side-Scan Sonar and Bathymetric Survey Program, 2 vols., Novato, CA, 63 pp.+ appen.

LaBelle, J.C. and J.L. Wise. 1983. Alaska Marine Ice Atlas. produced by the Arctic Information and Data Center. University of Alaska, Anchorage, pp. 144 to 145.

Lanan, G.A., D.H. Maguire, B. Hazen, J.D. Hall, and C.J. Perry. 2008. Oooguruk Offshore Arctic Flowline Design and Construction. Proc., 2008 Offshore Technology Conference, OTC-19353.

Leidersdorf, C.B., G.E. Hearon, K.D. Vaudrey, and G. Swank. 2007. Strudel Scour Formation off Arctic River Deltas. Proc., 30th International Conference on Coastal Engineering, Vol. 5, World Scientific, Hackensack, New Jersey, p. 5312-5324.

Lewis, R. 2001. New Real-Time DGPS Source. In *GPS-GIS News, Spring 2001, p. 3.*

Magellan Corporation. 2001. *Powered by WAAS*. San Dimas, CA.

Mahoney, A., Eicken, H., Shapiro, L., Graves, A. 2005. Defining and locating the seaward landfast ice edge in Northern Alaska. 18th International Conference on Port and Ocean Engineering under Arctic Conditions, POAC '05. Potsdam, N.Y., June 26–30, 2005. 3, pp. 100−109.

Market Wire. 2008. True North Energy Announces Beaufort Sea Project Update. http://findarticles.com/p/articles/mi_pwwi/is_200802/ai_n21413016/print.

McClelland Engineers, Inc. 1982. Duck Island/Sag Delta Development Project, Strudel Scour Investigation. Ventura, CA 47 pp. + appen.

Milbert, D.G. 2001. GPS Fluctuations over Time on May 2, 2000. Interagency GPS Executive Board, Washington, D.C. 4pp, http://www.igeb.gov/sa.

Minerals Management Service. 2006. "Exploration Wells, Beaufort Sea", www.mms.gov/alaska/fo/wellhistory/bs_wells.htm. Northstar Project Team (BPXA, *et al*.). 1996. "Test Trench Project HSE Plan" Greenpeace USA, 1999, "Greenpeace Files Suit to Stop Illegal Construction of Ice Roads on Alaska's North Slope" www.commondreams.org/pressreleases/jan99/012099i.htm.

National Oceanic and Atmospheric Administration (NOAA), 2008, Center for Operation Oceanographic Products and Services. http://co-ops.nos.noaa.gov.

Northstar Project Team (BPXA, et al.). 1996. "Test Trench Project HSE Plan" Greenpeace USA, 1999, "Greenpeace Files Suit to Stop Illegal Construction of Ice Roads on Alaska's North Slope" www.commondreams.org/pressreleases/jan99/012099i.htm.

Petroleum News (Kay Cashman). 2007. Kupcake on Track for February Drilling.

Reimnitz, E.C. and E.W. Kempema. 1982. High Rates of Bedload Transport Measured from Infilling Rate of Large Strudel-scour Craters in the Beaufort Sea, Alaska. U.S.G.S. Professional Paper, Menlo Park, CA.

Reimnitz, E.C., Rodeick, C.A. and S.C Wolf. 1974. Strudel Scour, a Unique Arctic Marine Geologic Phenomenon. *Journal of Sedimentary Petrology, 44(2); 409-420.*

Sandwell Engineering. 2003. Thetis Ice Island Wells. For Pioneer Natural Resources Alaska, Inc.

Solomon, S. Weekly Reports – Mackenzie Delta Break-up 2007/08 (2006, 2007, 2008). Produced by the Bedford Institute of Oceanography for Natural Resources Canada. Dartmouth, NS. ssolomon@nrcan.ca

Smith, T.S., S.T. Partridge, S.C Amstrup, and S. Schliebe. 2007. Post Den Emergence Behavior of Polar Bears (Ursus Maritimus) in Northern Alaska. *Arctic, Vol. 60, No. 2, p. 187-194.*

State of Alaska, Dept. of Natural Resources. 2006. Nikaitchuq Development Royalty Modification Agreement.

Trans-Alaska Pipeline System Owners (TAPS). 2001. Environmental Report for Trans-Alaska Pipeline System Right-of-Way Renewal. Anchorage, AK: TAPS Owners.

US Army Corps of Engineers. 1998. Northstar Project Environmental Impact Statement.

U.S. Department of Agriculture, National Resources Conservation Service (NRCS), 2008, Alaska Snow Survey Program. http://www.ak.nrcs.usda.gov/Snow/index.html

U.S. Geological Survey, 2008, http://waterdata.usgs.gov.

Vaudrey, K.D. 1996. Design Basis Ice Criteria for the Northstar Development, Vaudrey & Associates, Inc., San Luis Obispo, CA, 54 pp.+ appen.

Vaudrey, K. 1984, 85, and 86. Breakup Study of the Alaskan Beaufort and Upper Chukchi Seas. separate reports for 1983 to 1985 seasons, AOGA Projects 224, 274 and 319, Vaudrey & Associates, Inc., San Luis Obispo, CA.

Walker. H.J. 1974. The Colville River and the Beaufort Sea: Some interactions. *The Coast and Shelf of the Beaufort Sea, Proceedings of a symposium on Beaufort Sea Coast and Shelf Research*. Eds., J,C. Reed and J.E. Sater, The Arctic Institute of North America, pp. 513-540.

Western Regional Climate Center (WRCC). 2008. http://www.wrcc.dri.edu

Workman, J. 2008. Personal Communication, Nanuq Construction, Inc.